INFORMATION TO USERS

This manuscript has been reproduced from the microfilm master. UMI films the text directly from the original or copy submitted. Thus, some thesis and dissertation copies are in typewriter face, while others may be from any type of computer printer.

The quality of this reproduction is dependent upon the quality of the copy submitted. Broken or indistinct print, colored or poor quality illustrations and photographs, print bleedthrough, substandard margins, and improper alignment can adversely affect reproduction.

In the unlikely event that the author did not send UMI a complete manuscript and there are missing pages, these will be noted. Also, if unauthorized copyright material had to be removed, a note will indicate the deletion.

Oversize materials (e.g., maps, drawings, charts) are reproduced by sectioning the original, beginning at the upper left-hand corner and continuing from left to right in equal sections with small overlaps. Each original is also photographed in one exposure and is included in reduced form at the back of the book.

Photographs included in the original manuscript have been reproduced xerographically in this copy. Higher quality 6" x 9" black and white photographic prints are available for any photographs or illustrations appearing in this copy for an additional charge. Contact UMI directly to order.

UMI

A Bell & Howell Information Company
300 North Zeeb Road, Ann Arbor MI 48106-1346 USA
313/761-4700 800/521-0600

System Modelling, Identification and Coordinated Control Design for an Articulated Forestry Machine

Bin Mu
B.Eng., (McGill University), 1994

Department of Mechanical Engineering
McGill University

June 1996

A thesis submitted to the Faculty of Graduate Studies and Research
in partial fulfillment of the requirements for the degree of
Master of Engineering

Abstract

This thesis describes the modelling of electrohydraulic actuation systems of a prototype forestry vehicle, the experimental identification of the dynamic models parameters and control strategies for forestry operations.

The linear graph method is selected to derive comprehensive models of three electrohydraulic actuation subsystems, i.e. the swing, boom and stick subsystems, on the vehicle based on modelling of individual components. A new approach is proposed, then, to integrate rigid-body dynamic models with the actuator dynamic models to result in a complete machine model.

Off-line parameter identification procedures are used, including the least-square method. A series of experiments is performed to obtain numerical values for the parameters involved in the system models. The experimental setups are described in detail and new procedures are explained. The model validation studies show that the mathematical models closely represent the dynamic characteristics of the forestry machine.

The concept of coordinated control in teleoperation is studied. The resolved motion rate control strategy shows superiority over conventional joint-based control in heavy-duty forestry machines. Two inverse Jacobian manipulator control schemes, based on velocity and on position servo schemes, are introduced and evaluated under various operating conditions. The results provide guidelines for the design and implementation of manipulator controllers on a forestry machine.

Résumé

Cette thèse décrit la modélisation de systèmes d'actuation électro-hydraulique pour un prototype de véhicule forestier, l'identification expérimentale de paramètres du modèle dynamique et des stratégies de commande lors d'opérations forestières.

La méthode des graphes linéaires est choisie pour obtenir les modèles détaillés de trois actionneurs électro-hydrauliques différents du véhicule, soit ceux de la base rotative, de la flèche et du balancier, à partir de la modélisation des composantes individuelles. Une nouvelle approche est alors proposée pour combinér les modèles dynamiques des corps rigides aux modèles dynamiques des actionneurs afin d'obtenir un modèle complet de la machine.

La méthode des moindres carrés est utilisée en différée pour l'identification des paramètres. Une série d'expériences a été effectuée afin d'obtenir les valeurs numériques de paramètres impliqués dans les modèles du système. Le montage expérimental détaillé est décris, et de nouvelles procédures sont justifiées. Les études de validation du modèle démontrent que les modèles mathématiques décrivent très bien les caractéristiques des systèmes.

Le concept de commandes coordonnées dans les téléopérations est étudiés. La stratégie de commande du type de la vitesse du mouvement résolue, démontre sa supériorité face aux modèles d'asservissement conventionnels basés sur les articulations, et ce pour les machines forestières à usage intensif. Deux schéma de commande, celui de la matrice Jacobienne inversée avec la vitesse du manipulateur, et celui d'un modèle asservi en position, sont introduits et évalués sous diverses conditions d'opération. Le résultat fournit des lignes directrices pour la conception et la réalisation de modèles d'asservissement pour le véhicule.

To my parents

Acknowledgments

I wish to wholeheartedly thank my supervisor Evangelos Papadopoulos for his invaluable guidance, assistance, scheduled and unscheduled discussions throughout the realization of my Master's degree. I truly appreciate his time, wisdom, effort not only in the preparation of this thesis, but in all aspects of academic life. His lectures on systems modelling and robotics I took back in the undergraduate years made up my mind to pursue research in this field.

I also wish to thank Real Frenette for his help with setting up experiments. His dedication, enthusiasm, patience under all weather conditions made this time consuming stage valuable experience for me. I also wish to thank Soumen Sarkar, one of my project partners, to discuss some issues related to this thesis. Also I would like to thank Paul Freedman at CRIM, Ismo Makkonen and Jean Coutu at FERIC, Robert Lessard at Autolog who were directly involved in the project and made contributions in the progress of my research.

To all my friends in the center, I owe a deep debt of thanks for making my stay here such a rewarding experience, even in the toughest of times. You are too numerous to name. Ali, Dan, Eric, Glen, Yves, my research group members; and many friends, Robert, Hamid, Mike, Oliver, Manuel, Dominik, and of course, my roommate, Nikolai. Special thanks to Eric for helping in the translation of the abstract into French. I wish to thank all the people who make the Center for Intelligent Machines such an amazing research unit.

This research has been made possible with the financial support made by the Ministère de l'industrie, du Commerce, de la Science et de la Technologie of Quebec, (MICST), under the program SYNERGIE.

Finally, I would like to thank my parents for their love and support during my Master's degree and throughout my entire university career.

Table of Contents

List of Figures

List of Tables

Nomenclature

Symbols

A	Area
B	Damping coefficient
C	Fluid capacitance
C_d	Orifice discharging coefficient
C_o	Velocity of sound in the fluid
C_R , $C_{R'}$	Valve orifice resistance
D	Diameter of pipes
D_m	Volumetric displacement of the motor
F, **F**	Forces and vector of forces
gy	Gyrator of pistons
G:	Joystick position and velocity gain
G(q)	Gravity matrix
i	Current
I	Fluid inertance
J	Jacobian matrices
K^-:	Pre-loop shaping gain
l	Length
M(q)	Mass matrix
N	Gear ratio of the gear train
P	Pressure
P_s	Pump pressure
q	Joint angles
Q	Flow rate
R	Fluid resistance
V	Voltage
$\mathbf{V(q,\dot{q})}$	Matrix include Coriolis terms and damping characteristics of links
x	Piston displacements
$\dot{x}$	Piston velocities
X_{real}, X_{des}:	Actual and desired end-effector position

Greek Symbols

β	Bulk modulus
β_x	Multipass ratio for measuring the separation characteristics of a filter
θ	Joystick deflection angles
$\theta_{real}, \theta_{des}$	Actual and desired actuator position
ρ	Fluid density
τ	Torque
Ω	Angular velocity

Notation

$(\cdot)$	Euclidian inner product
$\dot{(\ )}$	Differentiation with respect to time
$(\ )^T$	Matrix transpose
$(\ )^{-1}$	Matrix inverse
$\lvert\ \rvert$	Absolute value
$\mathbf{f}()$	Functions

Abbreviations

bm	Boom
DOF	Degree of freedom
in, out	Inlet, outlet
sk	Stick
sw	Swing

1. Introduction

1.1 Motivation

The forest sector is Canada's most important industry in terms of net contribution to the economy (in 1990, its contribution to the trade surplus was $19 billion, and it generates 3.1% of the GDP), numbers employed (293,000 jobs, of which 49,000 are in forest operations), and socioeconomic importance (300 communities are solely dependent on this industry), [5].

Forestry machines, typically located in remote areas, operating in rugged and arduous conditions set high demands for productivity, reliability, efficiency and operator safety and comfort.

Forestry machines, particularly feller machines, manufactured in Scandinavian countries are more technologically sophisticated and ergonomical. However, different operating conditions, sizes of trees and attached cutting tools slow down their penetration to the North American market. Nevertheless, we are facing direct competition and

therefore, many improvements should be made given the current development stage of forestry vehicles.

One of the most needed improvements is a better control strategy and man-machine interface. For some older machines, operators are required to use both feet, hands, knees and elbows simultaneously to actuate the throttle, winch clutches and brakes in order to complete one working cycle. In current machines, control requires individual command of each link by an operator, which in turn, requires significant visual feedback, judgment and skill. Both situations keep operators extremely busy with low-level mechanical manipulations instead of making high-level decisions, such as planning tree-cutting operations or choosing appropriate trees. Coordinated control, by which operators are enabled to command desired end-effector motions directly along axes relevant to the task environment, greatly decreases demands on operators, and thus, workload is reduced dramatically.

Tree-cutting operations involve highly repetitive working cycles. Tool engaging, cutting, delimbing and collecting are necessary steps in operations. With the advancement of computer technology, the procedures can be programmed or remembered. Ideally, intensive manual operations will be replaced by a single push button or single joystick commands. To accomplish these objectives, the dynamic behavior of the vehicles, of their actuation systems and of their manipulators must first be well understood.

1.2 ATREF Project

ATREF, a French acronym for "Application des Technologies Robotiques aux Equipements Forestiers" (Application of robotics technologies to forestry equipment), has been carried out since 1994 with these goals in mind. The project is partly funded by the

Quebec government's SYNERGIE program, whose objectives stress the acceleration of technology transfer from Quebec's research community to the private sector. The remainder of the funding comes from the project's industrial partners: the Forest Engineering Research Institute of Canada (FERIC), Denharco Inc. and Autolog Inc. The research members are the Centre de recherche informatique de Montreal (CRIM), McGill University, and Université Laval.

The test vehicle of the project, a modified FERIC C-180 forwarder, is shown in Figure 1.1. Both mobility and maneuverability of the vehicle come from hydraulic systems powered by a diesel engine sitting at the back of the vehicle platform. Four wheels are independently driven by four hydraulic motors. The bogies connected to these wheels are designed to minimize tilt of the overall machine when the vehicle is climbing slopes. An articulated three-degree-of-freedom manipulator is actuated by a hydraulic motor and two cylinders. The stick, the link which rests on the ground as shown in the picture, was extended on the tip to increase the reachability of the manipulator. The end-effector, not shown in the picture, will be attached to the stick.

Figure 1.1 The test vehicle - modified FERIC C-180 forwarder.

Four main activities were planned for the project. Activity 1 is the preparatory stage. It involves modifying C-180 forwarder, comprehensive modelling and parameter identification of the test vehicle, and generating a database of current feller machines on the market. Activity 2 focuses on the computerized control of the machine. A Coordinated control strategy is to be implemented and tested. Activity 3 concerns designing a graphical simulator with a multimedia component, to be used for novice operator training. Finally, in activity 4 interactive CAD tools are developed to assist designing similar type of forestry equipment in the future.

1.3 Related Work

The starting point for designing good control laws is to mathematically model the physical system such that the system can be controlled as accurately as possible in the following stage. Modelling methodologies vary mainly depending on the purpose of modelling and on individual preferences. While the majority is using classical modelling tools and *ad hoc* approaches, systems methods, such as linear graph and bond graph methods, used to derive lumped-parameter models of multi-domain systems in unified ways, are gradually becoming important. With the advancement of computer technology, detailed dynamic models studies which require substantial computing power can be carried out systematically and easily.

The linear graph methodology [28], represents the topological relationships of lumped element interconnections within a system. The term *linear* in this context denotes a graphical lineal (line) segment representation, and is not related to the concept of mathematical linearity. A linear graph is used to represent system structure in many energy

domain, and is a unified method of representing systems that involve multi-energy domains. They are similar in form to electrical circuit diagrams.

A significant amount of research efforts has been directed towards understanding the dynamic characteristics of electrohydraulic actuation systems through the implementation of mathematical models. The majority of previous work has been focused on modelling of servovalves, transmission lines and actuators separately. Often only linear models have been derived due to the complex nature of the systems. More recently, McLain *et al* [23] developed dynamic models for an electrohydraulic actuation system by taking into consideration non-linearity, such as valve hysteresis, orifice area, and piston damping. The level of accuracy of the models shown makes them a potentially valuable tool in analysis and design of electrohydraulic actuation systems. However, the models were derived for a single-stage, four-way, suspension-type of valve, which is not used in industry.

Electrohydraulic actuation systems are complex non-linear systems. It is difficult both to obtain accurate dynamic models, and to identify the corresponding physical parameters. The high cost of hydraulic actuation systems, the additional cost of data-acquisition systems and sensors, and the lack of experience in hydraulics, intimidate many robotics research laboratories from having hydraulic actuation systems with reliable sensing and acquisition capabilities. Even those who can afford to carry out experiments, very often deal directly with linearized models only, which limit the range of validity of models. The consequence of this approach results in extra difficulties during the controller design stage [41], [21]. Nevertheless, different identification methods for transmission lines [40], [19], actuators [38], and servovalves [22], [25], were proposed and implemented, and some specific servo actuation systems were investigated [23], [13].

Forestry operations demand heavy-duty machines which have articulated mechanical structures, actuated through coupled and complex hydraulic actuation systems to perform in

diverse and harsh environments. Operators often find themselves in a situation that requires significant visual feedback, judgment and skill for low-level felling operations. However, there is not enough time to spend on higher-level decision making, such as choosing trees and planning cutting paths. Whitney [39] proposed a resolved motion rate control method such that operators are enabled to call for the desired end-effector motion directly along axes relevant to the task environment, which substantially reduces the complexity of operations.

For the control of relatively slow, wide-workspace telemanipulators like forestry feller machines, Kim [17] later compared human operator performance by using two modes, position and rate control, under different workspace sizes. Rate control (regulating manipulator velocity signals) is found preferable to position control (regulating manipulator position signals). Das *et al.* [7] further evaluated operator performance with seven manual control modes in teleoperation, which are combinations of manual position or resolved motion rate control with alternative control schemes for force reflection and remote manipulator compliance. The resolved mode teleoperated control method was implemented successfully by researchers at UBC on excavator machines [20], [30], [32].

1.4 Thesis Outline

The thesis begins with a survey on components of electrohydraulic actuation systems and design guidelines used in mobile machines. Then two types of dynamic models of the actuation systems on the test vehicle are derived. Once the models are given, the procedures to identify parameters involved in the models are described. The results of experiments then lead to model validation studies. The valid dynamic models finally allow for the design of a resolved-motion controller.

The organization of this thesis is as follows:

Chapter 2 gives the fundamentals of mobile machine actuation systems. The comparison of hydraulic systems to other actuation systems is illustrated. The choices of power sources, valves, and actuators are discussed.

Chapter 3 introduces the linear graph method, which is implemented in deriving mathematical models of three actuation subsystems used on the vehicle, namely, the swing, boom and stick subsystems. The nonlinear state-space models are presented. Also, the integration of the actuation system dynamics with manipulator dynamics equations is discussed.

Chapter 4 describes the experimentation involved to estimate physical parameters required in the dynamics models derived in Chapter 3. The data-acquisition system, experimental setup and measurement procedures are described. Model validation studies and a refinement of the proposed hydraulic actuation models are described. An analysis of the experimental data and comparison studies are presented.

Chapter 5 addresses the concept of teleoperation. Formulation and design of the coordinated control strategies based on validated dynamic models of the vehicle are discussed. Computer simulation results are also presented.

Chapter 6 concludes the thesis with a summary of the work done. Some further research developments concerning the project are mentioned.

2. Electrohydraulic Actuation Systems

The term *hydraulics* is defined as that branch of engineering that deals with fluids as a transmitting medium for energy. While the use of hydraulic power goes far back in the history of man's effort to harness nature, it was not until the first few decades of the twentieth century that hydraulic power came to prominence. With the help of sophisticated electronics, electrohydraulic actuation systems are widely applied in high-power-demand applications, such as aerospace and heavy-duty mobile equipment.

In this chapter, the fundamentals of mobile machine electrohydraulic actuation are presented. A comparison of hydraulic systems to other actuation systems is illustrated first. An overview of components used in hydraulic actuation system follows next, including the choices of fluid power sources, valves, actuators and other related components. Some modifications of the electrohydraulic systems of the experimental vehicle are also described.

2.1 Why hydraulics?

There are many unique features of hydraulic actuation systems compared to others, e.g. electrical, mechanical, etc. These fundamental features explain the dominant presence of hydraulics in the aerospace, forestry, construction, mining, and agriculture sectors. Some of the advantages are:

1. Efficient cooling. Heat generated by internal losses is a basic limitation of any machine. Lubricants deteriorate, mechanical parts wear down, and insulation breaks down as temperature increases. Hydraulic components are superior to others in this respect because the working fluid carries away the heat generated. This feature permits the use of smaller and lighter components. Hydraulic pumps and motors are currently available with horsepower to weight ratios greater than 2000 W/kg. Obviously, small compact systems are attractive in mobile and airborne installations.

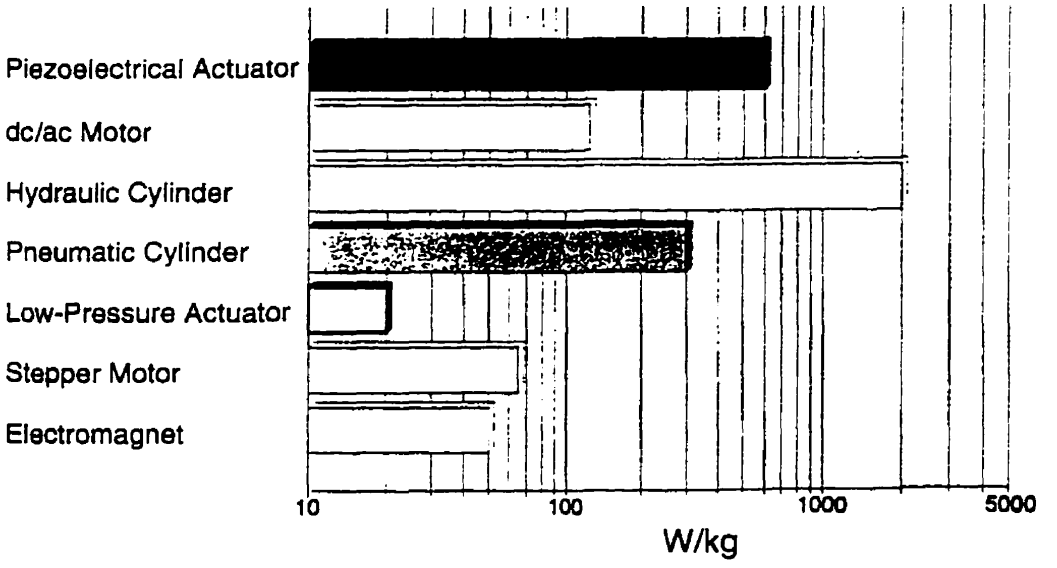

Figure 2.1 Power-to-weight ratios for common actuator principles, [10]

2. Large force or torque output. There is no phenomenon in hydraulic components comparable to saturation and losses in magnetic materials of electrical machines. The torque developed by an electric motor is proportional to the current through its windings and is limited by magnetic saturation. The torque developed by hydraulic actuators (i.e., motors and cylinders) is proportional to the pressure difference and is limited only by safe stress level. Therefore, hydraulic actuators develop relatively large torque or forces for comparatively small devices.

3. High stiffness. Hydraulic actuators have higher stiffness, that is, inverse of slope of speed-torque curve, compared to other drives. Hence, there is little drop in speed as loads are applied. In closed-loop systems, this results in greater positional stiffness and less positional error.

4. Fast speed of response. Hydraulic actuators have a higher speed of response with fast starts, stops, and speed reversals. Torque to inertia ratios are large, resulting in a high acceleration capability. On the whole, higher loop gains and bandwidths are possible with hydraulic actuators in servo loops.

5. Superb lubrication. The hydraulic fluid also acts as a lubricant and makes possible long component life.

Although hydraulic actuation systems offer many distinct advantages, several disadvantages limit their application.

1. Hydraulic power is not so readily available as electrical power. This is not a threat to mobile and airborne applications but most certainly affects stationary applications.

2. Small allowable tolerances result in high costs of hydraulic components.

3. It is almost impossible to maintain the working fluid free of dirt and contamination. Contaminated oil can clog valves and actuators and, if the contaminant is abrasive, cause a permanent loss in performance and even failures.

4. Basic design procedures are lacking or are difficult to use because of the complexity of the system. For example, there is no single law to describe the hydraulic resistance. Some of the components introduce highly non-linear behavior. This factor limits the degree of sophistication of the controllers for such systems.

Overall, the outstanding characteristics of hydraulic actuation systems, combined with their comparative stiffness at low power levels, make them indispensable in high-power-demand systems, such as aerospace and heavy-duty mobile applications.

2.2 Positive-displacement pumps

Positive-displacement pumps are energy-conversion devices that convert mechanical energy to fluid energy, [12]. In the rapidly expanding field of hydraulic power, positive-displacement pumps of widely varying designs have been developed to meet the demands of high-pressure, high-speed applications. These designs are based upon three main types, which are designated as gear, vane and piston pumps as shown in Figure 2.2.

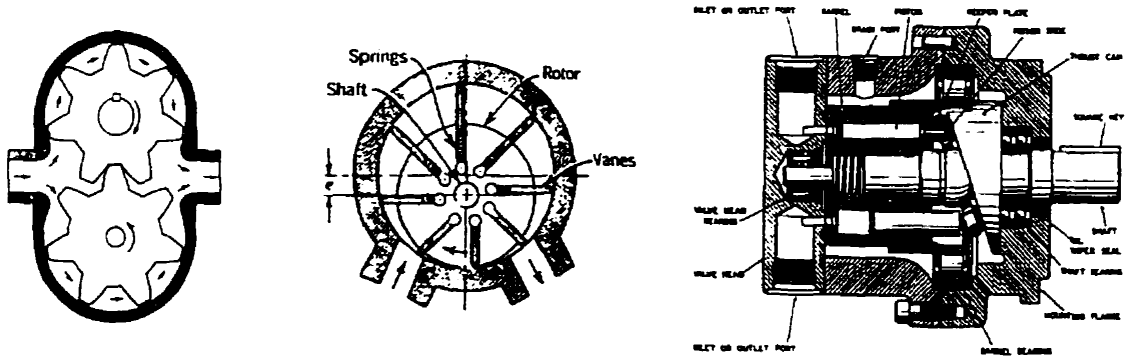

(a) Spur gear pump (b) Sliding vane pump (c) Axial piston pump

Figure 2.2 Three basic types of positive-displacement hydraulic pumps.

Up to a few years ago, pressure ratings for gear and vane pumps were well below those of piston pumps, due to strength limitations and unbalanced pressure effects. The situation, however, has been changing gradually. High pressure gear and vane pumps with maximum pressure ratings of 200 to 250 bar are now available (Note that, still, piston type of pumps can provide 400 bar or higher if desired). As the majority of the hydraulic actuation systems operate within this range, the determining factor in choosing a pump will often be a compromise between volumetric efficiency and cost. Gear pumps are, as a rule, cheaper than comparably rated piston pumps, while vane pumps occupy the middle ground. The high volumetric efficiency of piston pumps can not normally be matched by either gear or vane pumps.

Three types of pump operating modes are used in practice, namely, constant flow, constant pressure, and load-sensing modes. A constant flow system provides full flow at any value of pressure. A constant pressure system has a mechanism to keep constant pressure at different flow rates. When no flow is needed, the pump delivers just enough fluid to make up for internal leakage. A load-sensing system provides only the flow and pressure demanded to meet load requirements. Almost no energy is wasted.

Although constant flow pump systems have been a common choice for a wide range of machines in the past few decades, the trend is towards constant pressure or load-sensing systems. With the requirements of energy efficiency and increasing demand for fast response and sophisticated control systems, more designers turn to these two pump systems. A comparison of energy consumption of the three types is shown in Figure 2.3. Although a load-sensing system demands less energy, the speed of response is slower than that of a constant pressure system. Since fast speed of response is one of the design criteria in our project, we decided to use a constant pressure system.

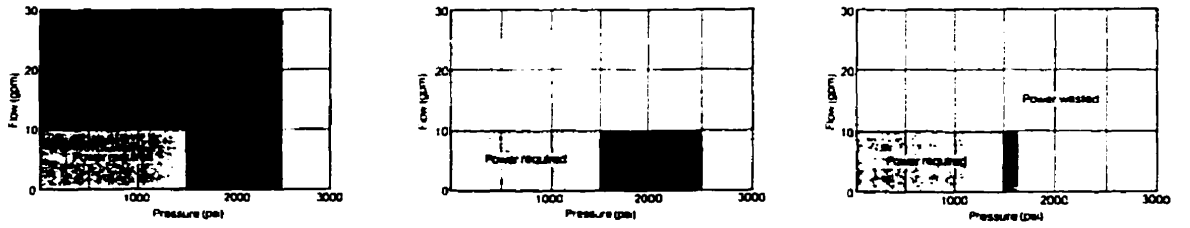

(a) Constant flow pump (b) Constant pressure pump (c) Load-sensing pump

Figure 2.3 Power consumption of typical hydraulic systems, [12].

2.3 Valves

Hydraulic control valves are devices that use mechanical motion to control a source of fluid power. They vary in arrangement and complexity, depending upon their functions. Control valves are mechanical, electromechanical or hydromechanical devices, and knowledge of their dynamic performance is very important for design and analysis purposes, [24].

2.3.1 Valve configurations

Valves may be divided into three classifications: sliding, seating, and flow dividing. Examples of these are the spool, flapper, and jet pipe valves, respectively, which are shown schematically in Figure 2.4.

The most widely used valve is the sliding valve employing a spool type construction. It can be further classified by (a) the number of 'ways' flow can enter and leave the valve, (b) the number of lands on spools, and (c) by the type of centering when the valve spool is in neutral position. Because all valves require a supply, a return, and at least one line to the load, valves are either three-way or four-way (two-way valves cannot provide reversal in the direction of flow). A three-way valve requires a bias pressure acting on one side of an unequal area piston for direction reversal. A four-way valve would have two lines to the

load. The number of lands on a spool vary from one in a primitive valve to the usual three or four, and special valves may have as many as six lands. If the width of the land is smaller than the port in the valve sleeve, the valve is said to have an open center or to be underlapped. A critical center or zero lapped valve has a land width identical to the port width. Closed center or overlapped valves have a land width greater than the port width when the spool is at neutral. The typical flow vs. orifice opening profiles (the slope is defined as the *flow gain*) is shown in Figure 2.5 for these three types of centering positions.

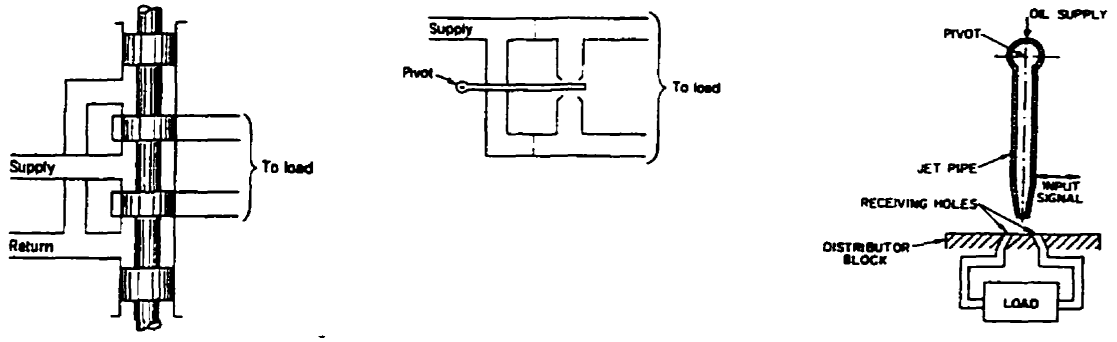

(a) Spool valve (b) Jet flapper valve (c) Jet pipe valve

Figure 2.4 Typical hydraulic control valves.

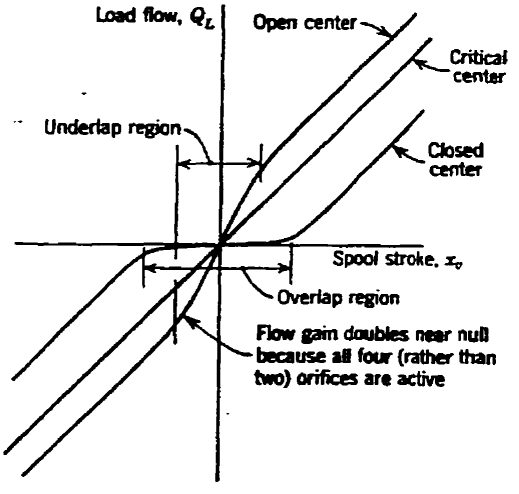

Figure 2.5 Flow gain of different center types.

Spool valve manufacture requires that close and matching tolerances be held, thus the valves are relatively expensive and sensitive to fluid contamination. Tolerances required for flapper valves are not as stringent. However, the relatively large leakage flow limits their application to low power levels. Flapper valves are used extensively as the first stage in two-stage electrohydraulic and hydromechanical servovalves.

Jet pipe valves are not used as widely as flapper valves because of large null flows. Their characteristics are not easily predictable and the speed of response is slower than that of the flapper type. The main advantage of jet pipe valves is their insensitivity to dirty fluids. However, the more predictable flapper valves have similar performance characteristics and are usually preferred, [24].

2.3.2 Valves in closed-loop control

For closed-loop control purposes, critical center type is always desired due to the linear flow gain. However, the high manufacturing cost and safety considerations have prevented its implementation in certain applications. Closed center is not desirable in closed-loop control because of the deadband characteristic in the flow gain. Deadband results in steady state error and, in some cases, can cause backlash which may lead to stability problems. However, with the assistance of electronics, the deadband can be well compensated during operation.

Historically, electrohydraulic closed-loop applications for controlling position, velocity or pressure have been left to industrial servovalves, which, in closed-loop control allow operation as precise-metering and fast-acting elements. Servovalves have critical center configurations. With the internal mechanical feedback loops, their bandwidth can be over 100 Hz. However, high cost, high sensitivity to contamination, and relatively high pressure drops across ports, make room for state-of-the-art proportional valves, which

have been improved to the point where they can be used as cost-effective and less-troublesome alternatives to servovalves.

Proportional control valves are directional control valves designed to meet commercial performance standards. They include interfacing and pilot stages resulting in proportional control characteristics, i.e. infinitely variable positioning of a control element in a defined relationship to an input signal, [12]. Like servovalves, proportional valves convert an electrical input signal e.g. voltage V or current i, into a proportional, hydraulic output, e.g. a corresponding spool position. The traditional design of a proportional valve is much more tolerant of contamination than that of a servovalve with sacrificing precision and fast response. However, with features such as additional spool position control and two-stage pilot-operating, disturbances created by flow forces and friction on the main spool are substantially eliminated. Operating the valve through the entire signal range generates such low hysteresis that it often cannot be measured. In addition, valves of this type demonstrate much quicker response than older types. For valves which have an overlap in the neutral position to minimize internal leakage, additional electronic deadband compensators in the external control loop can assure a smooth transition when changing flow direction. In consideration of the characteristics described above, proportional valves were chosen in this project for controlling the three-degree-of-freedom articulated manipulator.

2.4 Actuators

The function of actuators in hydraulic systems is to convert the hydraulic energy supplied by the pump and processed by the control elements into useful mechanical work. Actuators have either a linear or a rotary output and can be classified into two basic types:

(1) Cylinders.

(2) Motors.

2.4.1 Cylinders

The most commonly used hydraulic actuator is the cylinder or jack. A cylinder can be either single-acting or double-acting. Single-acting cylinders are power driven in one direction only, whereas double-acting cylinders are power-driven in both directions. Cylinders can be constructed as single-ended or double-ended, as shown in Figure 2.6. Double-ended symmetrical cylinders, Figure 2.6.(a), are frequently used for high performance servo systems, but have greater overall body length and are more expensive than single-ended actuators for the same work output. Because of lower cost and smaller size, single-ended cylinders are widely used for both industrial and mobile applications. Although single-ended cylinders are asymmetrical, they are suitable for closed-loop systems, provided the effect of the asymmetry on performance and stability is taken into account when carrying out a system analysis.

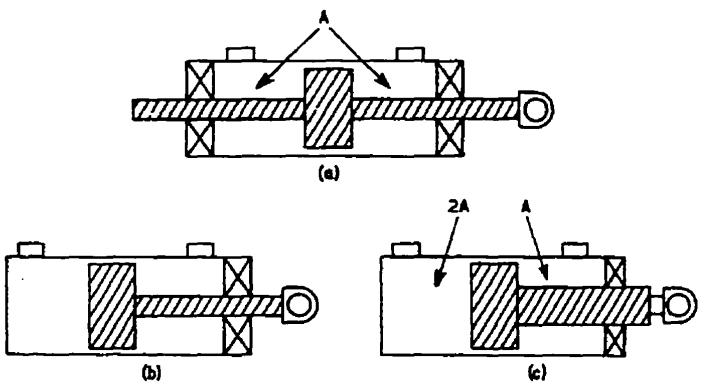

Figure 2.6 Typical types of cylinders (a) double-acting. (b) single-ended. (c) differential.

2.4.2 Motors

Hydraulic motors are essentially hydraulic pumps in which the energy conversion sense is reversed. While a pump converts mechanical energy supplied to its drive shaft by a prime mover into hydraulic energy, the motor converts the hydraulic energy provided by the pump into mechanical energy at its output shaft. Because of this basic similarity pumps and motors are, except for some minor differences, identical in construction. Three groups fall into the classification, namely, gear, vane and piston motors.

As with pumps, piston motors operate at the highest working pressure ranges among the three. Motors can be further subdivided into two categories:

(1) High-speed, low-torque.

(2) High-torque, low-speed.

Once the required output power of the motor has been established, it has to be decided which of the two is the most suitable for the given application. Industrial high-speed, low-torque motors are considerably cheaper than high-torque motors of equivalent power rating, although the former invariably necessitates the provision of reduction gearing, which is considered to be a disadvantage for closed-loop applications. A high-speed, low-torque motor was chosen in the original machine design, and we decided to stay with it.

2.5 Other Components

2.5.1 Filters

It is estimated that as much as 75 percent of hydraulic system failures can be attributed to dirt or contaminants. A hydraulic valve on a machine tool stuck or jammed by

contamination can place the tooling, machine, and/or operator in jeopardy. As the sophistication of fluid power components and circuits has grown, so has recognition of the need for high-efficiency filtration. Higher system pressures and faster cycle times means tighter clearances between the moving surfaces of hydraulic components, and more stress and shock for the components themselves.

Two types of devices are used to remove particles from hydraulic fluids: strainers and filters. A strainer is generally a large-pore-size device used at the inlet of a hydraulic pump. It employs a 100-mesh screen that removes particles bigger than 150 μm. A filter is a device that generally has a finer pore size than a strainer. The function of a filter is to remove dirt and contaminants above a specific size from the hydraulic fluid. The degree of filtration is generally determined by the needs of the most sensitive component in the hydraulic system, which, in many cases, is a valve.

The multipass β_x ratio is used for measuring the separation characteristics of a filter

$$\beta_x = \frac{\text{Number of upstream particles larger than x } \mu m}{\text{Number of downstream particles larger than x } \mu m} \tag{2.1}$$

Thus, a β_x ratio of 1 indicates that no contaminant particles are being removed, and a filter element with β_x=100 is 99% efficient to remove particles size x μm and larger.

2.5.2 Conductors

The channeling of hydraulic fluids under pressure from point to point in a hydraulic system is accomplished through a number of conveyance systems. These systems would include pipes, tubing, hoses, couplings, drilled holes, adapters, and manifolds. The function of the conveyance system is to provide a leak-proof carrier for the fluid that will be able to

withstand vibration, extreme temperatures (both externally and internally), adverse environmental conditions, and general abuse.

Conductors may be divided into three classes: pipe, tubing and hose. Piping and tubing are rigid conductors. They are not suitable for applications requiring the two ends of a conductor to move relative to one another. A typical example would be where machine elements move during a work cycle. There is better selection of hoses to choose from than for pipes or tubing. In addition to the freedom and convenience of relative motion between components, hoses provide other advantages.

1. Absorb hydraulic impulse shocks and smooth fluid flow.
2. Compensate for manufacturing tolerances in piping.
3. Provide freedom in routing conductors on a machine.

The five basic types of industrial hoses are classified by the amount of fluid pressure they can withstand. The type of reinforcement used is the chief difference between these hose types because high-pressure hoses require stronger reinforcement to handle the pressurized fluid in a system. Low pressure hoses are generally reinforced with a fabric braid. Medium and high-pressure hoses have single and multiple-wire braid reinforcement depending on need. Spiral-wire wrap hoses were developed for special, high-impulse pressure applications.

2.5.3 Hydraulic fluids

Fluids used in hydraulic systems on mobile equipment are usually divided into two categories: petroleum-based fluids and fire-resistant fluids. Petroleum-based fluids are the most-widely used in mobile equipment systems, but there is an increasing demand for fire-resistant fluids for mobile equipment used in hazardous locations.

A good hydraulic fluid serves a number of important functions:

(1) It transmits fluid power.

(2) It lubricates the components in a hydraulic system.

(3) It is capable of resisting oxidation.

(4) It holds its viscosity through a wide range of temperatures.

The selection of proper hydraulic fluid is important, as it has a direct bearing on the efficiency of the hydraulic system, the cost of maintenance, and the service life of the system components.

2.6 Summary

The fundamental components of a hydraulic actuation system were reviewed in this chapter. The advantages and disadvantages of the hydraulic components and technology described in this chapter were taken into account during the modification of the project's test vehicle, the FERIC C-180 forwarder. Some of the components used in the electrohydraulic actuation system are listed in Table 2.1. In addition, the detailed understanding of system components provided the foundation for the comprehensive dynamic modelling presented in the next chapter.

Table 2.1 Related hydraulic components of the C-180 forwarder test vehicle.

Pumps	Constant Pressure Piston Pump Rexroth - A10V045DF R/30L -PSC62N00
Valves	Proportional Valves

	Moog 641-204B
Motor	Fixed Displacement Piston Motor Rexroth - Model AA2FM45/61W-PSD52
Cylinders	Single-ended Cylinder Hayes-Dana 024-8849-0 (boom) Hayes-Dana 024-8848-0 (stick)
Hoses	Very High Pressure - 4000 psi[1] SAE 100R12 - 4 Spiral Steel Piles
Hydraulic fluids	PetroCanada Harmony Plus
Filters for propulsion system	HYCON Beta Spin Filter MFBN 160/1
Filters for valves	PALL 9660 $\beta_6 \geq 200$

[1] $1\ psi = 6.895 \times 10^{3}\ Pa = 6.895 \times 10^{-2}\ bar$

3. Modelling of the Electrohydraulic Actuation Systems of the FERIC Machine

The main objective of modelling physical systems is to describe and predict their performance characteristics operating under specified environmental conditions. Valid models, then, can be used in designing various controllers, developing systematic design tools, or developing graphical simulators for training.

There exists two basic modelling approaches. When modelling from *fundamental principles*, important physical processes taking place in the system are identified, and equations are written to describe these processes and their interrelations. Then the parameters involved in the equations are estimated by experiments. At the other end, lies the *black-box* approach: actual inputs and outputs are observed, and a model is fitted based on observations without considering the internal mechanism or physics involved.

A significant amount of research efforts has been directed towards understanding the dynamic characteristics of electrohydraulic actuation systems through derivation of mathematical models. With the advancement of measuring instruments and computer

technology, the complicated dynamic behaviors are observed and studied. Systems methods, which represent the topological relationship of interconnections between different systems and assist in developing series of lumped-parameter models in a unified fashion, are gradually gaining importance in modelling these systems. Such methods include bond graph, and linear graph, which are used in this thesis.

In this chapter, the linear graph method is implemented in developing a set of dynamic models for various components involved in the electrohydraulic actuation systems of the modified FERIC C-180 test vehicle shown in Figure 1.1. Then two different models are derived for the swing, boom and stick actuation subsystems, based on models of individual elements. Finally, the integration of the electrohydraulic actuation system with the manipulator dynamic models is presented.

3.1 Actuation Systems Overview

The experimental vehicle, the modified FERIC C-180 forwarder, was originally designed to collect trees felled and left by other machines and to carry trees out from the forest. In this project, a processing head is attached to the end of the stick through a Hooke-type mechanism. Therefore, it now functions as a single-grip harvester instead of a forwarder, i.e. it can fell trees and process them with its need. As described in Chapter 1, both mobility and maneuverability of the vehicle come from the hydraulic system powered by a diesel engine sitting at the back of the vehicle platform. The four wheels are independently driven by four hydraulic motors. The bogies connected to these wheels are designed to minimize tilt of the overall machine when the vehicle is climbing slopes. An articulated three-degree-of-freedom manipulator is actuated by a hydraulic motor and cylinders. The stick is extended to increase the reachability of the vehicle and the processing head is

attached to the stick. Commands, issued by a human operator sitting inside the cabin, are processed and sent to the actuators by an on-board computer system.

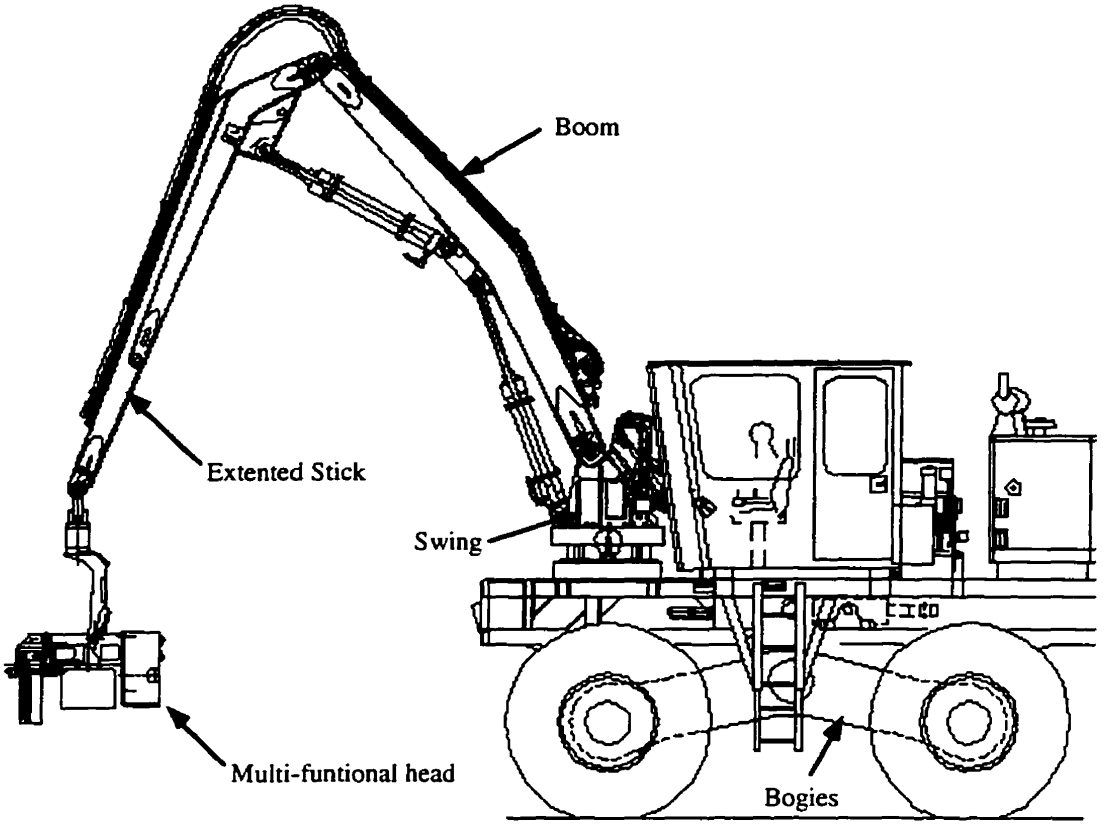

Figure 3.1 Schematics of the modified FERIC C-180 forwarder.

The swing actuation subsystem of the modified FERIC C-180 test vehicle consists of a two-stage, four-way proportional spool valve coupled with a hydraulic motor as shown in Figure 3.2. Voltage commands sent to the valve modulate the position of the spool which serves to regulate the orifice areas of supply and return paths. The hydraulic motor actuates the swing through a gear train. Except for the type of actuator used, the boom and stick subsystems have a similar setup, i.e. instead of a hydraulic motor, cylinders are connected to the boom and stick valves, as shown in Figure 3.3.

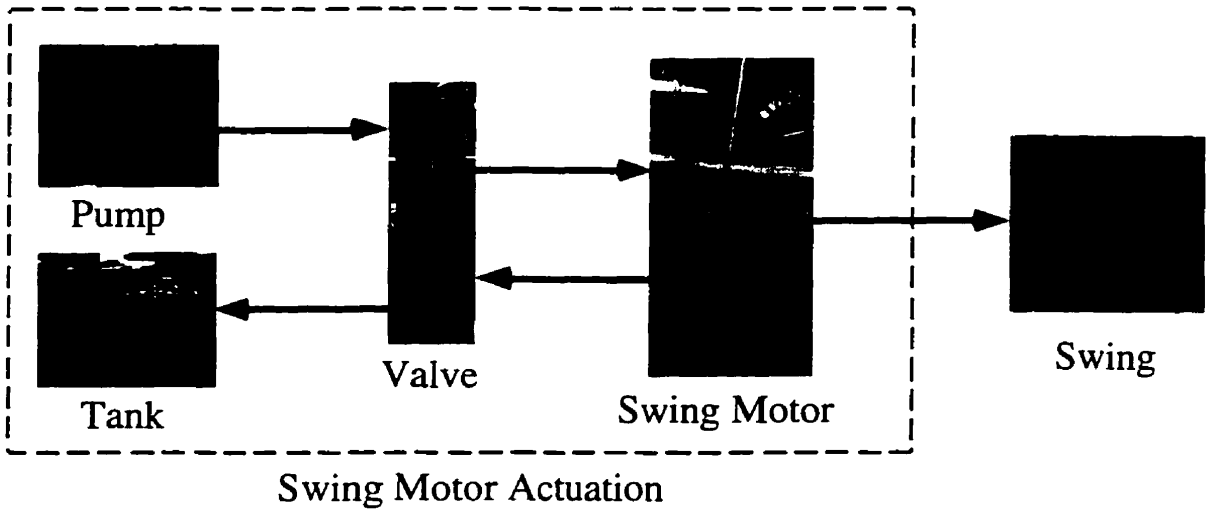

Figure 3.2 The swing actuation subsystem.

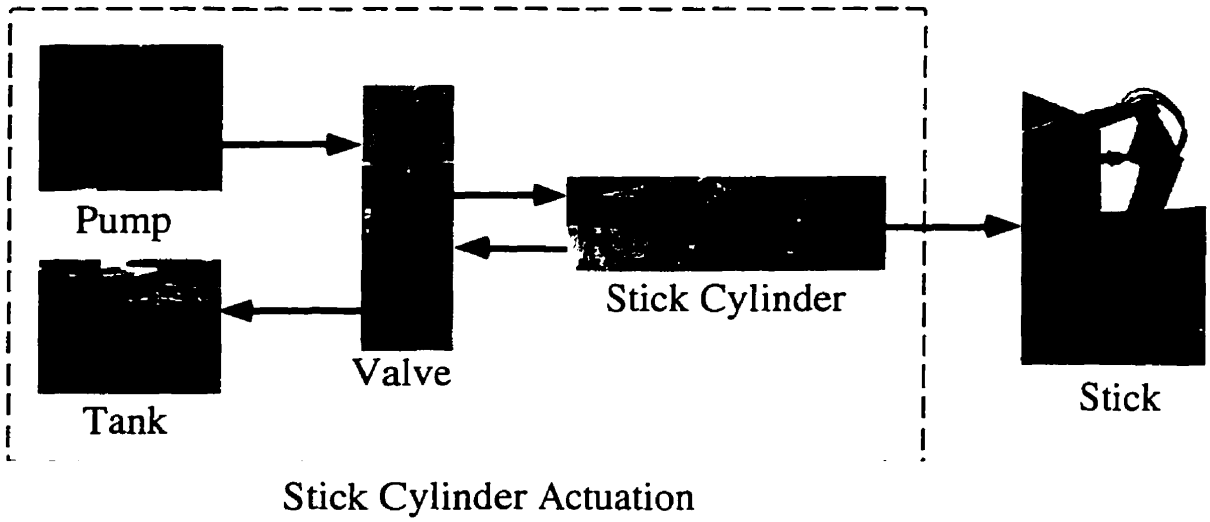

Figure 3.3 The stick actuation subsystem.

The actuation systems operate at 3,000 psi, provided by two constant pressure pumps which, in turn, are driven by a diesel engine, rated 152 hp[1] at 2,500 rpm[2].

[1] 1 hp = 745.7 Watts
[2] 1 rpm = 0.1047 rad/s

3.2 Electrohydraulic Components

3.2.1 Pump

Two pressure compensated, piston pumps provide hydraulic power to the test vehicle. An ideal power source is capable of supplying constant pressure at any flow required. Real pressure sources, on the other hand, have limits on the power that they can supply. In practical hydraulic pump analysis, leakage flows and friction are counted as sources of power loss as shown in Figure 3.4. Although this is certainly true in reality, hydraulic machines are quite efficient. For piston pumps, their efficiencies are always around 90% within the normal operating range. The test vehicle is operated in a way such that the pump saturation point is normally avoided. Therefore, we assume that the pumps are ideal sources of pressure.

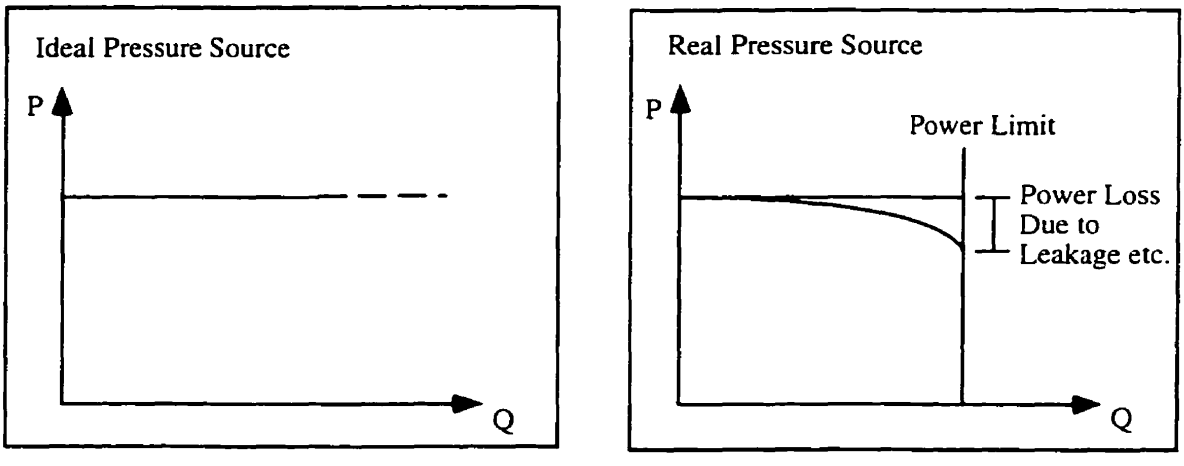

Figure 3.4 A comparison between ideal and real pressure source.

3.2.2 Valves

Three two-stage, four-way proportional spool valves are used to actuate the swing, boom and stick subsystems. Overlapped spool-port setup is chosen due to safety considerations

in spite of the undesirable resulting deadband. By using external compensation circuits, e.g. a small magnitude of voltage added to the normal operating command, the deadband effect can be eliminated. In such a case, valves can operate as critically centered, an essential requirement for closed-loop control.

One of the criteria in selecting valves is to consider their response time. If the resonant frequency of the spool is sufficiently high, its dynamic behavior is negligible compared to the relatively low resonant frequency of the controlled system. A typical industrial manipulator has a natural frequency in the range of 1 to 5 Hz, while the cut-off frequency of the selected proportional valves, when operating under maximum command is about 10 to 15 Hz. Thus only the resistive effect of the valves is considered.

The fluid resistance, resulting when fluid passes through a valve orifice, is given by the orifice equation. Two assumptions are made for further analysis:

(1) The fluid is ideal.

(2) The geometry of the valve is ideal.

(3) The flow is turbulent.

The assumption of an ideal non-viscous and incompressible fluid is close to reality under most conditions, and is also justified as far as phenomena inside the valve are concerned. At normal operating pressures, the finite compressibility of real liquids has only a negligible effect upon the flow through the metering orifices, although it is often very important in other parts of the system, [3].

'Ideal geometry' implies that the edges of the metering orifices are sharp and that the working clearance is zero so that the geometry of the orifice is independent of valve stem positions, [3].

Under these assumptions, the orifice equation that relates pressure drop across the valve and flow rate through it is of the form

$$\Delta P = C_R \cdot Q \cdot |Q| \tag{3.1}$$

where the coefficient C_R is a function of fluid density ρ, the orifice area A, and the orifice discharging coefficient C_d

$$C_R = \frac{\rho}{2 \cdot C_d^2 \cdot A^2} \tag{3.2}$$

For the geometry of most sliding-type valves at small openings, C_d is fairly constant when the Reynolds number is greater than 260. If the orifice edges are sharp as assumed previously, $C_d = 0.60$ to 0.65. If they are rounded or truncated by even a small flat, C_d will be 0.8 to 0.9 or higher, [24].

Therefore, valves are modelled as variable resistors. Input voltage commands modulate the orifice areas, which, in turn, affect the magnitude of C_R.

3.2.3 Transmission lines

Traditionally, transmission lines are modelled by distributed-parameter methods in the form of partial differential equations. They are difficult to derive and troublesome to employ in computer simulations. Lumped-parameter line models can be integrated easily into the control engineering domain provided that the frequency of oscillations in the system is significantly less than that corresponding to wave propagation, [36]. Therefore, if f is the frequency of oscillation that exists, and l is the line length, then a single lump model is valid provided that:

$$f < \frac{C_o}{2\pi \cdot l} \quad \text{and} \quad C_o = \sqrt{\frac{\beta}{\rho}} \tag{3.3}$$

where C_o is the velocity of sound in the fluid, and β is the bulk modulus. For a typical hydraulic oil with $\beta = 1.6 \times 10^9 N/m^2$, and $\rho = 970\, kg/m^3$, and for the longest hose on the test vehicle of 4 meters, the wave propagation frequency f is 51 Hz, which is far above

the frequencies possibly occurring in the actuation system. In addition, this calculation further ensures that only one lump is required for any of the hoses used on the test vehicle.

Several assumptions are made before deriving the detailed model:

(1) Turbulent flow is assumed (non-linear pressure-flow relationship) for the boom and stick model. In contrast, laminar flow is assumed for the swing model because the hoses for the swing subsystem are very short, and turbulent flow can not develop completely.

(2) Fluid compressibility and line compliance effects are linear. They hold for relatively small pressure fluctuations from the steady state pressure and for small expansions in the hoses.

(3) In defining fluid inertance, the momentum of the fluid on the inlet and outlet sides of the control volume is assumed to be the same.

There are many alternatives of arranging inertance, capacitance and resistance elements. For specific problems, one scheme may be better than another. A commonly used 'T' type model is chosen for modelling purposes, as shown in Figure 3.5.

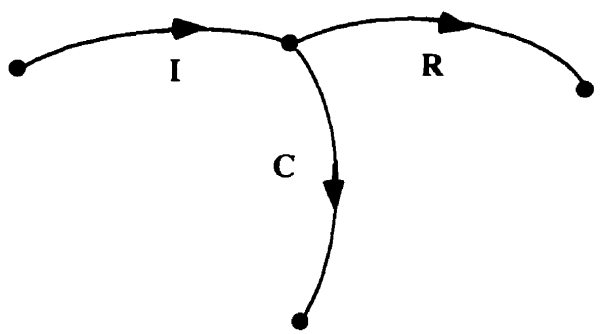

Figure 3.5 'T' type hose model.

3.2.4 Hydraulic Cylinders

Two single-ended type of cylinders are used to actuate the boom and stick subsystems. Cylinders seem to be relatively simple fluid power components. Mathematical models of different types of cylinders are provided in the literature. However, the single-ended type, which is the most commonly used in mobile machines, is often neglected. Here we are proposing its mathematical model in the linear graph form.

Several assumptions are made before the model derivation:

(1) The cylinder chambers are assumed to be rigid, i.e. no compliance in the wall. The stiffness of the cylinder chamber is more than 10 times higher than that of the hoses. Therefore, when operating at the same pressure range, the compliance effect from cylinders is negligible.

(2) Viscous friction effects in the piston seals are assumed. Hydraulic oil lubricates gliding passages in the cylinder and greatly reduces the effect of coulomb friction. Viscous friction is considered to be dominant.

(3) There is no significant leakage past the piston. Under normal operating pressure, the volumetric efficiency for cylinder is usually around 85-90%. The amount of slip flow is minimal for well-designed cylinders. In addition, the single-ended type of cylinders further prevent any internal leakage.

Hydraulic cylinders are devices transferring fluid energy to its mechanical form, i.e. the pressure difference at two chambers drives piston to move around. The linear graph identify this type of elements as transducers. However, due to the single-ended configuration, the general two-port element transducer can not be applied directly. Instead, a combination of two two-port elements are formed to model this device, as shown in Figure 3.6.

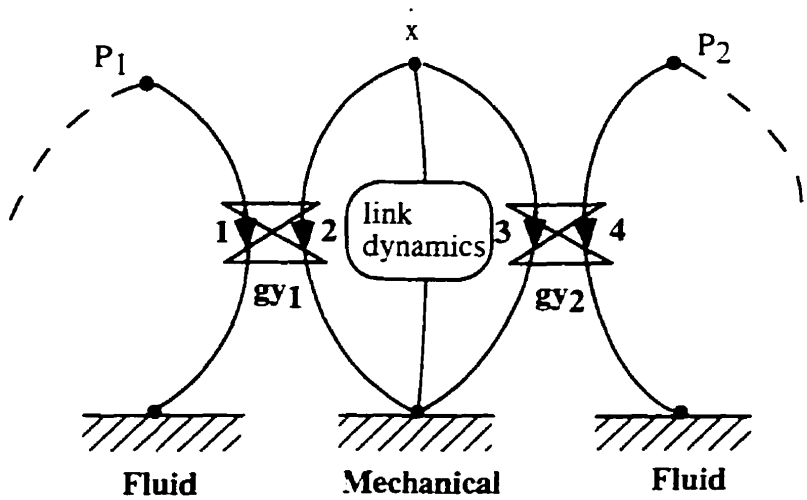

Figure 3.6 Cylinder model in the linear graph representation.

In this figure, P_1 and P_2 represent the inlet and outlet pressures of the cylinder, and gy_1, gy_2 are the areas on each side of the piston.

3.2.5 Hydraulic Motor

A fixed-displacement, piston motor is used to drive the swing subsystem. Contrary to cylinder modelling, hydraulic motors are typical transducers which can be modelled easily as two-port gyrators.

Several assumptions are made as follows

(1) Viscous friction of the motor is lumped into the damping of the gear train connected to its output shaft.

(2) Both internal and external leakage exist inside the motor, and slip flow is laminar. Although, in general, the volumetric efficiency of hydraulic motors is quite high, at low speeds the slip flow effect becomes more prominent. Very often, the motor on the test vehicle is working within this speed range.

The linear graph model of the hydraulic motor is shown in Figure 3.7.

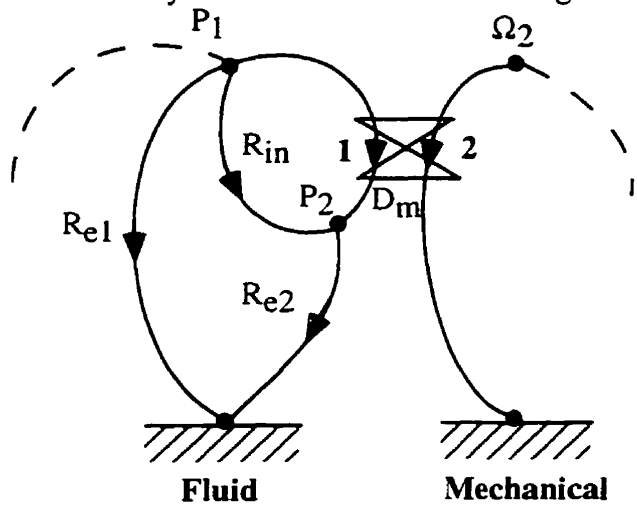

Figure 3.7 Hydraulic motor model.

P_1 and P_2 represent inlet and outlet pressures in the motor, R_{in} is the resistance of the internal leakage, R_e is the resistance of the external leakage, and D_m is the volumetric displacement of the motor.

3.2.6 Other Related Components

There are a few other hydraulic components which need some consideration. Filters and check valves in the circuits behave as fluid resistance and may affect the accuracy of the models. However, the manufacturing specifications show that their resistance is smaller compared to that of valves, actuators and hoses, and therefore, their effects are neglected at the modelling stage.

3.3 Swing Subsystem

Based on the system's configuration and the modelling assumptions made in the previous sections, a swing subsystem model is formulated in the form of a linear graph as follows.

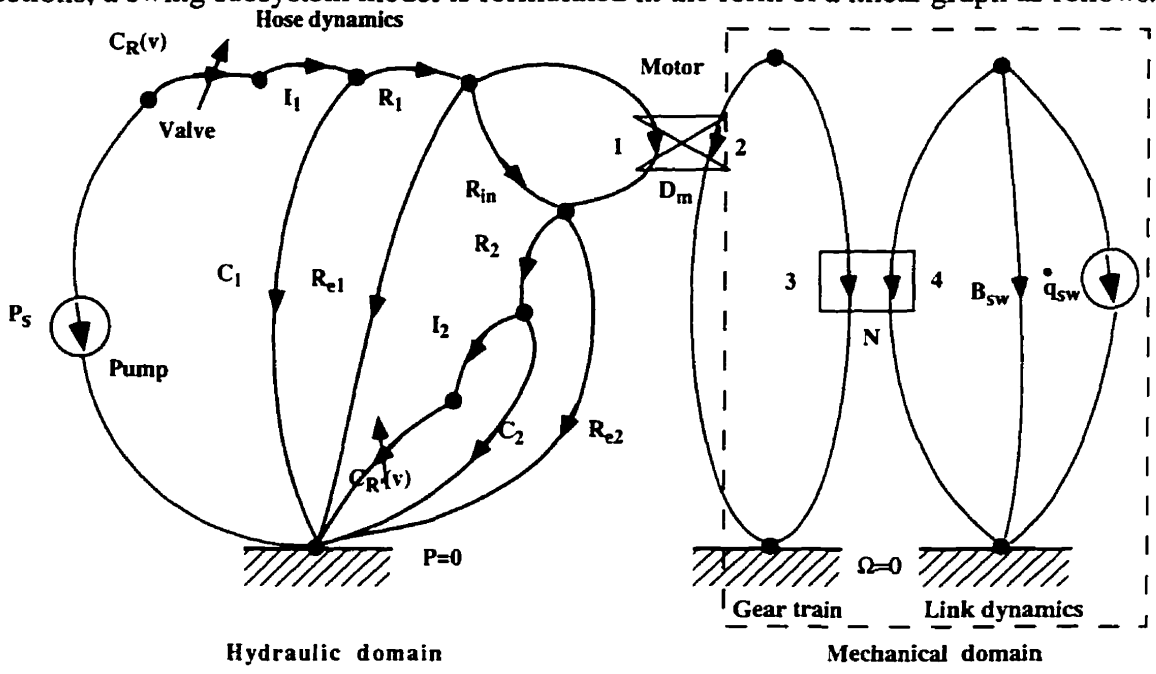

Figure 3.8 The swing subsystem model.

The parameters showed in Figure 3.8 are defined as:

P_s :	pump pressure.
C_R , C_R :	valve orifice resistance modulated by input voltage.
I_1 , I_2 :	supply and return line inertance.
C_1 , C_2 :	supply, return line capacitance.
R_1 , R_2 :	supply, return line resistance.
R_{in} , R_{e1} , R_{e2} :	internal and external leakage of the motor.
D_m :	volumetric displacement of the motor.
N :	gear ratio of the gear train.

B_{sw} : viscous damping coefficient in the gear train.

$\dot{q}_{sw}$: angular velocity of the swing.

As shown in Figure 3.8, high pressure oil is pumped through the valve whose orifice is modulated by the input voltage. Then it arrives at the inlet of the motor through the entry hose. The motor shaft drives the manipulator through the gear train. Some leakage flow is generated inside the motor due to its construction. Finally the fluid is pushed from the outlet of the motor back to the tank through the returning hose and valve. Note that the swing link interacts with the hydraulic subsystem through the swing angular velocity $\dot{q}_{sw}$. This angular velocity will be specified by the non-linear manipulator dynamics similarly to the element equation $d\Omega_j/dt = 1/J \cdot \tau_j$, although it is shown as a velocity source in Figure 3.8. Also the dynamics structure of the entry and return hoses are arranged in a symmetric way to simplify the computer simulation on direction variations of swing motion. The switch of R_2 and I_2 will not affect the orders of the system, although the values of these parameters might change in order to reflect the behavior of the actual system.

From the graphical representation, dynamic equations are derived using the linear graph procedure as follows. First, elemental equations are written for each linear graph element involved in the graph. Then, an equal number of constraint equations are derived from interconnection laws for these elements, namely, continuity and compatibility equations. These equations are used to result in a group of state equations in terms of state variables and inputs. The states of elements can then be represented in terms of the state variables.

For the swing subsystem, four state variables are chosen to represent its characteristics, namely, P_{c_1}, P_{c_2}, Q_{i_1}, and Q_{i_2}. P_{c_1} is the pressure across the capacitance C_1 of the entry hose, P_{c_2} is the pressure across the capacitance C_2 of the return hose, Q_{i_1} is the flow rate through the inertance I_1 of the entry hose, and Q_{i_2} is the flow rate through the inertance I_2

of the return hose. Four state equations are derived and pressure drops across other elements and flow rates through them are expressed in terms of the state variables as shown below.

Elemental Equations

$$\begin{aligned}
&\frac{dP_{c_1}}{dt} = \frac{1}{C_1} Q_{c_1} && P_{C_R} = C_R \cdot Q_{C_R}{}^2 \cdot sign(Q_{C_R}) && Q_{R_{e2}} = \frac{P_{R_{e2}}}{R_{e2}} \\
&\frac{dP_{c_2}}{dt} = \frac{1}{C_2} Q_{c_2} && P_{R_{in}} = R_{in} \cdot Q_{R_{in}} && Q_1 = D_m \cdot W_2 \\
&\frac{dQ_{i_1}}{dt} = \frac{1}{I_1} P_{i_1} && P_{R_2} = R_2 \cdot Q_{R_2} && t_2 = -D_m \cdot P_1 \\
&\frac{dQ_{i_2}}{dt} = \frac{1}{I_2} P_{i_2} && P_{C_R} = C_R \cdot Q_{C_R}{}^2 \cdot sign(Q_{C_R}) && W_3 = N \cdot W_4 \\
& && Q_{R_1} = \frac{P_{R_1}}{R_1} && t_4 = -N \cdot t_3 \\
& && Q_{R_{e1}} = \frac{P_{R_{e1}}}{R_{e1}} && t_B = B_{sw} \cdot W_B
\end{aligned} \tag{3.4}$$

Continuity Equations

$$\begin{aligned}
&Q_{C_R} = Q_{i_1} \\
&Q_{i_1} = Q_{c_1} + Q_{R_1} \\
&Q_{R_1} = Q_1 + Q_{R_{in}} + Q_{R_{e1}} \\
&Q_{R_1} = Q_{R_{e2}} + Q_{R_2} + Q_{R_{e1}} \\
&Q_{R_1} = Q_{R_{e2}} + Q_{C_2} + Q_{i_2} + Q_{R_{e1}} \\
&Q_{i_2} = Q_{C_R} \\
&\tau_2 + \tau_3 = 0
\end{aligned} \tag{3.5}$$

Compatibility Equations

$$\begin{aligned}
&P_s = P_{C_R} + P_{i_1} + P_{c_1} \\
&P_{c_1} = P_{R_1} + P_{R_{in}} + P_{R_2} + P_{c_2} \\
&P_{R_{e1}} = P_{R_{in}} + P_{R_2} + P_{c_2} \\
&P_{R_{in}} = P_1 \\
&P_{R_{e2}} = P_{R_2} + P_{c_2} \\
&P_{c_2} = P_{i_2} + P_{C_R} \\
&W_2 = W_3 \\
&W_4 = \dot{q}_{sw} \\
&W_B = \dot{q}_{sw}
\end{aligned} \tag{3.6}$$

State Equations

$$
\begin{aligned}
\frac{dP_{c_1}}{dt} &= \frac{1}{C_1}\left(Q_{i_1} - \frac{P_{C_1} - P_{R_{in}} - P_{R_2} - P_{C_2}}{R_1}\right) \\
\frac{dP_{c_2}}{dt} &= \frac{1}{C_2}\left(\frac{P_{C_1} - P_{R_{in}} - P_{R_2} - P_{C_2}}{R_1} - \frac{P_{R_{in}} + P_{R_2} + P_{C_2}}{R_{e1}} - \frac{P_{C_2} + P_{R_2}}{R_{e2}} - Q_{i_2}\right) \\
\frac{dQ_{i_1}}{dt} &= \frac{1}{I_1}\left(P_s - C_R \cdot Q_{i_1}{}^2 \cdot sign(Q_{i_1}) - P_{C_1}\right) \\
\frac{dQ_{i_2}}{dt} &= \frac{1}{I_2}\left(P_{C_2} - C_R \cdot Q_{i_2}{}^2 \cdot sign(Q_{i_2})\right)
\end{aligned}
\tag{3.7}
$$

and

$$
\begin{aligned}
P_{R_{in}} &= R_{eq4} \cdot \left[R_{eq3} - R_{eq1} \cdot \left(\frac{1}{R_1} + \frac{1}{R_{e1}}\right) \cdot \left(\frac{P_{C_1} - P_{C_2}}{R_1} - \frac{P_{C_2}}{R_{e1}} - \frac{P_{C_2}}{R_{e2}}\right)\right] \\
P_{R_2} &= R_{eq1} \cdot \left(\frac{P_{C_1} - P_{R_1} - P_{C_2}}{R_1} - \frac{P_{R_{in}} + P_{C_2}}{R_{e1}} - \frac{P_{C_2}}{R_{e2}}\right) \\
R_{eq1} &= 1 \Big/ \left(\frac{1}{R_1} + \frac{1}{R_2} + \frac{1}{R_{e1}} + \frac{1}{R_{e2}}\right) \\
R_{eq2} &= 1 \Big/ \left(\frac{1}{R_{in}} + \frac{1}{R_1} + \frac{1}{R_{e1}}\right) \\
R_{eq3} &= \frac{P_{C_1} - P_{C_2}}{R_1} - \frac{P_{C_2}}{R_{e1}} - D_m \cdot N \cdot \dot{q}_{sw} \\
R_{eq4} &= 1 \Big/ \left(\frac{1}{R_{eq2}} - R_{eq1} \cdot \left(\frac{1}{R_1} + \frac{1}{R_{e1}}\right)^2\right)
\end{aligned}
\tag{3.8}
$$

The pressure drops across the hydraulic motor and flow going through it are calculated as follows.

$$
\begin{aligned}
P_{in} - P_{out} &= \Delta P_1 = P_{R_{in}} \\
Q_{sw} &= Q_1 = D_m \cdot N \cdot \dot{q}_{sw}
\end{aligned}
\tag{3.9}
$$

3.4 Boom/Stick Subsystem

Based on the system configuration and modelling assumptions made in the previous sections, the boom and stick subsystem models are formulated in the form of the linear graphs as follows.

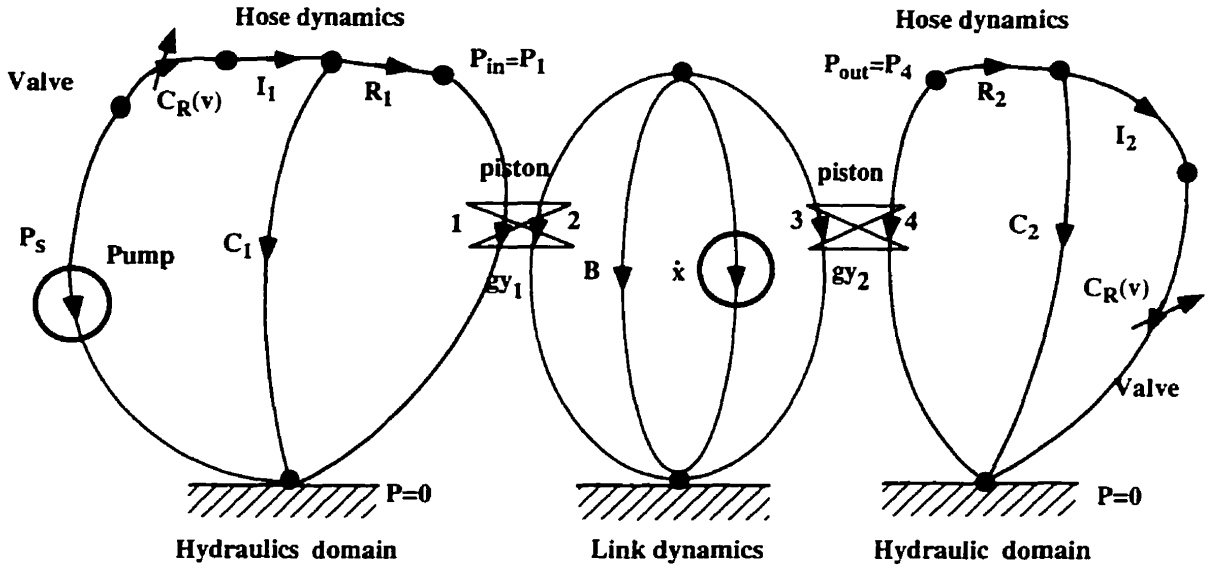

Figure 3.9 The boom and stick subsystem models.

The parameters shown in Figure 3.9 are defined:

P_s :	pump pressure.
C_R , C_R :	valve orifice resistance modulated by input current.
I_1 , I_2 :	supply and return line inertance.
C_1 , C_2 :	supply, return line capacitance.
R_1 , R_2 :	supply, return line resistance.
gy_1 , gy_2 :	rod and head side areas of the piston, $gy_1 = A_1$ and $gy2 = A_2$.
B :	viscous damping coefficients in the cylinders, B_{bm} or B_{sk}.

$\dot{x}$: pistons velocities, $\dot{x}_{bm}$ or $\dot{x}_{sk}$.

From the graphical representation, dynamic equations are derived as follows.

Elementary Equations

$$\frac{dP_{C_1}}{dt} = \frac{1}{C_1} Q_{C_1} \qquad P_{C_R} = C_R \cdot Q_{C_R}{}^2 \cdot sign(Q_{C_R}) \qquad F_B = B \cdot V_B$$

$$\frac{dP_{C_2}}{dt} = \frac{1}{C_2} Q_{C_2} \qquad P_{R_1} = R_1 \cdot Q_{R_1}{}^2 \cdot sign(Q_{R_1}) \qquad Q_1 = -gy_1 \cdot V_2$$

$$\frac{dQ_{i_1}}{dt} = \frac{1}{I_1} P_{i_1} \qquad P_{R_2} = R_2 \cdot Q_{R_2}{}^2 \cdot sign(Q_{R_2}) \qquad F_2 = gy_1 \cdot P_1 \qquad (3.10)$$

$$\frac{dQ_{i_2}}{dt} = \frac{1}{I_2} P_{i_2} \qquad P_{C_R} = C_R \cdot Q_{C_R}{}^2 \cdot sign(Q_{C_R}) \qquad F_3 = gy_2 \cdot P_4$$

$$Q_4 = -gy_2 \cdot V_3$$

Continuity Equations

$$\begin{aligned} Q_{C_R} &= Q_{i_1} \\ Q_{R_1} &= Q_1 \\ Q_{i_1} &= Q_{C_1} + Q_1 \\ Q_{i_2} &= Q_{C_R} \\ Q_4 &= -Q_{R_2} \\ Q_4 + Q_{i_2} + Q_{C_2} &= 0 \end{aligned} \qquad (3.11)$$

Compatibility Equations

$$\begin{aligned} P_s &= P_{C_R} + P_{i_1} + P_{C_1} \\ P_{C_1} &= P_{R_1} + P_1 \\ P_4 &= P_{R_2} + P_{C_2} \\ P_{C_2} &= P_{i_2} + P_{C_R} \\ V_2 &= \dot{x} \\ V_B &= \dot{x} \\ V_3 &= \dot{x} \end{aligned} \qquad (3.12)$$

State Equations:

$$\begin{aligned}
\frac{dP_{C_1}}{dt} &= \frac{1}{C_1}(Q_{i_1} - gy_1 \cdot \dot{x}) \\
\frac{dP_{C_2}}{dt} &= \frac{1}{C_2}(gy_2 \cdot \dot{x} - Q_{i_2}) \\
\frac{dQ_{i_1}}{dt} &= \frac{1}{I_1}(P_s - C_R \cdot Q_{i_1}^{\ 2} \cdot sign(Q_{i_1}) - P_{C_1}) \\
\frac{dQ_{i_2}}{dt} &= \frac{1}{I_2}(P_{C_2} - C_R \cdot Q_{i_2}^{\ 2} \cdot sign(Q_{i_2}))
\end{aligned} \tag{3.13}$$

The pressure drop across the piston and flow going through either side of the cylinder are calculated as follows.

$$\begin{aligned}
P_{in} &= P_1 = P_{C_1} + R_1 \cdot (gy_1 \cdot \dot{x})^2 \cdot sign(\dot{x}) \\
P_{out} &= P_4 = R_2 \cdot (gy_2 \cdot \dot{x})^2 \cdot sign(\dot{x}) + P_{C_2} \\
Q_{in} &= Q_1 = -gy_1 \cdot \dot{x} \\
Q_{out} &= Q_4 = -gy_2 \cdot \dot{x}
\end{aligned} \tag{3.14}$$

3.5 Integration with Manipulator Dynamics

One of the objectives of modelling the electrohydraulic actuation systems is to predict the dynamic behavior of the articulated links on the test vehicle by combining actuator and manipulator dynamics. The dynamic models of the manipulator, i.e. for the swing, boom and stick subsystems, were derived by S. Sarkar, [29]. We propose two procedures to integrate the swing, the boom and stick subsystems into the dynamic equations of manipulators. By given the amount of voltage commands to valves, the manipulator

dynamics can be computed to predict system response. The overall dynamic equations of the manipulators have the following form

$$\mathbf{M}(\mathbf{q})\cdot\ddot{\mathbf{q}} + \mathbf{V}(\mathbf{q},\dot{\mathbf{q}}) + \mathbf{G}(\mathbf{q}) = \boldsymbol{\tau} \tag{3.15}$$

where $\mathbf{M}(\mathbf{q})$ is the mass matrix, $\mathbf{V}(\mathbf{q},\dot{\mathbf{q}})$ includes Coriolis and centrifugal terms, $\mathbf{G}(\mathbf{q})$ includes gravity terms, and $\boldsymbol{\tau}$ is the input torque provided by the actuators.

3.5.1 Cylinder Actuation

Cylinder actuation exists in the boom and stick subsystems. Their configurations are shown in Figure 3.10.

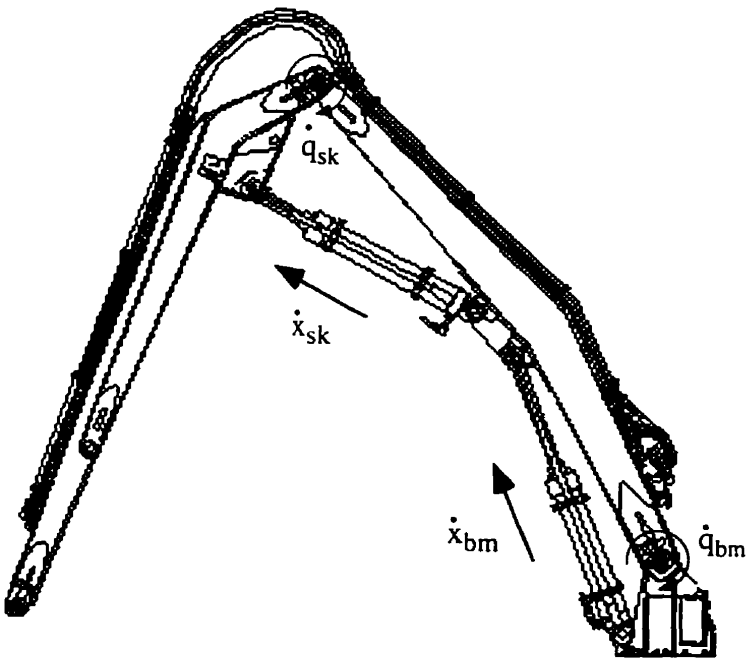

Figure 3.10 Cylinder actuation in the boom and stick subsystems.

From the knowledge of manipulator dynamics, we have the following well-known relationship:

$$\begin{aligned}\dot{\mathbf{x}} &= \mathbf{J}\cdot\dot{\mathbf{q}} \\ \boldsymbol{\tau} &= \mathbf{J}^{\mathrm{T}}\cdot\mathbf{F}\end{aligned} \tag{3.16}$$

where $\mathbf{x}$ is the vector of piston displacements, $\mathbf{q}$ is the vector of manipulator joint angles, $\mathbf{F}$ includes the forces generated by actuators, $\boldsymbol{\tau}$ is the corresponding torque. Since each link is independently actuated, the Jacobian $\mathbf{J}$ is a diagonal matrix. The complete Jacobian expressions of the boom and stick are given in Appendix A.

For single-ended type of cylinders, we have

$$\begin{pmatrix} F_{bm} \\ F_{sk} \end{pmatrix} = \begin{pmatrix} A_{in\_bm} & -A_{out\_bm} & 0 & 0 \\ 0 & 0 & A_{in\_sk} & -A_{out\_sk} \end{pmatrix} \cdot \begin{pmatrix} P_{in\_bm} \\ P_{out\_bm} \\ P_{in\_sk} \\ P_{out\_sk} \end{pmatrix}$$

$$\begin{pmatrix} Q_{in\_bm} \\ Q_{in\_sk} \\ Q_{out\_bm} \\ Q_{out\_sk} \end{pmatrix} = -\begin{pmatrix} A_{in\_bm} & 0 \\ 0 & A_{in\_sk} \\ A_{out\_bm} & 0 \\ 0 & A_{out\_sk} \end{pmatrix} \cdot \begin{pmatrix} \dot{x}_{bm} \\ \dot{x}_{sk} \end{pmatrix} \tag{3.17}$$

where A_{in_bm}, A_{out_bm}, A_{in_sk}, A_{out_sk} are inlet and outlet areas of the boom and stick pistons, F_{bm}, F_{sk} are the forces generated by boom and stick cylinders. Similarly, P_{in_bm}, P_{out_bm}, P_{in_sk}, P_{out_sk} are pressures at inlet and outlet of the boom and stick cylinders, and Q_{in_bm}, Q_{out_bm}, Q_{in_sk}, Q_{out_sk} are flow rates. The negative sign in the second equation comes from the assumption that the energy in two-port transduction process is lose-less. A schematic diagram of the cylinders is shown in Figure 3.11.

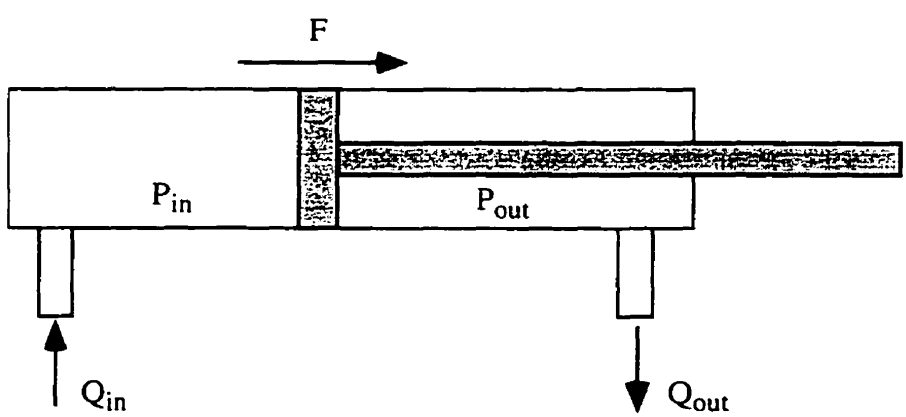

Figure 3.11 Schematics of cylinder actuation.

Thus

$$\begin{pmatrix}\tau_{bm}\\ \tau_{sk}\end{pmatrix} = \mathrm{J}^{T}(\mathrm{q})\cdot \mathrm{F} = \mathrm{J}^{T}(\mathrm{q})\cdot\begin{pmatrix}F_{bm}\\ F_{sk}\end{pmatrix} = \mathrm{J}^{T}(\mathrm{q})\cdot\begin{pmatrix}A_{in\_bm} & -A_{out\_bm} & 0 & 0\\ 0 & 0 & A_{in\_sk} & -A_{out\_sk}\end{pmatrix}\cdot\begin{pmatrix}P_{in\_bm}\\ P_{out\_bm}\\ P_{in\_sk}\\ P_{out\_sk}\end{pmatrix}$$

$$\begin{pmatrix}\dot{q}_{bm}\\ \dot{q}_{sk}\end{pmatrix} = \mathrm{J}^{-1}(\mathrm{q})\cdot\begin{pmatrix}\dot{x}_{bm}\\ \dot{x}_{sk}\end{pmatrix} = -\mathrm{J}^{-1}(\mathrm{q})\cdot\begin{pmatrix}1/A_{in\_bm} & 0\\ 0 & 1/A_{in\_sk}\end{pmatrix}\cdot\begin{pmatrix}Q_{in\_bm}\\ Q_{in\_sk}\end{pmatrix} \qquad (3.18)$$

$$= -\mathrm{J}^{-1}(\mathrm{q})\cdot\begin{pmatrix}1/A_{out\_bm} & 0\\ 0 & 1/A_{out\_sk}\end{pmatrix}\cdot\begin{pmatrix}Q_{out\_bm}\\ Q_{out\_sk}\end{pmatrix}$$

Therefore, the relationship between pressures of actuators and torque output to links is set up. Also the flows at the cylinders are determined by the angular velocities of the boom and stick.

3.5.2 Hydraulic Motor Actuation

By following similar procedures, hydraulic motors can be modelled as a gyrator for which the constant of gyration is the volumetric displacement of the motor, D_m. Here, the relationship is simpler because of the equal area configuration for the motor. Note also there is a gear train, with gear ratio N, connected directly to the output shaft of the motor in order to amplify torque output to the swing of the machine. By the definition in the linear graph, the gear train is a transducer of the transformer type. The transduction equation becomes

$$\begin{pmatrix}\dot{q}_{sw}\\ \tau_{sw}\end{pmatrix} = \begin{pmatrix}0 & D_m/N\\ -N\cdot 1/D_m & 0\end{pmatrix}\cdot\begin{pmatrix}P_{in\_sw}-P_{out\_sw}\\ Q_{sw}\end{pmatrix} \qquad (3.19)$$

Up to this step, the relationship between manipulator dynamics, in terms of variables $\boldsymbol{\tau}$ and $\dot{\mathbf{q}}$ and electrohydraulic actuator dynamics, in terms of variables $\mathbf{P}$, $\mathbf{Q}$ are set up. The

overall dynamic equations for the three-degree-of-freedom manipulator, the swing, boom and stick are in the form of

$$\dot{\underset{\sim}{q}}_1 = \underset{\sim}{q}_2$$

$$\dot{\underset{\sim}{q}}_2 = M\left(\underset{\sim}{q}_1\right)^{-1}\left\{-V\left(\underset{\sim}{q}_1, \underset{\sim}{q}_2\right) - G\left(\underset{\sim}{q}_1\right) + \underset{\sim}{t}\right\}$$

$$\begin{aligned}
\dot{P}_{c_1_sw} &= \left(1/C_{1_sw}\right)\cdot\left(Q_{i_1_sw} - \left(P_{C_1_sw} - P_{R_{in}}(\dot{q}_{sw}) - P_{R_2} - P_{C_2_sw}\right)/R_1\right)\\
\dot{P}_{c_2_sw} &= \left(1/C_{2_sw}\right)\cdot(\left(P_{C_1_sw} - P_{R_{in}}(\dot{q}_{sw}) - P_{R_2} - P_{C_2_sw}\right)/R_1\\
&\qquad -\left(P_{R_{in}}(\dot{q}_{sw}) + P_{R_2} + P_{C_2_sw}\right)/R_{e1} - \left(P_{C_2_sw} + P_{R_2}\right)/R_{e2} - Q_{i_2_sw})\\
\dot{Q}_{i_1_sw} &= \left(1/I_{1_sw}\right)\cdot\left(P_s - C_R\cdot Q_{i_1_sw}{}^2\cdot sign(Q_{i_1_sw}) - P_{C_1_sw}\right)\\
\dot{Q}_{i_2_sw} &= \left(1/I_{2_sw}\right)\cdot\left(P_{C_2_sw} - C_R\cdot Q_{i_2_sw}{}^2\cdot sign(Q_{i_2_sw})\right)
\end{aligned} \tag{3.20}$$

$$\begin{aligned}
\dot{P}_{c_1_bm} &= \left(1/C_{1_bm}\right)\cdot\left(Q_{i_1_bm} - gy_1\cdot\dot{x}_{bm}\right)\\
\dot{P}_{c_2_bm} &= \left(1/C_{2_bm}\right)\cdot\left(gy_2\cdot\dot{x}_{bm} - Q_{i_2_bm}\right)\\
\dot{Q}_{i_1_bm} &= \left(1/I_{1_bm}\right)\cdot\left(P_s - C_R\cdot Q_{i_1_bm}{}^2\cdot sign\left(Q_{i_1_bm}\right) - P_{c_1_bm}\right)\\
\dot{Q}_{i_2_bm} &= \left(1/I_{2_bm}\right)\cdot\left(P_{c_2_bm} - C_{R'}\cdot Q_{i_2_bm}{}^2\cdot sign\left(Q_{i_2_bm}\right)\right)
\end{aligned}$$

$$\begin{aligned}
\dot{P}_{c_1_sk} &= \left(1/C_{1_sk}\right)\cdot\left(Q_{i_1_sk} - gy_1\cdot\dot{x}_{sk}\right)\\
\dot{P}_{c_2_sk} &= \left(1/C_{2_sk}\right)\cdot\left(gy_2\cdot\dot{x}_{sk} - Q_{i_2_sk}\right)\\
\dot{Q}_{i_1_sk} &= \left(1/I_{1_sk}\right)\cdot\left(P_s - C_R\cdot Q_{i_1_sk}{}^2\cdot sign\left(Q_{i_1_sk}\right) - P_{c_1_sk}\right)\\
\dot{Q}_{i_2_sk} &= \left(1/I_{2_sk}\right)\cdot\left(P_{c_2_sk} - C_{R'}\cdot Q_{i_2_sk}{}^2\cdot sign\left(Q_{i_2_sk}\right)\right)
\end{aligned}$$

and $\underset{\sim}{q}_1 = \left[q_{sw} \quad q_{bm} \quad q_{sk}\right]^T$, $\underset{\sim}{\tau} = \left[\tau_{sw} \quad \tau_{bm} \quad \tau_{sk}\right]^T$.

The first two equations describe the dynamics of the manipulator mechanical structures. They contain three sets of first-order differential equations of the swing, boom and stick. The remaining equations illustrate the dynamic characteristics of the hydraulic actuation

subsystems. Three sets of first-order differential equations are listed for the swing, boom and stick actuation subsystems. The interconnection between the manipulator mechanical structure and the actuation systems is bridged by the piston velocity $\dot{x}_{bm}$, $\dot{x}_{sk}$ for the boom and stick subsystems and $\dot{q}_{sw}$ for the swing subsystem. A SIMULINK file written for simulating the overall dynamic behavior of the three degree of freedom manipulator, i.e. the swing, boom and stick, is given in Appendix B.

3.6 Summary

The linear graph method was selected and implemented to model various components involved in the electrohydraulic actuation systems on the modified FERIC C-180 test vehicle. Then, two sets of models, namely, the swing, boom and stick models were derived based on models of individual components. The integration procedure of the electrohydraulic actuation system models with the manipulator dynamic models were presented. The validity of these models is verified in the parameter identification stage. The detailed procedures are explained in Chapter 4.

4. Parameter Identification

In the previous chapter, two sets of dynamic models were derived for the swing, boom and stick actuation subsystems. However, good mathematical models depend not only on the structure of the equations, but also on the values of the physical parameters involved. Parameter identification can be considered as part of the process of constructing valid mathematical models for dynamic systems.

A brief discussion of the fundamentals of parameter identification is presented first. Then the data acquisition system, the experimental setup and measurement procedures used are described. Model validation studies are described by comparing computer simulation results with experimental data. A summary of the chapter follows.

4.1 Basics of Parameter Identification

4.1.1 Definition

Historically, parameter identification has been motivated by the need to design better control systems. In most practical systems, such as industrial processes, there is seldom

sufficient a priori information about a system and its environment to design an effective control strategy. Very frequently, we are faced with the necessity of experimentally determining some important physical parameters such as heat transfer coefficient, chemical reaction rate, damping ratio, and so on. The need for highly accurate models has been testified by the development of optimal and adaptive control theories, [15].

A wish to predict is a common and powerful motive for dynamic modelling. Prediction by a mathematical model is considered to be one of the final objects of the modelling stage in control system design. After the structure of the model is derived, parameters involved in the model have to be estimated by experiments. Therefore, *parameter identification is the process of measuring parameters, which are involved in a mathematical model of a dynamic system, from observations of physical experiments.*

4.1.2 Procedures

In general, we would like to identify parameters individually in order to reduce errors to a minimum. This requires that experiments are setup according to the definitions of parameters. Based on the sensors that are available and the electrohydraulic system configurations, simple analysis shows that we can design specific experiments for most of the parameters. However, standard identification procedures are demanded for other parameters. The following two sections give an overview on this topic.

4.1.2.1 Methods

Two methods are generally used to identify system parameters: on-line and off-line identification methods. Off-line identification assumes that systems are time invariant, i.e. parameters do not change with respect to time. It determines a model of a system using a

batch of measured data, where the whole batch is available at all stages of the procedure. On-line identification, on the other hand, infers the model at the same time as the data is collected. The model is then updated at each time instant when some new data becomes available. On-line methods have been adapted for use in adaptive control and filtering. For the actuation systems we are dealing with, the physical parameters involved are considered to be time-invariant. Therefore, off-line estimation procedure is chosen for processing the experimental data. A detailed comparison between on-line and off-line estimation is shown in Table 4.1.

Table 4.1 Comparison of off-line and on-line estimation.

Off-line estimation	On-line estimation
Available after a finite number of elementary operations	Available after (in principle) an infinite number of elementary operations
Requires considerable memory	Requiring less memory
Not available in an approximate form as an intermediate result	Available in an approximate form as an intermediate result
In open loop with respect to estimation	In closed loop with respect to estimation

4.1.2.2 Algorithms

Once the off-line identification approach is chosen, numerical values of the parameters are sorted by fitting the observations according to a deterministic measure of error between model output and observed output, totaled over all the observations. Least-squares

estimation is the simplest, yet most powerful, approach among several methods under this estimation framework.

The least-squares method estimates the numerical value of parameters of a given model through minimizing the sum of the squared errors between the model output and the observations of the output. There are two apparent advantages of it. First, large errors are heavily penalized: an error twice as large is four times as bad. The other advantage is the mathematical tractability. The formula giving the least-squares estimates is obtained by quite simple matrix algebra, and the estimates are computed as the solution to a set of linear equations, [26].

Whenever noise is present in the observations from which a model is estimated, the value of parameters are affected by it and are therefore random variables: taking another set of observations would not give precisely the same results. For white-noise, the least-squares method is considered to be sufficient enough to eliminate its effect. For other types of noise, depending on the amount of prior knowledge available, different levels of procedures can be implemented. These include the Markov estimator, the maximum likelihood estimator and the Bayes estimator.

4.2 Data-Acquisition System

4.2.1 Sensors

The experiments focus on identifying parameters of the electrohydraulic actuation systems, namely of the swing, boom and stick subsystems. Sensors are selected based on the structure of the proposed dynamic models. Summarized information on the sensors used is given in Table 4.2.

Table 4.2 Selected sensors for parameter identification.

Types of Measurements	No. of Sensors	Specifications of Sensors
Hydraulic measurements	12	Pressure transducers - TransInstruments 2000-BG-H50-02-A10A Range: 0 ~ 5,000 psi. Accuracy: ± 0.01% of full scale.
	2	Flow meters - EG&G FT-16AEU2-LEA-2 Range: 0.85 ~ 50 gallon/min. Accuracy: ± 0.05% of measurements. Time constant: 10 ms.
	3	Thermocouples - Thermokinetics K-125-316-S-4-A-720-YM2 Range: −270 °C ~ 1360 °C. Accuracy: ± 0.2 °C.
Mechanical measurements	3	Resolvers - Fasco 11BRCX-300-C 10m Range: 0 ~ 360 degree. Accuracy: ± 7/60 degree.
	2	Magnetostrictive linear transducers - Balluff BTL-2-L1-0914-Z-S50

		Range: 0 ~ 36.5 inches. Resolution: ± 0.04% of full scale.
Prime mover	1	Tachometer - speed of the diesel engine

4.2.2 Data-Acquisition System

Various types of sensors were selected for the purpose of experiments and control. A schematic drawing of the data-acquisition system is shown in Figure 4.1. Analogue signals from pressure transducers, spool sensors, cable sensors and inclinometers are digitized by A/D converters. A special A/D converter is used for digitizing signals sent by the thermocouple. Signals picked up from resolvers are processed by a R/D card, a special electronic card to generate reference signals and convert the readings into digital values. Magnetostrictive linear transducers, flow meters and the tachometer are connected to a Motorola HC11 micro-controller because their output needs to be processed and digitized before it is sent to the embedded system, a Ziatech-8902, 486 DX-2 computer installed at the back of the cabin on the vehicle. The STD-32 bus was chosen to transfer data within the embedded system, and the QNX real-time operating system is used for the experiments. Eventually, the on-board computer will function as the controller of the manipulator, i.e. processing sensor information and operator's inputs, monitoring the state of the vehicle, issuing commands to the actuation system and self-diagnosing possible malfunctions. The data sampling rate can go as high as 200 Hz. However, at the experimental stage, it is mainly used to collect sensor readings, buffer and send off data to another computer via Ethernet. This second 486 DX-2 computer is remotely located and it is also running the

QNX real-time operating system. Its main function is to store and process the experimental data. A picture of the embedded system is shown in Figure 4.2.

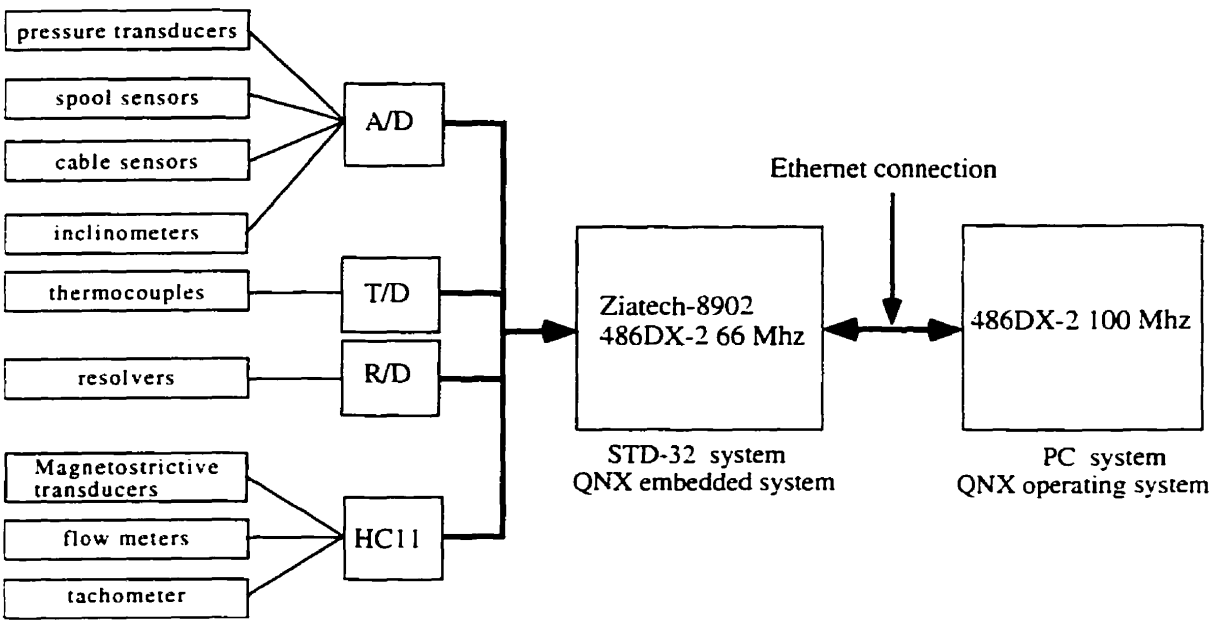

Figure 4.1 Schematics of data-acquisition system.

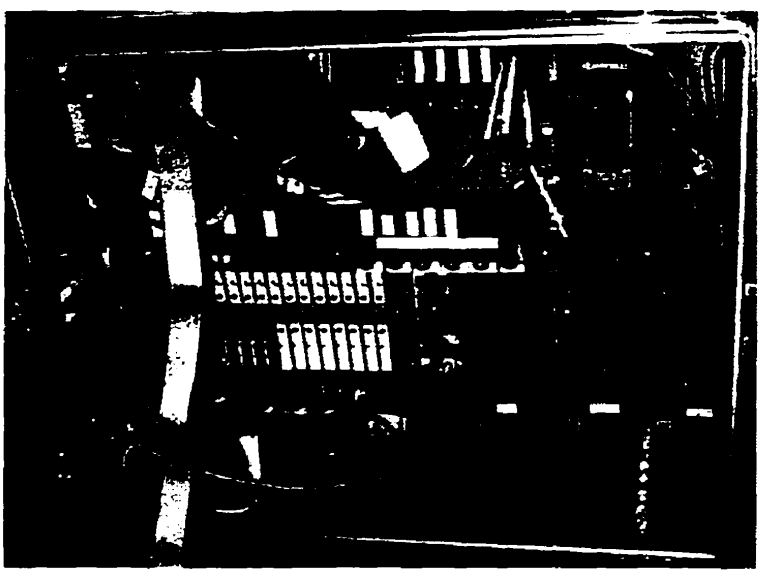

Figure 4.2 Embedded system.

4.3 Experimentation

Experiments were designed so that the parameters needed in the models of the electrohydraulic actuation system could be identified. These include parameters related to the hoses, valves, cylinders and motor.

4.3.1 Sensor Calibration

This is the preliminary stage of the experiments. The objective is to test the data-acquisition system and ensure that the sensor readings are within sensor nominal error bounds. Various methods were implemented to calibrate pressure transducers, flow meters, thermocouples, resolvers and magnetostrictive linear transducers. Pressure transducers were calibrated by measuring the ambient atmosphere pressure. One of the two flow meters was calibrated by the manufacturer, and the other one was calibrated by comparing its measurement with the first one. Thermocouples were calibrated by measuring both ice/water mixture and boiling water.

4.3.2 Valve Configurations

4.3.2.1 Objective

Here, the objective is to estimate the relationship between voltage input V to the valves and their coefficients C_R. Since the three valves used in the swing, boom and stick actuation are identical type, only one of them is tested and C_R is measured.

4.3.2.2 Approach

For incompressible flow through orifices, the orifice equation relating pressure and flow is given as

$$\Delta P = P_{in} - P_{out} = C_R \cdot Q \cdot |Q| \tag{4.1}$$

where the coefficient C_R is a function of the fluid density ρ, the orifice area A, and the orifice discharge coefficient C_d.

$$C_R(V) = \frac{\rho}{2C_d^2 \cdot A^2(V)} \tag{4.2}$$

By varying the magnitude of the input voltage command, several groups of pressure P_{in}, P_{out} and flow rate Q were collected. Then, a MATLAB curve-fitting algorithm was implemented to find a polynomial relationship of C_R as a function of the voltage input V

$$C_R = \frac{P_{in} - P_{out}}{Q \cdot |Q|} \tag{4.2a}$$

Note that although measurements for only one valve port are described here, the other port was also tested. It was found that the two port characteristics are very similar.

Required measurements: Pressure P_{in}, P_{out} at inlet and outlet of the valve

Flow rate Q across the valve

Voltage V sent to the valve

4.3.2.3 Experimental Setup

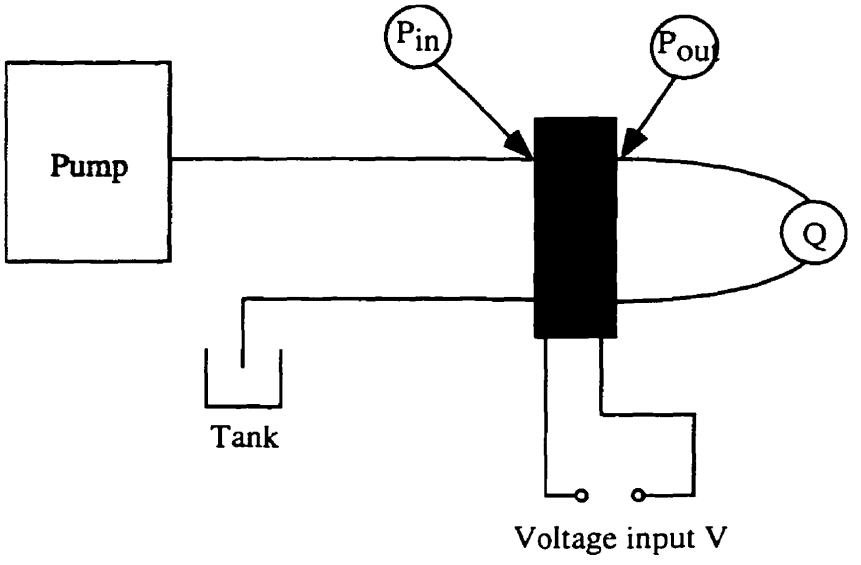

Figure 4.3 Apparatus setup for valve configuration measurement.

4.3.2.4 Results

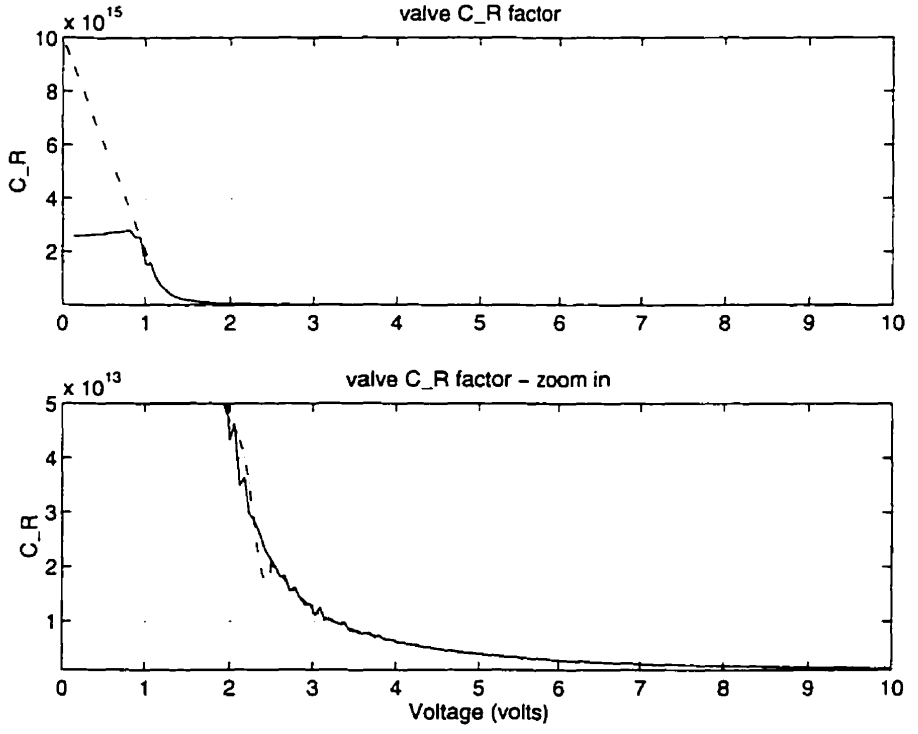

Figure 4.4 Valve characteristics.

The solid line stands for the experimental results and the dotted line results from curve fitting. Note that the flat region between 0 and 1 volt in the first half of the figure is due to both the lower measurement limit of the flow meter and the mechanical deadband (closed center) of the valve. The signal from the flow meters can only be picked up if the rotation frequency of blades inside them is greater than 31 Hz, which is equivalent to 0.85 gallon per minute. Any values less than 31 Hz are ignored and assigned a value of 31 Hz.

4.3.3 Hose Resistance

4.3.3.1 Objective

To estimate the *static* relationship between pressure and flow rate, i.e. the resistance, for all hoses used on the test vehicle.

4.3.3.2 Approach

Given a nominal flow rate and hose dimensions, the approximate Reynolds number calculation shows that the flow is turbulent under normal operating conditions of the vehicle. For incompressible, fully developed turbulent flow, the equation relating pressure and flow is given as, [24]

$$\Delta P = \alpha \frac{\mu^{0.25} \rho^{0.75} L}{D^{4.75}} Q^{1.75} \tag{4.3}$$

Where α is a constant depending on the units, μ is the absolute viscosity, ρ is the fluid density, L is the pipe length, and D is the inside diameter of the pipe. The factor $Q^{1.75}$ can be further approximated by $Q \cdot |Q|$. Therefore, for a given specific fluid, we have the equation in the form

$$\Delta P = P_{in} - P_{out} = R_{hose} \cdot Q \cdot |Q| \tag{4.4}$$

where fluid viscosity, density, hose diameter and length are lumped into a single parameter R_{hose}. Note also that R_{hose} is proportional to hose length.

The SAE 100R12 very-high-pressure hydraulic hose is the only type of hose used on the vehicle. For hoses with different diameters and lengths, their resistance can be calculated by a linear approximation according to Equation (4.3).

By varying valve opening conditions, a set of flow rates and the corresponding pressure differences across the hose were measured. Note that data must be collected when flow dynamics die out to eliminate the effects of fluid inertance and capacitance.

Required measurements: Pressure P_{in}, P_{out} at the entrance and exit of the hose.

Flow rate Q through the hose.

4.3.3.3 Experimental Setup

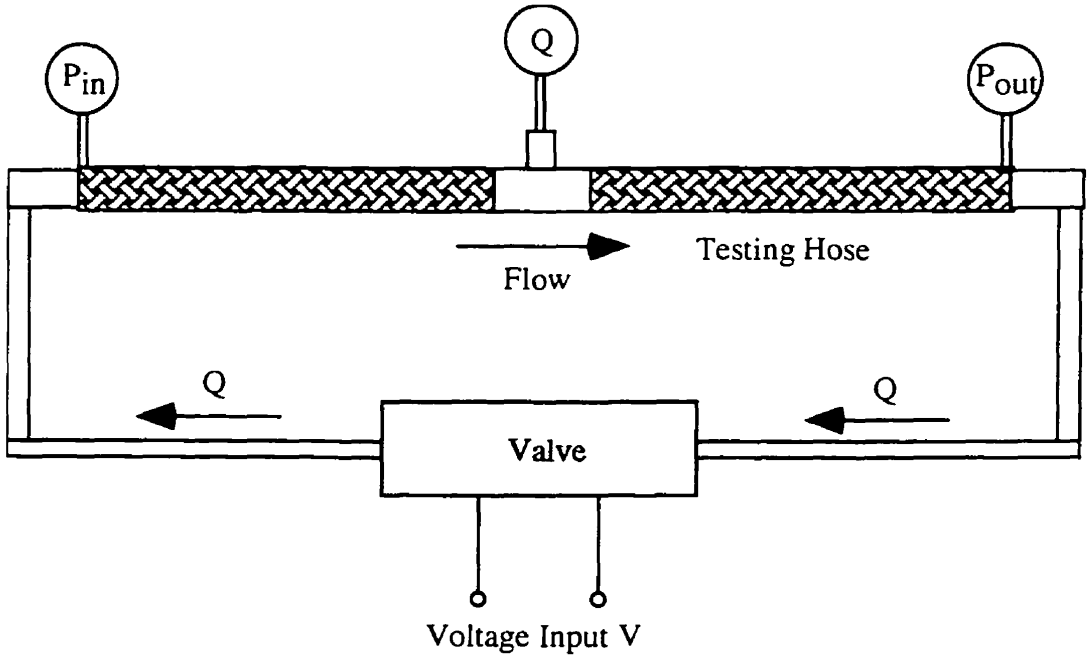

Figure 4.5 Hose resistance measurement.

4.3.3.4 Results

The least-squares method is used to find the value of R_{hose} as shown in Equation (4.4). For a SAE 100R12 very high pressure hose with length of 4 meters and diameter of 3/4 inches, the relation of ΔP and $Q$is shown in Figure 4.6 by using the estimated value of R_{hose}. The solid line represents the experimental measurements and the dotted line represents the estimation. Again, the flat region at the beginning of the experimental curve comes from the measuring limitation of the flow meters and the mechanical deadband of the valve.

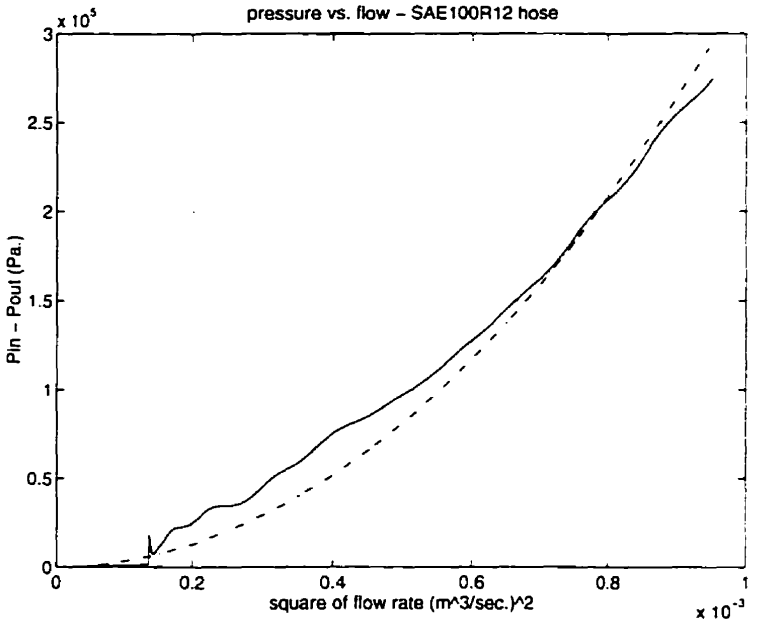

Figure 4.6 Resistance measurement of a SAE 100R12 hose with length of 4 meters and 3/4 inches diameter.

4.3.4 Inertance and Capacitance

4.3.4.1 Objective

To estimate the *dynamic* characteristics of the given transmission lines, i.e. capacitance and inertance.

4.3.4.2 Approach

If the fluid is assumed incompressible and frictionless, that is, if it is assumed to have only inertia, application of Newton's second law of motion to the fluid control volume yields

$$\Delta P = I\frac{dQ}{dt} \tag{4.5a}$$

where I is called the *fluid inertance*, and depends upon the pipe geometry and fluid properties. According to simplified theoretical considerations, [28]

$$I = \frac{\rho \cdot L}{A} \tag{4.5b}$$

where ρ is the fluid density, L is the length of the hose and A is the hose inner diameter. After measuring the inertance of a given hose, its value for other hoses can be approximated based on the hose length and size. Because of the coexistence of capacitance and inertance in hoses, inertance effect can not be measured independently. The experimental procedure is described after the discussion of fluid capacitance.

For a hose in which only the fluid capacitance is considered, that is, in which the fluid density is negligible, the following equation relates the incoming and outgoing flow rate with the time rate of change of pressure:

$$Q = C\frac{dP}{dt} \tag{4.6}$$

The capacitance, C, is a combined coefficient of fluid compressibility and wall expansion in hoses. Detailed calculations were shown in [27] for cylinders by knowing the values of Young's modulus E and Poisson's ratio ν of the material. For flexible hoses, those values are hardly available. The inertance and the capacitance of various hoses on the test vehicle can be estimated by knowing the capacity of a standard hose and their length and diameter. The following is the data-processing procedure used to compute inertance and capacitance of the same hose used for estimating resistance.

Required measurements: Pressure P at the entrance and exit of the hose.

Flow rate Q at the entrance and exit of the hose.

Linear Graphs Model	Data Processing
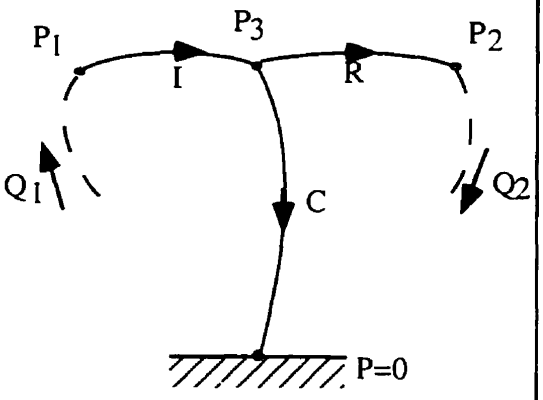	1. Calculate P_3 by adding P_2 to the pressure drop across R, $P_3 = R \cdot Q_2 \cdot \lvert Q_2 \rvert + P_2$ 2. Calculate C by the definition $C = {(Q_1 - Q_2)}/{dP_3/dt}$ 3. Calculate I by the definition $I = {(P_1 - P_3)}/{dQ_1/dt}$

4.3.4.3 Experimental Setup

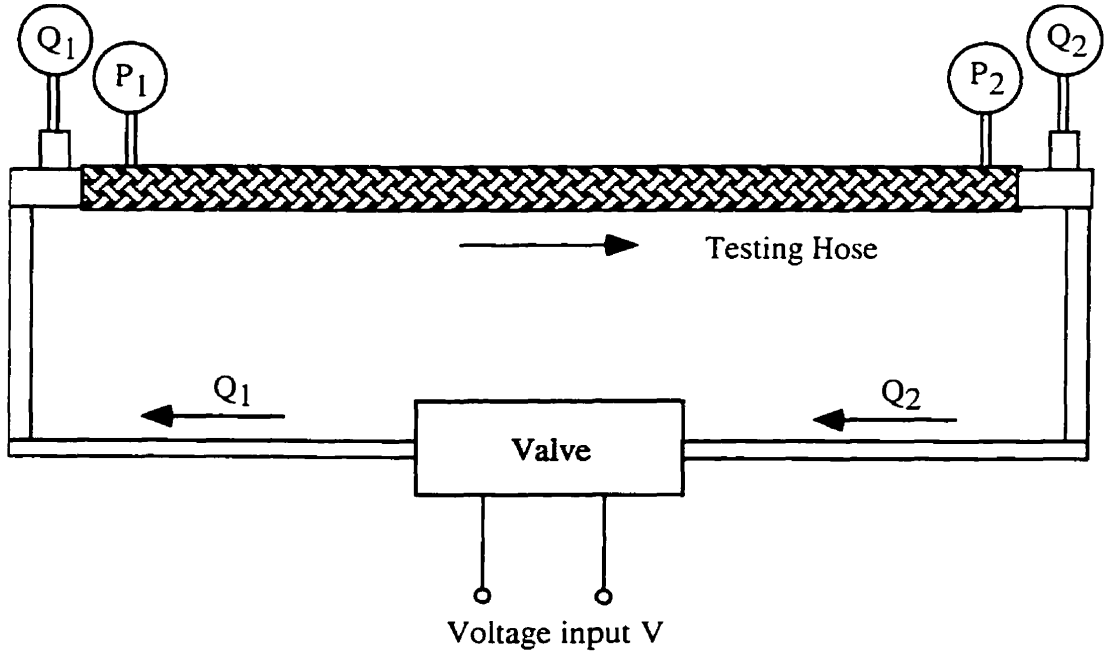

Figure 4.7 Inertance and capacitance measurement setup.

4.3.4.4 Results

For a SAE 100R12 very high pressure hose with length of 4 meters and diameter of 3/4 inches, four groups of data were collected for the inertance and capacitance measurements. Note that some negative values appear in the capacitance and inertance calculation. These are due to the phase difference between ΔQ and ΔP_3 in C, ΔP and $d\dot{Q}_1$ in I in the measurements. Their effects are minimized by taking the average value of each group of experimental results. The final values of I and C are the average of these mean values of the four measurements.

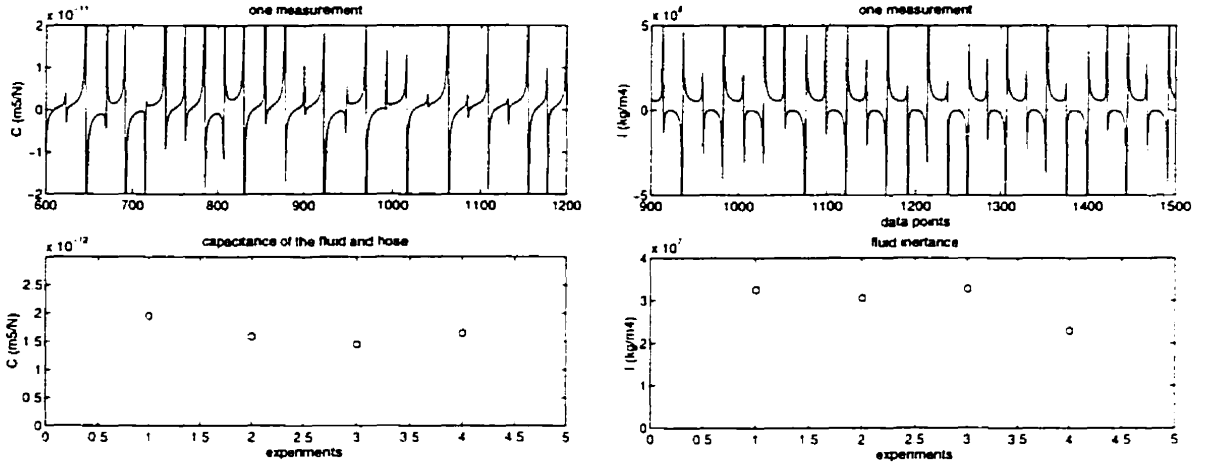

$$C = 1.585 \times 10^{-12} m^5 / N \qquad I = 3.062 \times 10^7 kg / m^4$$

Figure 4.8 Capacitance and inertance estimation for a SAE 100R12 hose with length of 4 meters and 3/4 inches diameter.

4.3.5 Motor Leakage

4.3.5.1 Objective

To estimate the internal and external leakage of the piston motor in the swing actuation subsystem.

4.3.5.2 Approach

Leakage flow and friction are the causes of power losses in hydraulic motors. The friction effect is lumped into the gear train connected to the shaft of the motor, and it will be considered in the next section. In general, two types of leakage flows exist inside motors: internal or cross-port leakage between higher and lower pressure chambers and external leakage from each motor chamber passing pistons to case drain. Because all mating clearances in a motor are intentionally made small to reduce losses, these leakage flows are laminar and, therefore, proportional to pressure.

The internal leakage is proportional to the pressure difference across the inlet and outlet ports of a motor, and may be written as:

$$\Delta P = P_1 - P_2 = R_{in} \cdot Q_{in} \tag{4.7}$$

where R_{in} is the internal or cross-port leakage resistance, and ΔP is the pressure difference across the two ports of a motor as shown in Figure 4.9.

The external leakage in each piston chamber is proportional to the particular chamber pressure and may be written as:

$$\begin{aligned} P_1 &= R_{ex} \cdot Q_{ex1} \\ P_2 &= R_{ex} \cdot Q_{ex2} \end{aligned} \tag{4.8}$$

where R_{ex} is external resistance, P_1 is pressure in the forward chamber and P_2 is pressure in the return chamber.

From the definition of an ideal motor we have

$$Q = D_m \cdot \dot{\theta}_m \tag{4.9}$$

where D_m is the ideal volumetric displacement and available from motor specification sheet, while $\dot{\theta}_m$ is the motor shaft speed which can be measured using a resolver.

Required measurements for external leakage:

Pressure P_1 , P_2 at the inlet and outlet of the motor.

Volume of oil collected from the case drain in a period of time for measuring slip flow rate.

Data processing:

The external leakage can be calculated from Equation (4.8) as $R_{ex} = (P_1 + P_2)/Q_{ex}$.

Required measurements for internal leakage:

The manipulator is turned 90 degrees from its normal forward position with respect to the swing motor axis. Then, the platform of the test vehicle is tilted in order to use gravity force to push the swing motor. Due to the existence of internal leakage, the manipulator is rotating slowly under the effect of gravity even when the swing valve is completely shut. In addition, external leakage does not exist in this situation. Two types of measurement are needed: pressure P_1 , P_2 at the inlet and outlet of the motor and swing resolver reading.

Data processing:

The flow rate of internal leakage can be calculated as $Q_{in} = D_m \cdot \dot{\theta}$.

Then $R_{in} = (P_1 - P_2)/Q_{in}$.

4.3.5.3 Experimental Setup

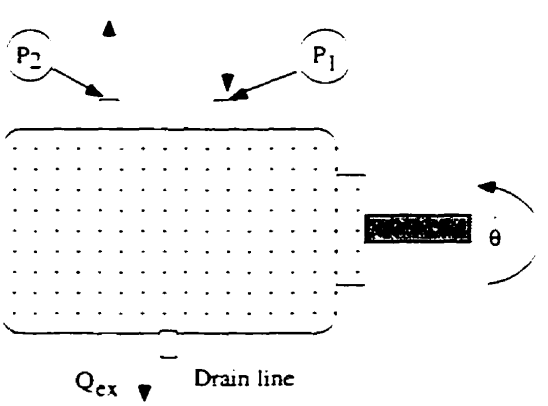

Figure 4.9 Leakage measurement setup.

4.3.5.4 Results

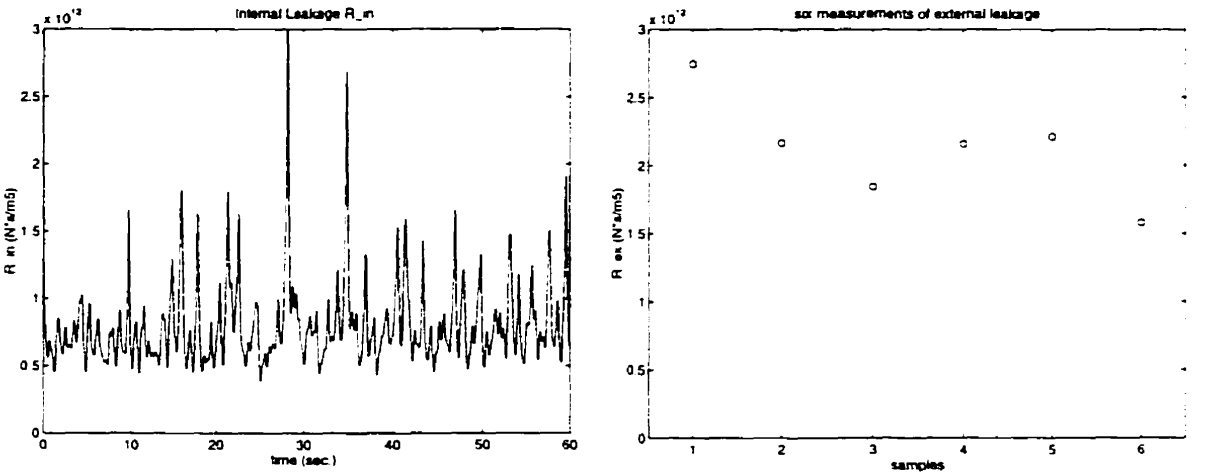

$$R_{in} = 8.002 \times 10^{11} N \cdot s / m^5 \qquad R_{ex} = 2.119 \times 10^{12} N \cdot s / m^5$$

Figure 4.10 Internal and external leakage measurements.

4.3.6 Piston and Motor Damping

4.3.6.1 Objective

To estimate damping coefficient B of the cylinders and the gear train attached to the hydraulic motor.

4.3.6.2 Approach

By assuming that the contacting surfaces are sufficiently lubricated, only viscous damping effects inside the cylinders and gear train need to be considered. For an ideal viscous damper, the constitutive relationship is in the form

$$F = B \cdot v \quad \text{or} \quad \tau = B \cdot \omega \tag{4.10}$$

where B is defined as the damping coefficient.

The physical connections of the manipulator prevent the actuators from being disconnected from the structure. Therefore, we can not estimate B without considering the

effect of other parameters. Values of B are estimated after other parameters are identified, and accumulative errors are lumped solely into them. The procedure for identifying the damping coefficient for the swing, boom and stick subsystems is described next.

The general form of manipulator dynamic equation can be written as

$$\ddot{\mathbf{q}} = \mathbf{M}(\mathbf{q})^{-1} \cdot \{-\mathbf{V}(\mathbf{q},\dot{\mathbf{q}}) - \mathbf{G}(\mathbf{q}) + \boldsymbol{\tau}\} \tag{4.11}$$

where $\ddot{\mathbf{q}}$ is the angular acceleration of the links, which can be calculated by differentiating the resolver readings twice. $\mathbf{M}(\mathbf{q})$ is the mass matrix and is a function of link mass and geometry properties and joint angles, and can be found by proper modelling and measurements. $\mathbf{V}(\mathbf{q},\dot{\mathbf{q}})$ contains Coriolis terms and joint damping. $\mathbf{G}(\mathbf{q})$ is the gravity matrix. It is also a function of link mass and geometric properties and joint angles. The torque term $\boldsymbol{\tau}$, which is defined in Equation (3.20), connects the hydraulic actuation systems to the manipulator and can be calculated based on measurements of pressures, flow rates and actuator velocities. Least-square estimation, then, is used to estimate the damping coefficient of the gear train in the swing subsystem and of the boom and stick cylinders.

Required measurements:

Pressure P_{in}, P_{out} at the inlet and outlet of the swing motor, boom and stick cylinders.

Resolver readings of the swing, boom and stick motion.

Data processing:

Reformulate $\ddot{\mathbf{q}} = \mathbf{M}(\mathbf{q})^{-1} \cdot \{-\mathbf{V}(\mathbf{q},\dot{\mathbf{q}}) - \mathbf{G}(\mathbf{q}) + \boldsymbol{\tau}\}$ into the form of $\dot{\mathbf{q}}_{sw} \cdot B = \boldsymbol{\alpha}$ for the swing subsystem, and $\dot{\mathbf{x}} \cdot B = \boldsymbol{\alpha}$ in the boom and stick subsystem cases. Also we assume that the mass and geometric properties are known and joint angle measurements are valid.

Then we have $B = \left[\dot{\mathbf{q}}^T\dot{\mathbf{q}}\right]^{-1}\dot{\mathbf{q}}^T\boldsymbol{\alpha}$ or $B = \left[\dot{\mathbf{x}}^T\dot{\mathbf{x}}\right]^{-1}\dot{\mathbf{x}}^T\boldsymbol{\alpha}$.

4.3.6.3 Results

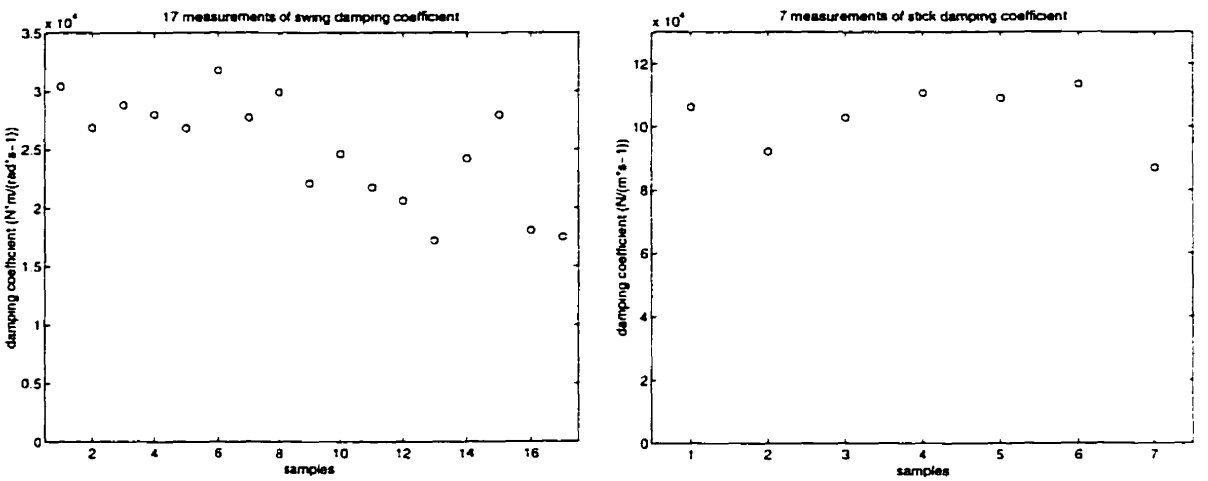

$B_{sw} = 2.450 \times 10^4 N \cdot m/(rad \cdot s^{-1})$ $B_{sk} = 1.030 \times 10^5 N/(m \cdot s^{-1})$

Figure 4.11 Damping coefficient measurement for the gear train and the stick cylinder.

4.4 Model Validation Studies

The capability to predict is the ultimate validation criterion for derived dynamic models. Up to this point, all the parameters involved in the electrohydraulic actuation systems have been identified. The inertia properties of manipulators were estimated by S. Sarkar, [28] using a solid modelling package available in AutoCad. Computer simulation results are compared next with the actual system response to various types of input.

4.4.1 Swing Subsystem

Input to the swing system and its state variables are shown below. The solid line stands for actual measurement and the dotted line is the prediction from the derived dynamic models.

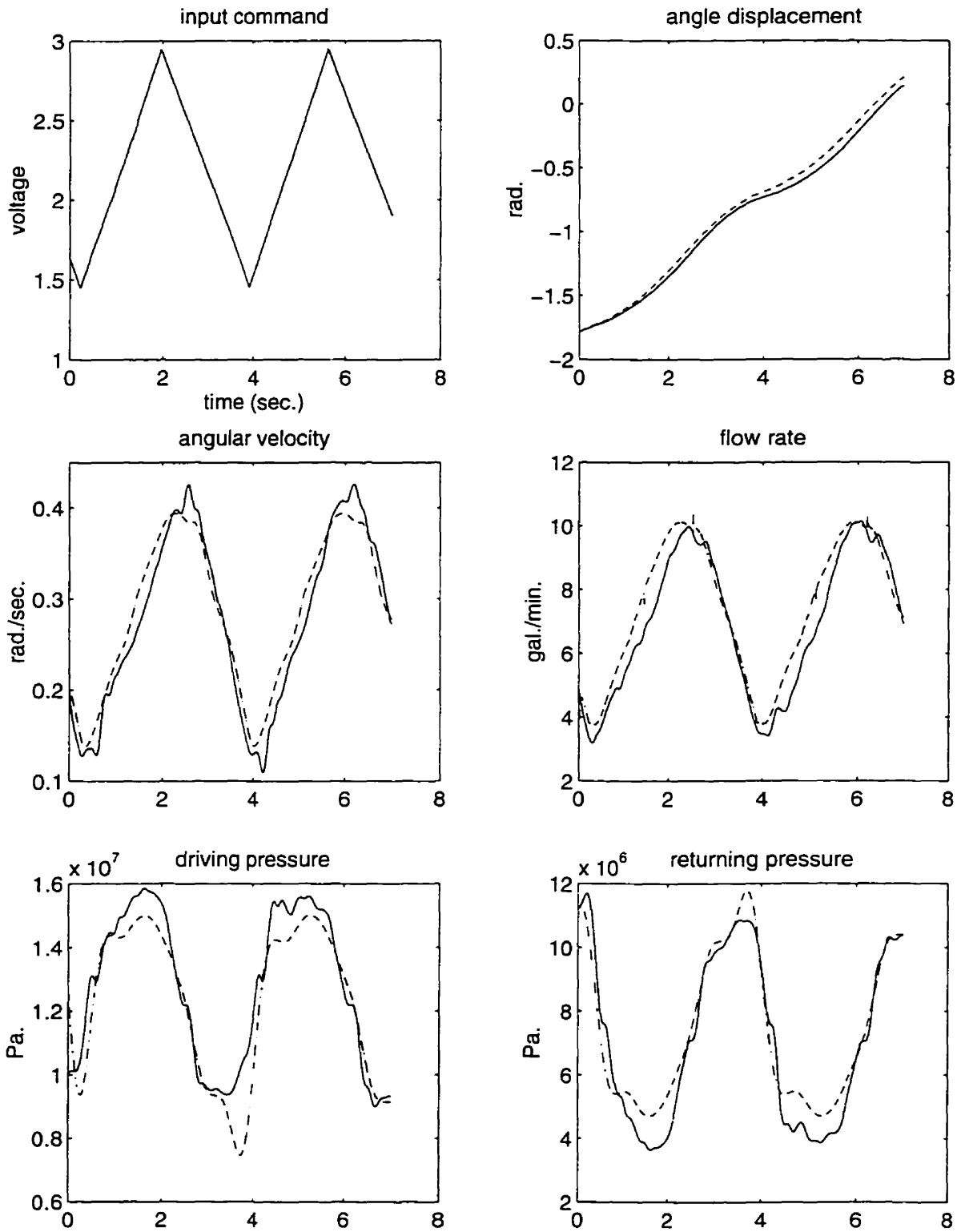

Figure 4.12 Model validation studies for swing model.

The prediction for the angular displacement and angular velocity are very close compared to the actual ones. The prediction for flow rate is also very good because of its relation to angular velocity. The predicted pressure profiles are close to the real ones, although part of the peaks were missed. The inertia properties were estimated by using AutoCad. Any discrepancies between the actual and the calculated mass components could cause inaccuracies in the estimation of the inertia matrix. Furthermore, just before conducting the experiments, a 2-DOF pendulum mechanism was attached to the end of the stick link. Therefore, the periodic motions of the manipulator caused swinging motions of the pendulum. Although its mass properties are known, the dynamic effects of this motion were neglected due to the lack of sensing capabilities. A more complicated friction model might also contribute in improving the results to some extent.

4.4.2 Stick Subsystem

The commanded input to the stick system and its associated variables are shown in Figure 4.10. Same line symbols are adopted, i.e. the solid line stands for actual measurement and dotted line is the prediction from dynamic models.

The predictions for the angular displacement and angular velocity are very close to the actual ones. The prediction for flow rate is also very good because of its relation to angular velocity. The predicted returning pressure profiles, however, are not close to the actual ones, although the driving pressures are close. The same reasons as that of the swing case can be applied to explain those minor discrepancies. Note also that the 2-DOF pendulum mechanism is assumed to be a point mass in the dynamic models. Its inertia properties, which have a bigger effect on the stick than on the swing, were not taken into account here.

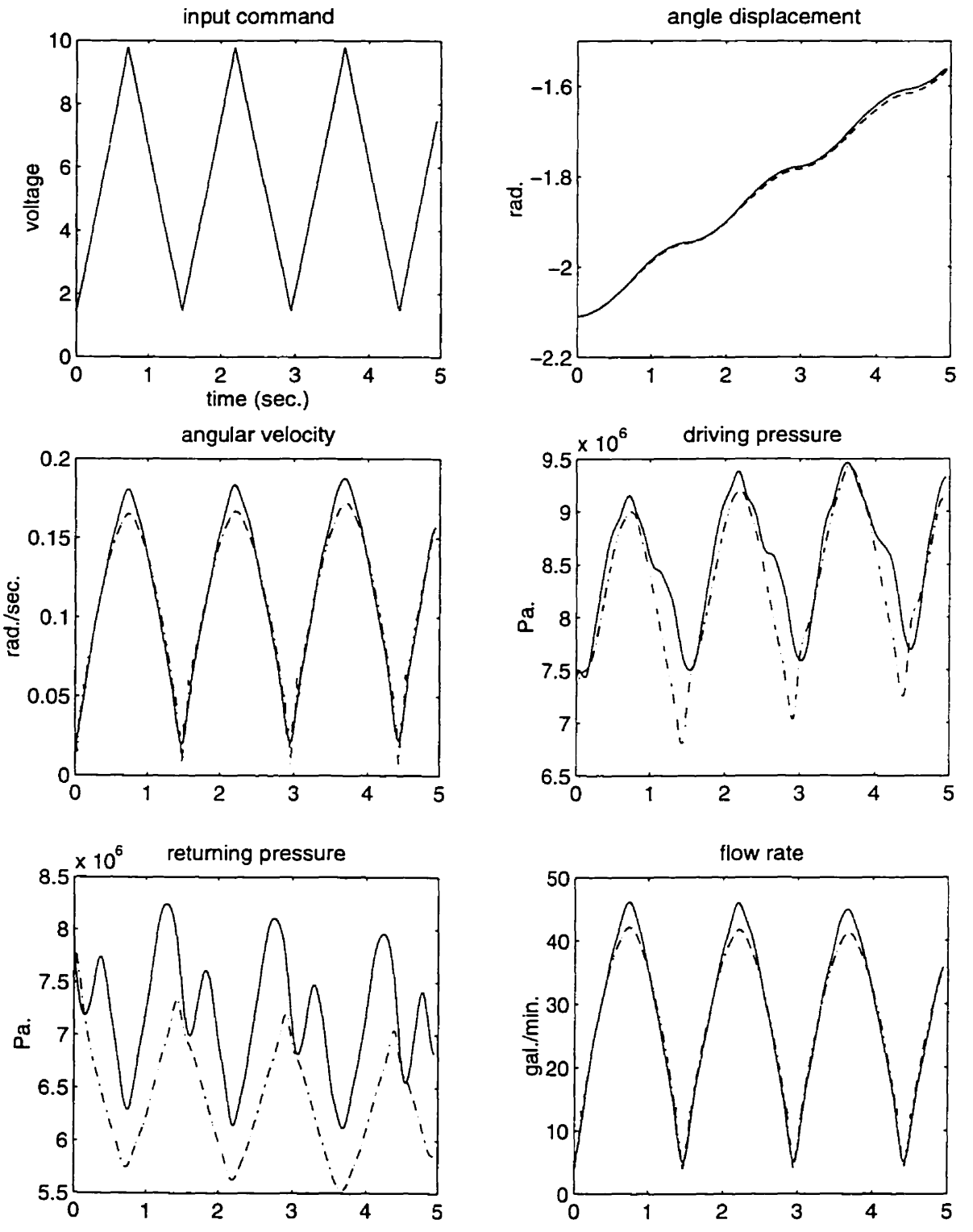

Figure 4.13 Model validation studies for stick model.

In addition, the overall inertia properties of the stick need to be reconsidered. The reason for the bumpy shapes of the returning pressure are not clear to us. Some further analysis showed that they could be attributed to the interaction of the single-ended cylinder configuration with symmetrical spool in the valves.

Although the dynamic model of the stick can not predict accurately the returning pressure, the main objective of these studies was to provide good prediction for angle displacement and joint angular velocity of manipulators. From this point of view, both the swing and the stick models are well-behaved and sufficient.

4.5 Summary

An overview of parameter identification was given first, including definitions, procedures and algorithms. Then, the sensors and the data-acquisition system used for the experiments were described. The detailed procedures and experimental setups for identifying each parameter were explained followed by the results. Discussions were provided explaining the model validation studies.

Two comprehensive dynamic models, i.e. the swing, boom and stick subsystems, were verified through a series of experiments. These models can be used to design control laws to improve the overall performance of the test vehicle.

5. Coordinated-Motion Controller Design

System modelling and parameter identification provided us with the foundation for model-based controller design. The test vehicle, the modified FERIC C-180 forwarder, like many other heavy-duty machines, has an articulated mechanical arm, actuated through coupled and complex hydraulic systems. The present control of these machines is by an operator who is actuating each link individually. This type of control requires significant visual feedback, judgment and skill to complete tasks. The operator is very busy with low-level mechanical manipulations instead of concentrating on high-level tasks, such as planning tree-cutting operations and choosing proper trees. Better control strategies that can ease the operating burden, are therefore needed.

In this chapter, some of the control strategies for teleoperation are reviewed and compared. Then several controller structures for resolved motion rate control schemes are evaluated from computer simulation results. Some guidelines for designing controllers for the test vehicle are given at the end.

5.1 Control Strategies in Teleoperation

Extensive studies have been carried out on the subject of teleoperation in the last two decades. Many control algorithms were proposed for different applications. Therefore, we have to identify which control modes are preferable in the heavy-duty forestry vehicles, and how they should be designed.

Position and rate control are the two common manual control modes in teleoperation. Kim *et al* evaluated the two modes based on the results of human operator performance, [17]. Position control is recommended for small-workspace teleoperation tasks. Such applications can be found in nuclear reactor teleoperators, surgical micromanipulators, and small dexterous telerobotic hands attached at the end of a main telemanipulator. Rate control, on the other hand, is suggested for slow wide-workspace teleoperation tasks. Most felling forestry tasks belong in the later category.

Currently, the control strategy implemented on heavy-duty forestry machines is a one-to-one mapping between lever displacements and corresponding link motions. This type of control, although easy to implement, requires the experience and skill of the operator to produce coordinated-motion necessary for most routine operations. The operator is required to learn what joint speeds are necessary at each instant to obtain the desired direction and speed of the end-effector. Since the control levers in these machines do not directly translate the intuitive actions initiated by the operator into the end-effector motion, the operator is kept busy with low-level adjustments. Not only lengthy and costly training periods are required, but also much of the operator's concentration is demanded to concurrently accomplish the work at hand while avoiding damage to the machine, or worse yet, inflicting personal injuries.

In 1969, Whitney proposed the resolved motion rate control algorithm to assist amputees to learn the usage of artificial prostheses and to perform contact tasks. Resolved

motion means that Cartesian space commands or trajectories are resolved to individual actuator commands, so that coordinated motion in Cartesian space is achieved, [38]. This algorithm was further implemented by Lawrence to control excavator-type machines. With the help of computer-control technology, the multi-lever system is reduced to a single joystick. The computer translates desired direction of motion of the end-effector from movement of the joystick into the necessary motion of each manipulator joint to achieve the desired end-effector motion.

Several advantages of resolved motion rate control can result if implemented to forestry machines:

1. Simplified machine operation. The controls are intuitive and relate intuitively to the tasks. Machine operation will be much simpler.

2. Improved productivity. Easier operation requires less correction to the position of the links of the machine and therefore, the task can be completed more rapidly.

3. Reduced learning time. Simpler operation allows novices to concentrate on task planning as opposed to learning the operation of the machine.

4. Improved safety. Operator's concentration is devoted to plan tasks and observe surroundings. Therefore, less accidents should occur.

Several advanced control modes were studied and operator performance in teleoperation was evaluated. Das *et al.* evaluated seven manual control modes which are combinations of manual position or resolved motion rate control with alternative control schemes for force reflection and remote manipulator compliance, [7]. It was found that force reflection significantly improves operator performance in all the tested control modes. However, the studies were conducted for a particular task, the repair of the Solar Maximum Satellite using teleoperators. The application of their results to forestry operations might not be appropriate due to the complex and different nature of these tasks. Even if applicable, non-

technical reasons, such as cost, may also prevent application of force feedback. For the needs of this project, it was decided to implement a resolved motion rate control without force reflection.

5.2 Coordinated-Motion Control Schemes Evaluation

5.2.1 Choices of Control Schemes

The objective of resolved motion rate control is to make the end-effector follow joystick commands given by an operator in Cartesian coordinates. A highly simplified control schematic diagram is shown in Figure 5.1.

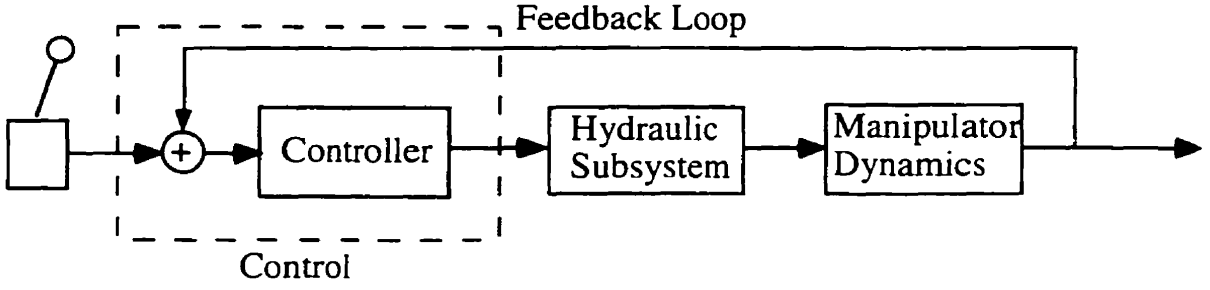

Figure 5.1 Generalized control schematic diagram.

In general, implementation of control laws requires knowledge of the kinematics, and the dynamics of the manipulator and hydraulic actuation system. However, a simplified three-degree-of-freedom manipulator model mimicking the swing, boom and stick operation is set up for the purpose of this evaluation. A first-order system model (manipulator velocity output to voltage input to valves) with natural frequency of 2 Hz is used for the three degree-of-freedom manipulator and actuator dynamics. However, the actual kinematics relationship is preserved.

The resolved motion rate control can be implemented by using either a position servo or a rate servo for each link. The basic difference between position and velocity servo is what type of output the controller is responsible for. The position servo uses a position signal and regulates manipulator joint positions, while the velocity servo uses a velocity signal and regulates manipulator joint velocities. In the resolved motion control regime, the desired manipulator joint velocity is integrated once before it is fed back to position servo and that is not required for the velocity servo.

Four possible control schemes can be composed by using inverse Jacobian or inverse kinematics in conjunction with a position or velocity servo, as shown in Figure 5.2. Among them, inverse kinematics seems to be an intuitive choice for position servo at first glance, see Figure 5.2(b). However, in order to integrate the end-effector velocity signals, its position has to be continuously fed to the integrators. This requires the measurements of the joint angles and performing forward kinematics computation to convert joint positions into end-effector positions. Therefore, extra computing time is demanded and can cause problems in realization of real-time control algorithms. In Figure 5.2(a), the combination of inverse kinematics and a velocity servo model needs a differentiator to process position signals within the control loop, which is not preferred in practice due to noise concerns. Note also that there are integrators in (b) and (d). However, they are outside of the control loops and are present only to calculate the end-effector velocities in computer simulations. Eventually, two control schemes, (c) and (d), were chosen for further evaluation. Note that K^- is a pre-loop shaping gain aiming at bringing the steady-state error to zero.

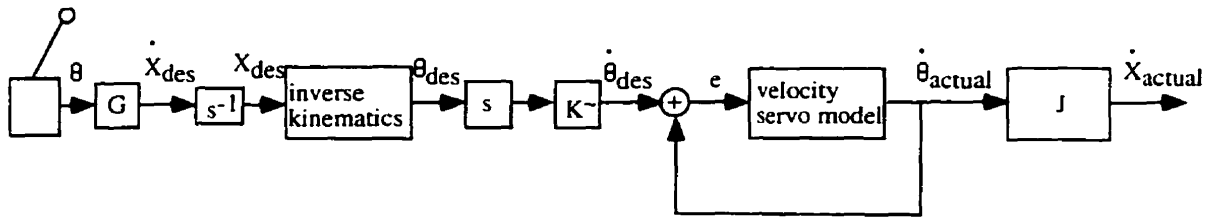

(a) inverse kinematics with velocity servo model

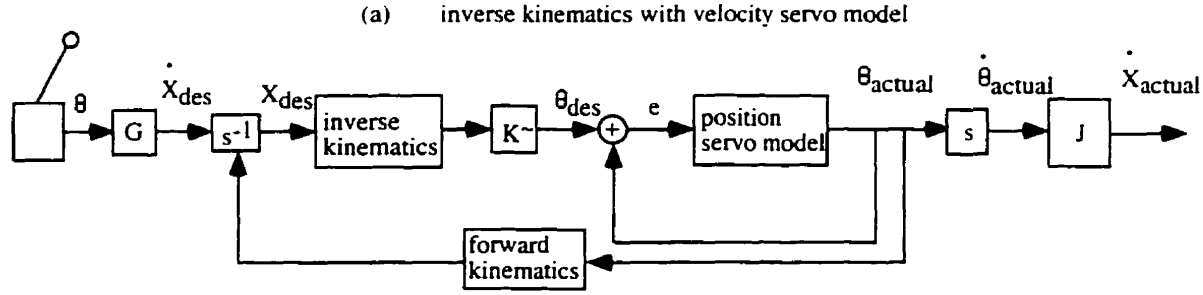

(b) inverse kinematics with position servo model

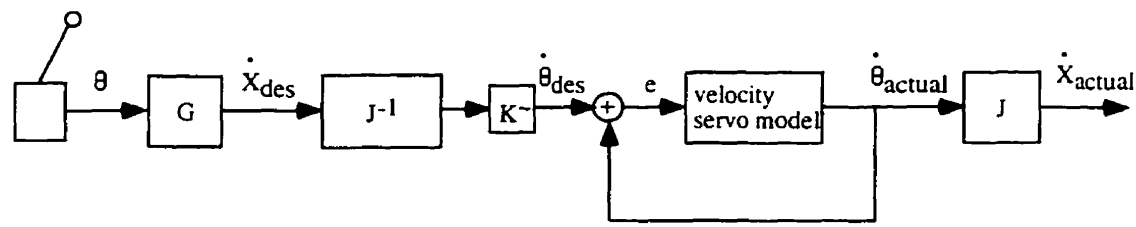

(c) inverse Jacobian with velocity servo model

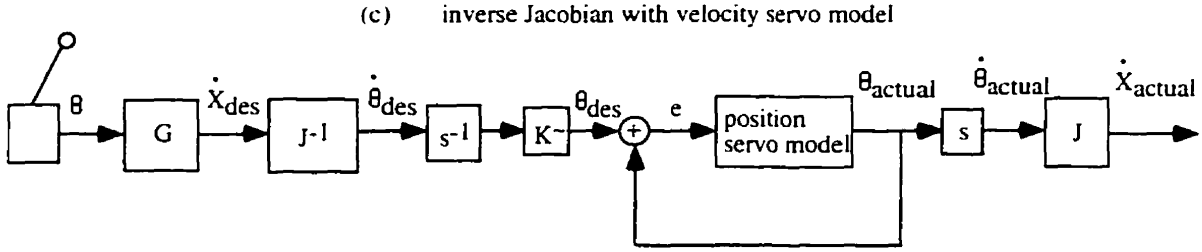

(d) inverse Jaconbian with position servo model

Figure 5.2 Control schematics for velocity and position servo controllers.

The symbols used in Figure 5.2 are defined as the following

θ: joystick deflection angle

θ_{real}, θ_{des}: actual and desired manipulator joint position

$\dot{\theta}_{real}$, $\dot{\theta}_{des}$: actual and desired manipulator joint velocity

X_{real}: actual end-effector position

$\dot{X}_{real}$, $\dot{X}_{des}$: actual and desired end-effector velocity

G: joystick position and velocity gain

J, J^{-1}: Jacobian and inverse Jacobian relationship between actuators and end-effector

K^{-}: pre-loop shaping gain

The position and velocity servo controllers per manipulator degree-of-freedom are shown in Figure 5.3. The gains in the feedback loop were chosen such that both models have the same closed-loop frequency for comparison.

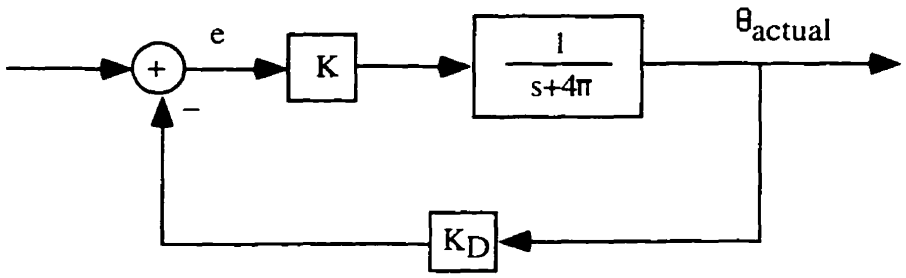

(b) velocity servo model

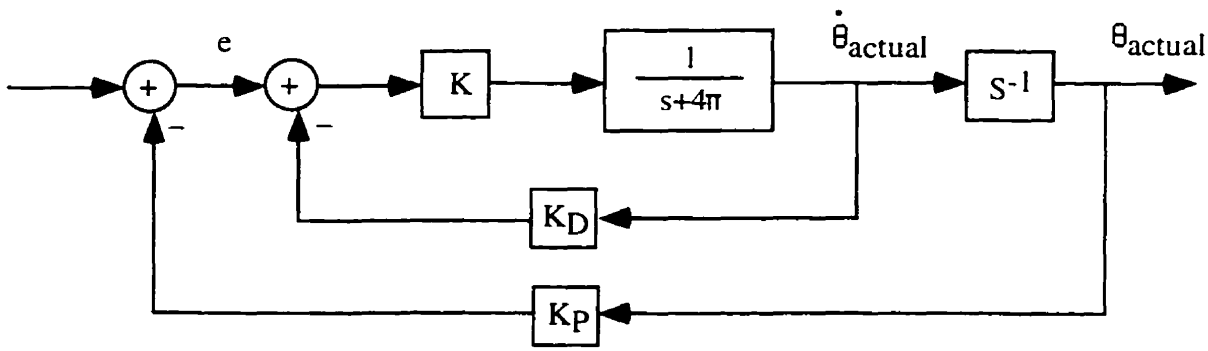

(a) position servo model

Figure 5.3 Schematics of simplified velocity and position servo controllers.

As shown in Figure 5.2, end-effector desired velocities indicated by joystick deflections are directly transformed to desired joint angular velocities (e.g. swing) or

As shown in Figure 5.2, end-effector desired velocities indicated by joystick deflections are directly transformed to desired joint angular velocities (e.g. swing) or translational velocities of joint (e.g. boom and stick) by employing the inverse Jacobian transformation. The desired velocity of each joint is then applied to the position or velocity servo controllers. Then the actual end-effector position or velocity is obtained using either a Jacobian or direct kinematics.

Computer simulation results of end-effector velocity and position comparison are shown in Figure 5.4 and Figure 5.5. Note that in the first four graphs of both figures, the solid lines represent the desired end-effector velocity or position, and dashed lines are for velocity servo while dotted lines for position servo. Then, in the last four graphs, the solid lines represent velocity servo error, and the dashed lines are for the position servo error. Step inputs are given in the x and z axis at different times, and a sinusoidal command is specified for the y axis end-effector motion. By comparing the end-effector velocity and position response of both models in Figure 5.4 and Figure 5.5, it can be observed that the velocity servo has faster response than the position servo. Therefore, much smaller velocity error is generated, and in correspondence, more accurate positioning results for the end-effector. If the linear manipulator model is known exactly, by carefully choosing pre-loop shaping gains, the combination of inverse Jacobian with velocity servo shows superior characteristics compared with the combination of inverse Jacobian with position servo.

5.2.2 Effects of Manipulator Natural Frequency

In the nominal linear model, we assumed that the natural frequency of the system is 2 Hz, which is a reasonable frequency for the mechanical system. However, actual manipulator systems have nonlinear characteristics and the natural frequencies change at different operating conditions. For the worst case scenario, the natural frequency of the system is

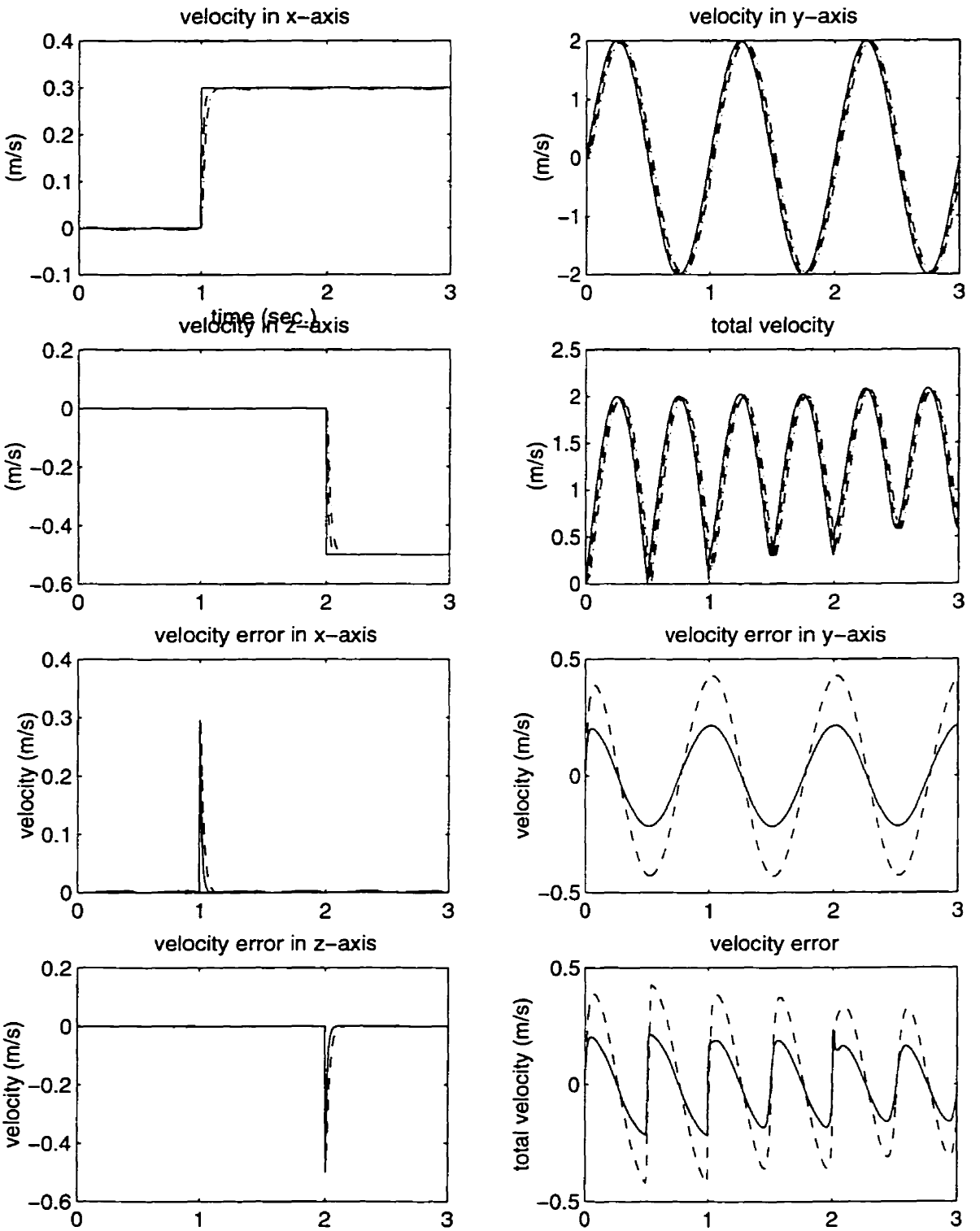

Figure 5.4 End-effector velocity comparison.

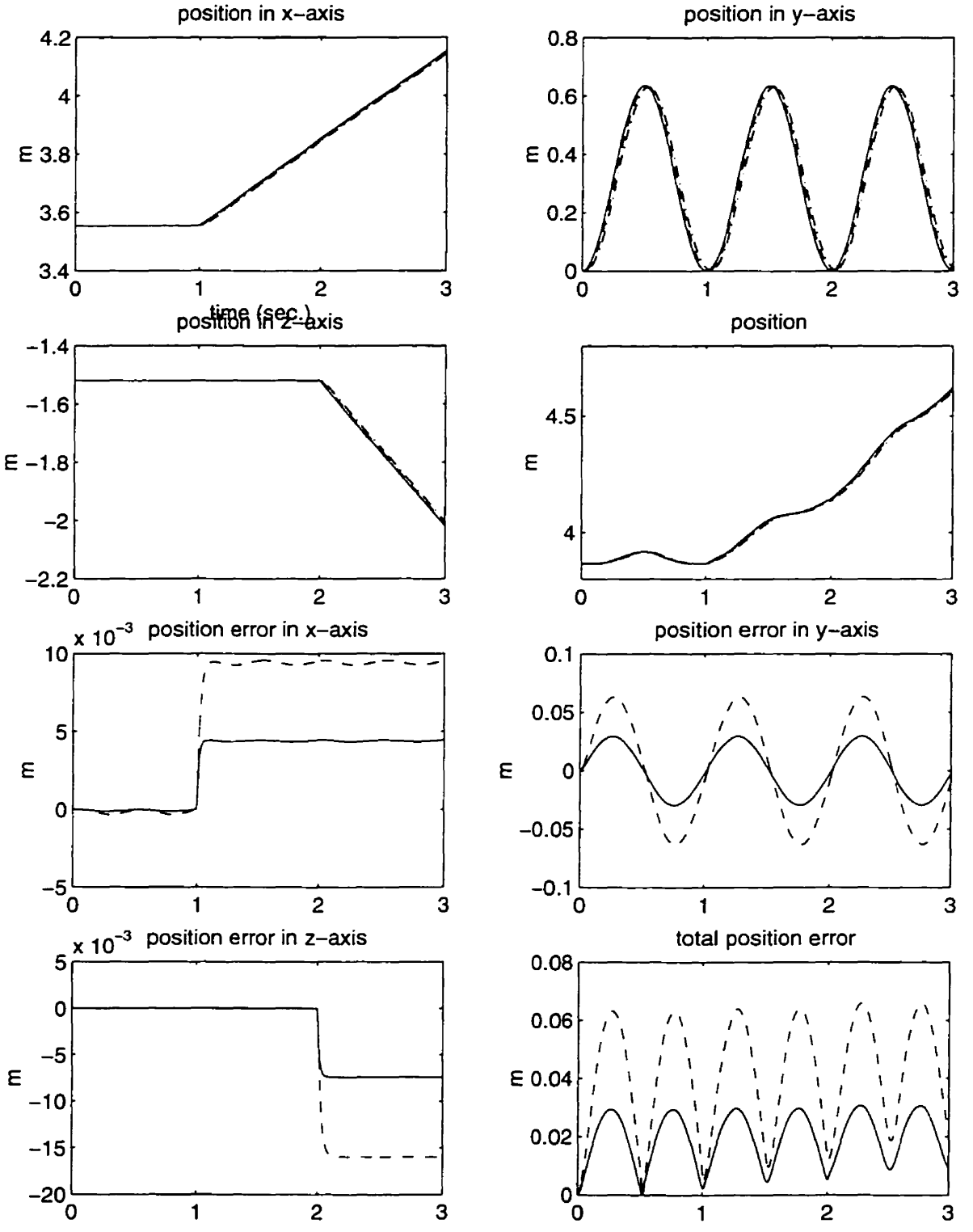

Figure 5.5 End-effector position comparison.

assumed to decrease 10 times to 0.2 Hz. After readjusting the pre-loop shaping gains for both models, simulation results show that velocity servo model is superior over the position servo, although the error in both cases increases comparing to the system with natural frequency at 2 Hz, as shown in Figures 5.6 and 5.7. In these two figures same line symbols are used for each variables as in the previous figures. For the first four graphs of both figures, the solid lines represent desired end-effector velocity or position, dashed lines are for velocity servo and dotted lines for position servo. Then, in the last four graphs, the solid lines represent velocity servo error and the dashed lines are for position servo error. As we observed from the figures, the velocity error in the y-axis increases slightly from $0.20\,m/s$ to $0.25\,m/s$ for the velocity servo, and from $0.4\,m/s$ to $0.5\,m/s$ for the position servo. Also, the corresponding position error increases from $0.025\,m$ to about $0.035\,m$ for velocity servo and from $0.065\,m$ to about $0.075\,m$. The result can be explained by evaluating the transfer functions of the systems. Since the poles move closer to the origin, the system response is slower and this sluggishness deteriorates the tracking capability of both systems.

5.2.3 Effects of the Accuracy of Manipulator Models

A linear dynamics model was chosen to evaluate the two control schemes discussed in the previous sections. The pre-loop shaping gain is adjusted according to the model. However, the non-linearity of the actual system makes a fixed pre-loop shaping gain effective only for operations in certain ranges. As shown in Figures 5.8 and 5.9, by using the nominal pre-loop shaping gain, the superiority of velocity servo model disappears even with only a 20% variation of the natural frequency in the systems. The position servo model, on the other hand, is very robust to this test. Note that in these two figures same line symbols are

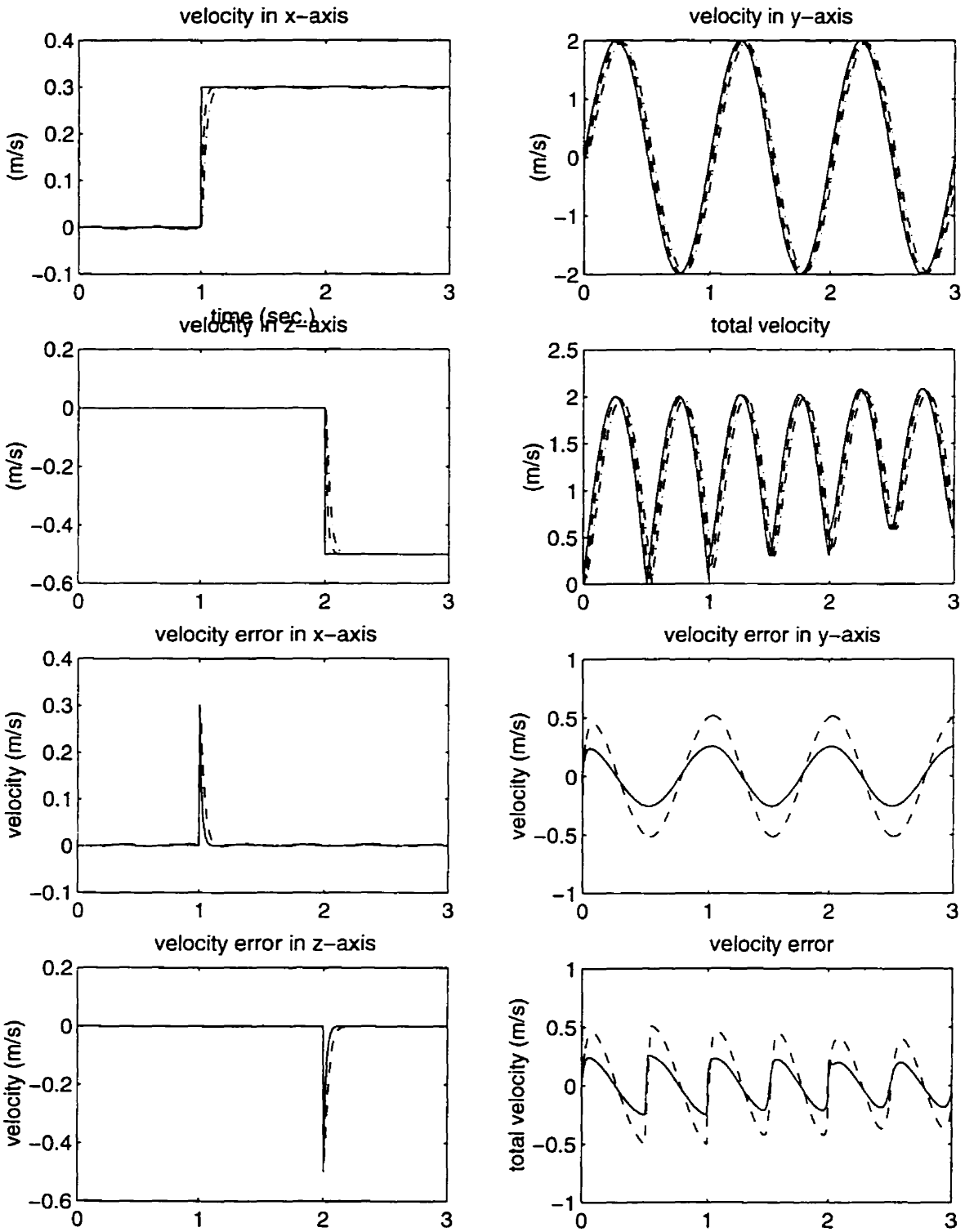

Figure 5.6 End-effector velocity comparison for actuator natural frequency at 0.2 Hz.

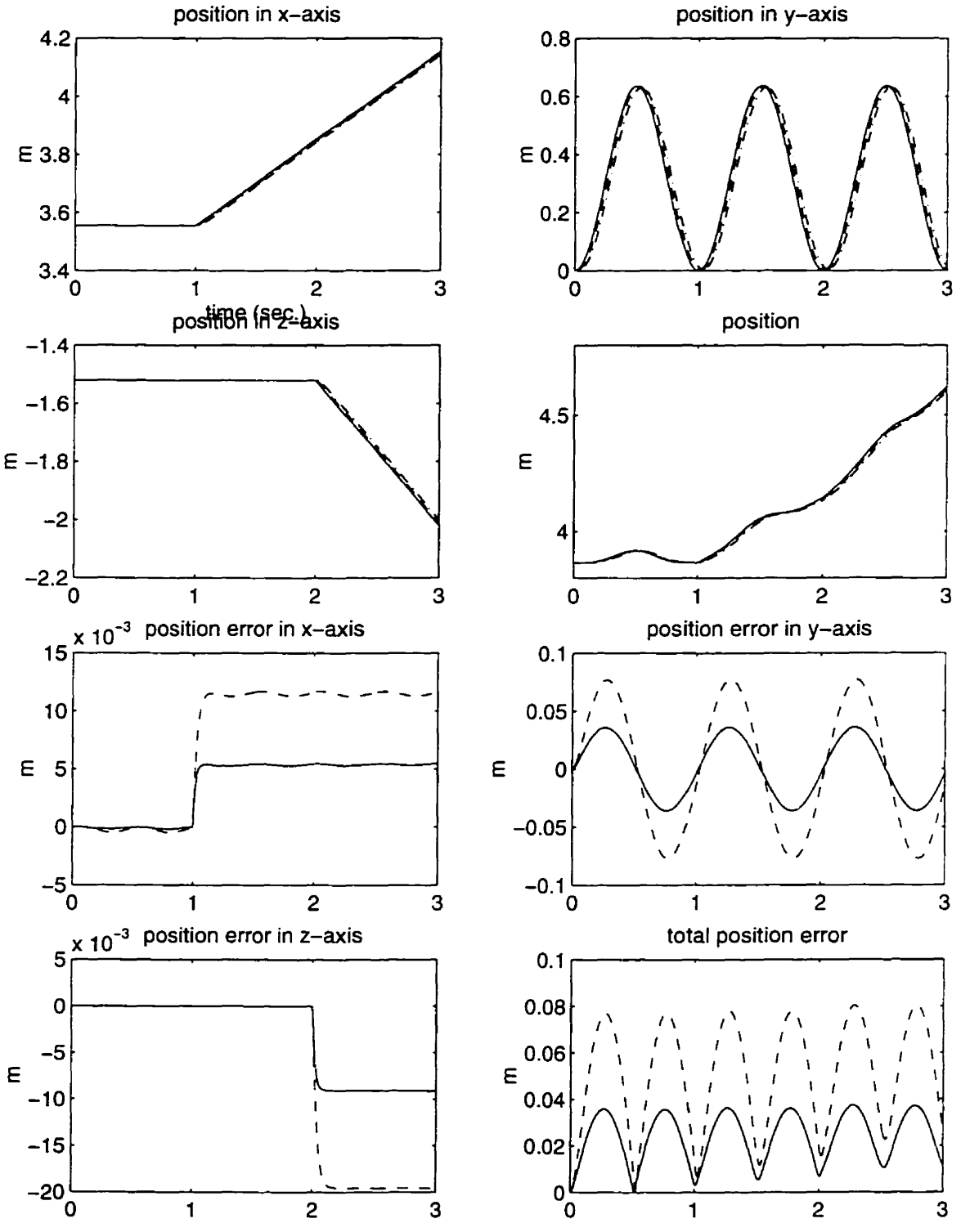

Figure 5.7 End-effector position comparison for actuator natural frequency at 0.2 Hz.

used for each variables as in the previous figures. As we observed from the two figures, the control scheme with velocity servo model does not behave properly, especially to a step input. The end-effector can not follow the input commands in the x and z directions as closely as in the previous situations. That results in a bigger error in these two directions, as compared to the control scheme with position servo. Also, the corresponding position error simply drifts away in response to the step inputs, which results bigger end-effector position error than that with the position servo.

We have evaluated two control schemes, using an inverse Jacobian with a position and a velocity servo scheme, and employing a linear dynamic model. The control scheme with velocity servo results in a faster response and generates more accurate end-effector velocity and position than that with position servo model, provided that the system dynamic models are known or do not deviate much from the nominal operating conditions. Due to time constraints, the performance of the system with actual dynamic models is not evaluated in this thesis. Nevertheless, computer simulation on both schemes are necessary before implementing either of them on the test vehicle.

5.3 Summary

Controller design follows naturally after completion of modelling and parameter identification. For heavy-duty forestry machines, like the FERIC forwarder, the resolved motion rate control strategy offers advantages over conventional joint-based control in the sense of improvements on productivity, operation easiness and operator safety. Under this framework, four control schemes, i.e. the combination of inverse Jacobian and inverse kinematics with velocity and position servo, were introduced and evaluated. Two of them,

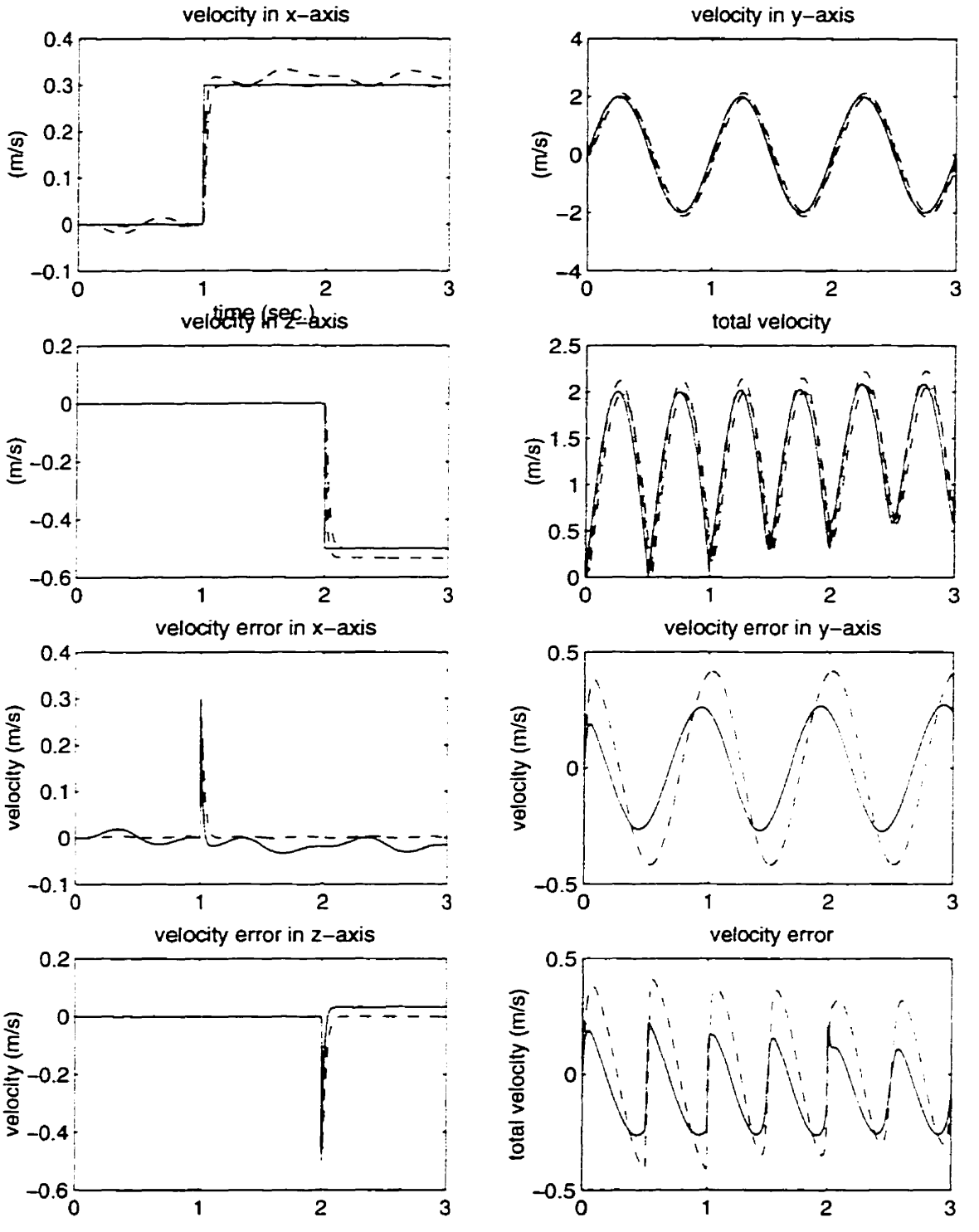

Figure 5.8 End-effector velocity comparison at nominal pre-loop shaping gain, but with a 20% change in nominal system natural frequency.

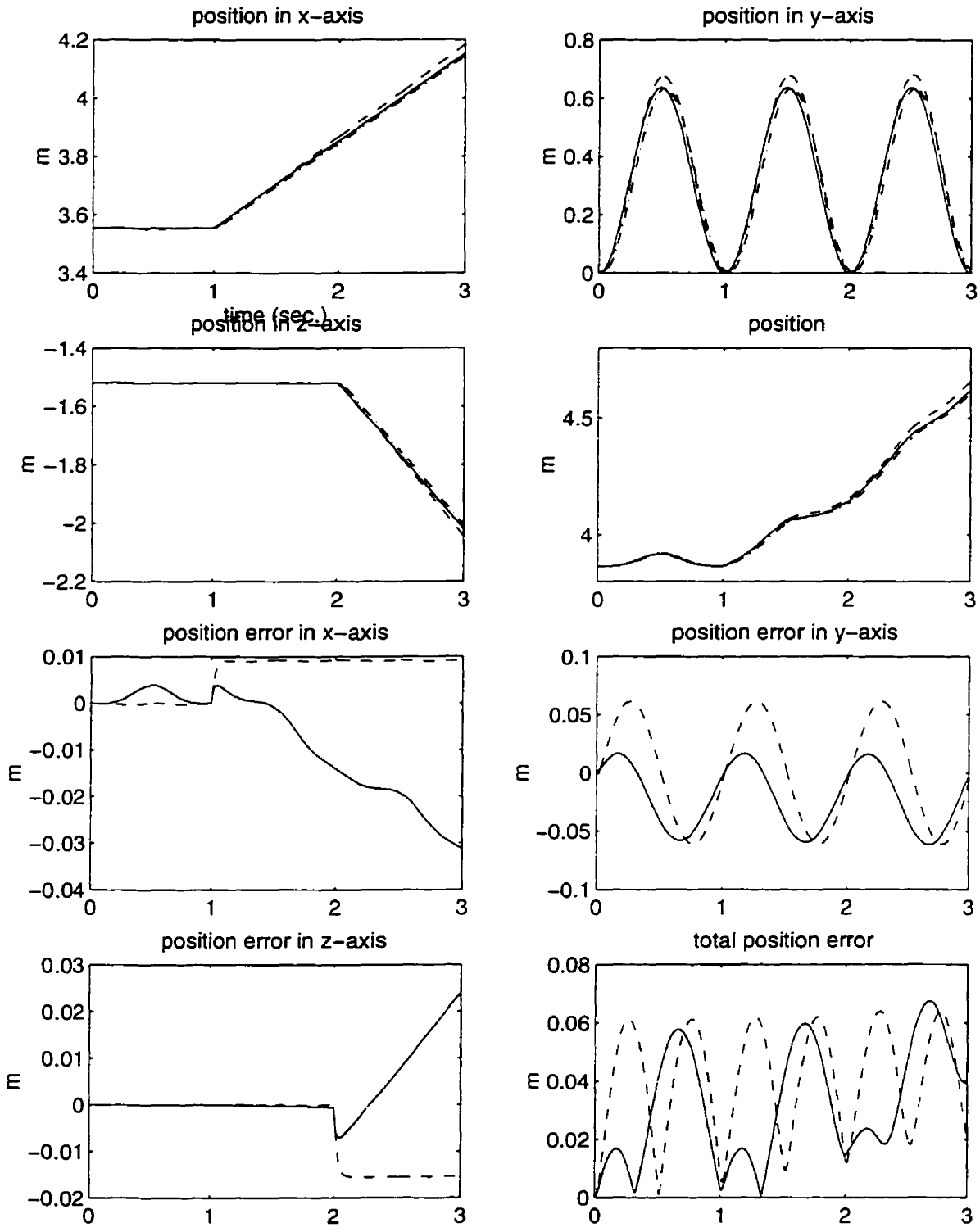

Figure 5.9 End-effector position comparison at nominal pre-loop shaping gain, but with a 20% change in nominal system natural frequency.

employing an inverse Jacobian with either a position or a velocity servo were further studied under various conditions. The velocity servo scheme resulted in a faster response and generated more accurate end-effector velocity and position than that of the position servo scheme, provided that the system dynamic model is known or does not deviate much from nominal operating conditions. The results can be further analyzed by using the actual non-linear dynamic models of the swing, boom and stick systems.

6. Conclusions

Fundamentals of the electrohydraulic actuation in mobile machines were reviewed. Comparisons of hydraulic systems with other actuation systems were illustrated in terms of their merits on important characteristics such as high power-to-weight ratios, high stiffness and fast speed of response. Those advantages make hydraulics widely applied in high-power-demand systems, such as aerospace and heavy-duty mobile equipment. An overview of components used in hydraulic actuation systems, including choices of fluid power sources, valves, actuators and some other related parts were explained in detail.

A mathematical model that closely describes system characteristics can be implemented in designing controllers, for developing CAD tools, and in this project, developing graphical simulators for training novices. The linear graph method, which represents the topological relationship of interconnections between different systems and assists in the development of a series of lumped-parameter models in a unified fashion, was employed to develop a set of dynamic models. Individual models for each electrohydraulic components were derived under some mild assumptions. These include models for pumps, valves,

transmission lines, hydraulic cylinders and motors existing on the test vehicle. Then, two sets of fourth-order state-space nonlinear dynamic models of the swing subsystem, and of the boom and stick subsystems were derived based on the models of individual components.

One of the objectives of modelling the electrohydraulic actuation systems is to predict the dynamic behavior of the articulated manipulator of the test vehicle by combining their dynamics with manipulator dynamics. The relationship between pressure difference across actuators and torque output to links, corresponding angular velocity generated from torque and flow rate in the hydraulic systems, is setup in gyrator form by the linear graph method.

A valid mathematical model not only has the right structure, but also the numerical values of the parameters involved must be also accurate. Identification methods were used to identify all the parameters in the actuation models. Off-line least-square identification methods were implemented. The experiments were designed to estimate the smallest possible number of parameters at one time. A series of new experimental procedures for identification were proposed and explained. The model validation studies show that the values of parameters are accurate and the two models closely represent the characteristics of the systems.

Finally, accurate models provide the foundations for controller design. For heavy-duty mobile machines, like the modified FERIC forwarder, the resolved motion rate control strategy shows superiority over the conventional joint-based control in the sense of improvement on productivity, operation easiness and operator safety. Under this framework, control schemes, namely, an inverse Jacobian with velocity and position servo controllers, were introduced and evaluated under various assumptions. The velocity servo scheme results in a faster response and generates more accurate end-effector velocity and position than that of a position servo model, provided that the system dynamic models are known or do not deviate much from nominal operating conditions.

Several interesting issues remain to be further explored and developed from the present work. The results of control strategy studies can be further analyzed by using non-linear dynamic models of the swing, the boom and stick systems instead of a first-order transfer function. Eventually, the results of this study will guide the implementation of controllers on the test vehicle. Further analysis for the prediction of returning pressure profiles on the boom and stick subsystems are needed for the sake of perfecting the model, although from a control point of view, accurate prediction of joint angle and joint velocity is far more important.

References

[1] Atkeson, C. G., An, C. H., Hollerbach, J. M., Estimation of Inertial Parameters of Manipulator Loads and Links. *The International Journal of Robotics Research*, 5(3):101-119, 1986.

[2] Bangert, H., Update on Proportional Valve Performance. *Hydraulics & Pneumatics*, page 41-46, June, 1992.

[3] Blackburn, J. F., Reethof, G., Shearer, J.L., *Fluid Power Control*. Technology Press of M.I.T. and John Willey, 1960.

[4] Blackwell, W. A., *Mathematical Modeling of Physical Networks*. Macnillan Publishing Co., 1967.

[5] Courteau, J., Robotics in Canadian Forestry. *IEEE Canadian Review - Winter*, pages 10-13, 1994.

[6] Craig, J. J., *Introduction to Robotics: Mechanics and Control, 2nd edition*. Addison-Wesley Publishing Co., 1989.

[7] Das, H., Zak, H., Kim, W. S., Bejczy, Schenker, P. S., Operator Performance with Alternative Manual Control Modes in Teleoperation. *Presence*, 1(2):201-217, 1992.

[8] De Silva, C. W., *Control Sensors and Actuators*. Prentice Hall, 1989.

[9] Franklin, G.F., Powell, J. D., Emami-Naeini, A., *Feedback Control of Dynamic Systems, 3rd edition*. Addison-Wesley Publishing Co., 1994.

[10] Gupta, M. M., Sinha, N. K., *Intelligent Control Systems*. IEEE Press, 1996.

[11] Harwick, W., Hydraulic Filtration Technology for the 90's. *Hydraulics & Pneumatics*, page 55-59, September, 1990.

[12] Henke, R. W., *Fluid Power Systems & Circuits*. Hydraulics & Pneumatics, 1983.

[13] Herman, T., Bonicelli, B., Sevila, F., Monsion, M., Bergeon, B., Bond-Greph Modelling and Identification of a High Power Hydraulic System. *Eleventh IASTED International Conference Modelling, Identification and Control*, Innsbrunk, Austria, 1992

[14] Hollerbach, J. M., Hunter, I. W., Ballantyne, J., A Comparative Analysis of Actuator Technologies for Robotics. *The Robotics Review*, 2nd edition, pages 301-342, 1991.

[15] Hsia, T.C., *System Identification - Least Squares Methods*. Lexington books, 1977.

[16] Keyworth, I., Fluid Power in Action: Mobile Equipment. *Hydraulics & Pneumatics*, page 31-32, August 1991.

[17] Kim, W. S., Tendick, F., Ellis, S. R., Stark, L. W., A Comparison of Position and Rate Control for Telemanipulations with Consideration of Manipulator System Dynamics. *IEEE Journal of Robotics and Automation*, RA-3(5):426-436, 1987.

[18] Koenig, H. E., Tokad, Y., Kesavan, H. K., Hedges, H. G., *Analysis of Discrete Physical Systems*. McGraw-Hill Book Co., 1967.

[19] Krus, P., Weddfelt, K., Palmberg, J., Fast Pipeline Models for Simulation of Hydraulic Systems. *Journal of Dynamic Systems, Measurement, and Control*, 116:132-136, 1994.

[20] Lawrence, P.D., Sauder, B., Wallersteiner, U., Wilson, J., Teleoperation of Forest Harvesting Machines. Proceedings of the Symposium of Robotics in Forestry, Quebec, Canada, 1990.

[21] LeQuoc, S., Xiong, Y. F., Cheng, R. M. H., Identification and Control of Nonliear System. *International Off-Highway & Powerplant Congress & Exposition*, 921622, 1992.

[22] Martin, D. J., Burrow, C. R., The Dynamic Characteristics of an Electrohydraulic Servovalve. *Journal of Dynamic Systems, Measurement, and Control*, 1976.

[23] McLain, T. W., Iversen, C. C., Jacobsen, S. C., Development, Simulation, and Validation of a Highly Nonlinear Hydraulic Servosystem Model. *American Control Conference*, pages 385-391, Pittsburgh, Pennsylvania, June 1989.

[24] Merritt, H. E., *Hydraulic Control Systems*. John Willey & Sons, 1967.

[25] Nikiforuk, P. N., Ukrainetz, P. R., Tsai, S. C., Detailed Analysis of a Two-Stage Four-Way Electrohydraulic Flow-Control Valve. *Journal of Mechanical Engineering Science*, 11(2), 1969.

[26] Norton, J. P., *An Introduction to Identification*. Academic Press, 1986.

[27] Rivin, E. I., *Mechanical Design of Robots*. McGraw-Hill Book Co., 1987.

[28] Rowell, D., Wormley, D. N., *System Dynamics: An Introduction*. Lecture Notes, 1993.

[29] Sarkar, S., *Dynamic Modeling of an Articulated Forestry Machine for Simulation and Control* Master's Thesis, McGill University, 1996

[30] Sepehri, N., Lawrence, P. D., Sassani, F., Frenette, R., Resolved-Mode Teleoperated Control of Heavy-Duty Hydraulic Machines. The Journal of Dynamic Systems, Measurement and Control, 1994.

[31] Shearer, J. L., Murphy, A. T., Richardson, H. H., *Introduction to System Dynamics*. Addison-Wesley Publishing Co., 1967.

[32] Singh, N., Zghal, H., Sepehri, N., Balakrishnan, S., Lawrence, P.D., Coordinated-Motion Control of Heavy-Duty Industrial Machines with Redundancy. Robotica, 13:623-633, 1995.

[33] Stewart, H. L., *Hydraulics for off-the-road Equipment*. Theodore Audel & Co., 1985.

[34] Tonyan, M. J., *Electronically Controlled Proportional Valves*. Marcel Dekker, Inc., 1985.

[35] Walters, R. B., *Hydraulic and Electrohydraulic Control Systems*. Elsevier Applied Science, 1991.

[36] Watton, J., *Fluid Power Systems*. Prentice Hall, 1989.

[37] Watton, J., Tadmori, M. J., A Comparison of Techniques for the Analysis of Transmission Line Dynamics in Electrohydraulic Control Systems. *Applied Mathematics Modelling*, 12:457-466, 1988.

[38] Wells, D. L., Iversen, E. K., Davis, C. C., Jacobsen, S. C., An Investigation of Hydraulic Actuator Performance Trade-Offs Using a Generic Model. *Proceedings of IEEE International Conference on Robotics and Automation*, pages 2168-2173, 1990.

[39] Whitney, D. E., Resolved Motion Rate Control of Manipulators and Human Prostheses. *IEEE Transactions on Man-Machine Systems*, MMS-10(2):47-53, 1969.

[40] Yang, W. C., Tobler, W. E., Dissipative Modal Approximation of Fluid Transmission lines Using Linear Friction Model. *Journal of Dynamic Systems, Measurement, and Control*, 113:152-161, 1991.

[41] Zhou, J. J., Conrad, F., Identification for Modeling and Adaptive Control of Hydraulic Robot Manipulators. *Identification and System Parameter Estimation 1991*, 2:705-710, 1992.

APPENDIX A

The kinematics relationship from the position of the boom and stick cylinders to the boom and stick joint positions.

$$q_{bm} = \text{a}\cos\left(\frac{l_{1b}^{\ 2} + l_{2b}^{\ 2} - x_{bm}^{\ 2}}{2 \cdot l_{1b} \cdot l_{2b}}\right) - \text{delta} - \text{si2}$$

$$q_{sk} = \text{a}\cos\left(\frac{l_{1s}^{\ 2} + l_{2s}^{\ 2} - x_{sk}^{\ 2}}{2 \cdot l_{1s} \cdot l_{2s}}\right) - \pi - \text{si1}$$

The Jacobian from the velocity of the boom and stick cylinders to the boom and stick joint velocity.

$$\begin{bmatrix} \dot{q}_{bm} \\ \dot{q}_{sk} \end{bmatrix} = \begin{bmatrix} j_{bm} & 0 \\ 0 & j_{sk} \end{bmatrix} \cdot \begin{bmatrix} \dot{x}_{bm} \\ \dot{x}_{sk} \end{bmatrix}$$

$$j_{bm} = \frac{x_{bm}}{l_{1b} \cdot L_{2b} \cdot \sqrt{1 - (l_{1b}^{\ 2} + L_{2b}^{\ 2} - x_{bm}^{\ 2})^2 / (4 \cdot l_{1b}^{\ 2} \cdot L_{2b}^{\ 2})}}$$

$$j_{sk} = \frac{x_{sk}}{l_{1s} \cdot l_{2s} \cdot \sqrt{(1 - (l_{1s}^{\ 2} + L_{2s}^{\ 2} - x_{sk}^{\ 2})^2 / (4 \cdot l_{1s}^{\ 2} \cdot L_{2s}^{\ 2})}}$$

Constant terms in the above equations:

$l_{1s} = 1.933956$ m

$l_{2s} = 0.884292$ m

$l_{1b} = 0.5625397$ m

$l_{2b} = 1.786382$ m

$\text{si1} = 2.5 \cdot \pi / 180$

$\text{si2} = 0.31 \cdot \pi / 180$

$\text{delta} = 61.7 \cdot \pi / 180$

APPENDIX B

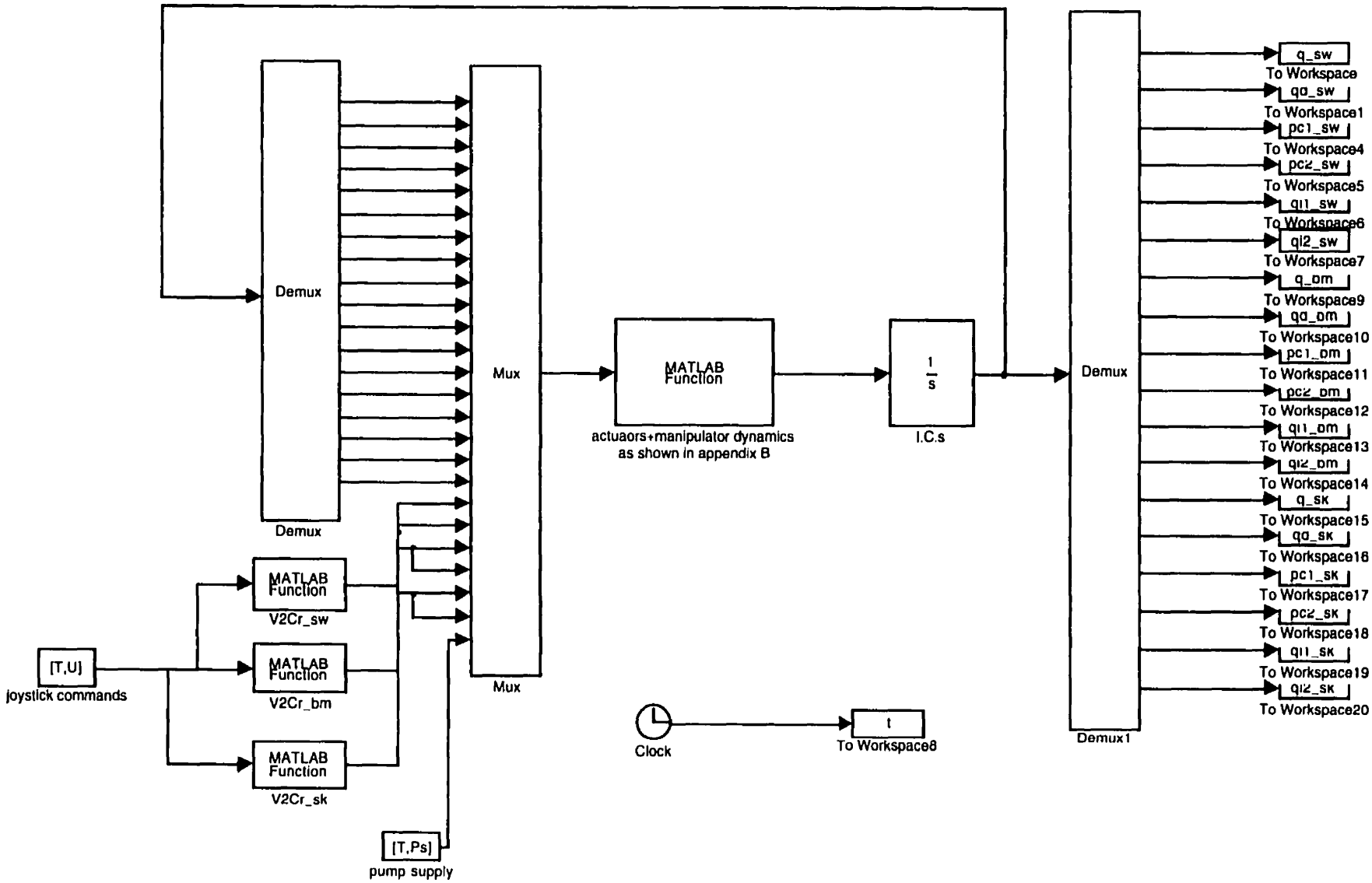
Demux
Demux
Mux
Mux
MATLAB Function
actuaors+manipulator dynamics as shown in appendix B
1/s
I.C.s
Demux
Demux1
q_sw
To Workspace
qa_sw
To Workspace1
pc1_sw
To Workspace4
pc2_sw
To Workspace5
ql1_sw
To Workspace6
ql2_sw
To Workspace7
q_bm
To Workspace9
qa_bm
To Workspace10
pc1_bm
To Workspace11
pc2_bm
To Workspace12
ql1_bm
To Workspace13
ql2_bm
To Workspace14
q_sk
To Workspace15
qa_sk
To Workspace16
pc1_sk
To Workspace17
pc2_sk
To Workspace18
ql1_sk
To Workspace19
ql2_sk
To Workspace20
MATLAB Function
V2Cr_sw
MATLAB Function
V2Cr_bm
MATLAB Function
V2Cr_sk
[T,U]
joystick commands
[T,Ps]
pump supply
Clock
t
To Workspace8

```
% swing-boom-stick file

%This is the M-file to simulate the dynamical characteristics of the
%havester with numerical values of parameters estimated from experiemtns.


function xdot = sbs_real(x)


%operation of valves - inputs to the system

Crv1_sw = x(19);
Crv2_sw = x(20);
Crv1_bm = x(21);
Crv2_bm = x(22);
Crv1_sk = x(23);
Crv2_sk = x(24);

Ps = x(25)*6894.7;      %actual pump pressure


%Assign estimated numerical values to parameters

lamda = 0*pi/180;
g = 9.81;
gx = 0;
gy = g*sin(lamda);
gz = g*cos(lamda);
m3s = 544.32;           % mass of stick in kg (1200 lbs)
%-------------------------------------------------------
m4 = 2.2 * 700 / 2.2;   % mass of the simulated head in  kg
%-------------------------------------------------------
m3 = m3s+m4;
m2 = 635.04;            % mass of boom in kg (1400 lbs)
m1 = 907.2;             % mass of base in kg (2000 lbs)
x3s = 1.6971698;        % c.m. of stick in m  page 34d
y3s = .193368;
z3 = 0;
l1 = .1524;             % length of base in m (6 ")
l2 = 4.118356;          % boom length in m (162.14 ")
l3 = 4.2991;            % stick length in m
x3 = (m3s*x3s+m4*l3)/m3;
y3 = m3s*y3s/m3;
x2 = 1.9882162;
y2 = .1453077;
z2 = 0;
x1 = .053975;
y1 = 0;

% LINKAGE GEOMETRY
l1s = 1.933956;
l2s = .884292;
l1b = .5625397;
l2b = 1.786382;
si1 = 2.5*pi/180;
si2 = .31*pi/180;
delta = 61.7*pi/180;

l = sqrt((x3-x3s)^2+(y3-y3s)^2);

% INERTIA MATRIX
I3zzs = 867.20018;
I3yys = 535.22412;
I3zz = I3zzs+m3s*l^2+m4*((l3-x3)^2+y3^2);
I3yy = I3yys+m3s*(x3-x3s)^2+m4*(l3-x3)^2;
I2zz = 833.6518;
I2yy = 756.0469;
I3xx = 0;
I2xx = 0;
I3xy = 0;
I2xy = 0;
I3yz = 0;
I2yz = 0;
I3xz = 0;
I2xz = 0;
I1xx = 0;
I1yy = 0;
I1zz = 27.524792;
I1xy = 0;
I1yz = 0;
I1xz = 0;

S23 = sin(x(7)+x(13));
C23 = cos(x(7)+x(13));
s1 = sin(x(1));
c1 = cos(x(1));
s2 = sin(x(7));
c2 = cos(x(7));
s3 = sin(x(13));
c3 = cos(x(13));

m11 = (m3*(l1^2+l2^2*c2^2+x3^2*C23^2+y3^2*S23^2+2*l1*l2*c2+ ...
        2*l1*x3*C23-2*l1*y3*S23+z3^2+l2*x3*(2*c2*C23)- ...
        l2*y3*(2*c2*S23)-2*x3*y3*(S23*C23))+m2*(l1^2+y2^2*s2^2+ ...
        x2^2*c2^2+z2^2+2*l1*x2*c2-2*x2*y2*s2*c2-2*l1*y2*s2)+ ...
        m1*(x1^2+y1^2)+I1zz+I2xx*s2^2+I2yy*c2^2-2*I2xy*s2*c2+ ...
        I3xx*S23^2+I3yy*C23^2-2*I3xy*(S23*C23));

m12 = (-m3*z3*(x3*S23+y3*C23+l2*s2)-m2*z2*(x2*s2+y2*c2)-(I3xz*S23+ ...
        I3yz*C23+I2xz*s2+I2yz*c2));

m13 = (-m3*z3*(x3*S23+y3*C23)-I3xz*S23-I3yz*C23);

m22 = (m3*(x3^2+y3^2+l2^2+2*l2*x3*c3-2*l2*y3*s3)+m2*(x2^2+y2^2)+ ...
        I3zz+I2zz);

m23 = (m3*(x3^2+y3^2+l2*x3*c3-l2*y3*s3)+I3zz);

m33 = (m3*(x3^2+y3^2)+I3zz);


denominator = (-(m13^2*m22) + 2*m12*m13*m23 - m11*m23^2 - ...
        m12^2*m33 + m11*m22*m33);


% ELEMENT OF INVERTED MASS MATRIX

im11 = (-m23^2 + m22*m33)/denominator;
im12 = (m13*m23 - m12*m33)/denominator;
im13 = (-(m13*m22) + m12*m23)/denominator;
im22 = (-m13^2 + m11*m33)/denominator;
im23 = (m12*m13 - m11*m23)/denominator;
im33 = (-m12^2 + m11*m22)/denominator;


G1 = ((m3*s1*(-l1-l2*c2-x3*C23+y3*S23)+m3*z3*c1+m2*s1*(-l1-x2*c2+y2*s2)+ ...
        m2*z2*c1-m1*(x1*si+y1*c1))*gx+(m3*c1*(l1+l2*c2+x3*C23-y3*S23)+ ...
        m3*z3*s1+m2*c1*(l1+x2*c2-y2*s2)+m2*z2*s1+m1*(x1*c1-y1*s1))*gy);


G2 = ((m3*(l2*c2+x3*C23-y3*S23)+m2*(x2*c2-y2*s2))*gz- ...
        (m3*s1*(l2*s2+x3*S23+y3*C23)+m2*s1*(x2*s2+y2*c2))*gy- ...
```

```
        (m3*c1*(l2*s2+x3*S23+y3*C23)+m2*c1*(x2*s2+y2*c2))*gx);

G3 = (m3*(x3*C23-y3*S23)*gz-(m3*s1*(x3*S23+y3*C23))*gy- ...
        (m3*c1*(x3*S23+y3*C23))*gx);


V1 = ((m3*(-2*l1*l2*s2-2*l1*x3*S23-2*l1*y3*C23-2*l2*y3*(c2*C23-s2*S23)- ...
        2*x3*y3*(C23^2-S23^2)-2*l2^2*s2*c2-2*l2*x3*(c2*S23+s2*C23)- ...
        2*x3^2*(S23*C23)+2*y3^2*(S23*C23))+m2*(-2*l1*x2*s2- ...
        2*l1*y2*c2-2*x2*y2*(c2^2-s2^2)-2*x2^2*s2*c2+2*y2^2*s2*c2)- ...
        2*I2xy*(c2^2-s2^2)+2*I2xx*s2*c2-2*I2yy*s2*c2-2*I3xy* ...
        (C23^2-S23^2)+2*I3xx*(S23*C23)-2*I3yy*(S23*C23))*x(2)*x(8)+ ...
        (m3*(-2*l1*x3*S23-2*l1*y3*C23-2*l2*y3*c2*C23- ...
        2*x3*y3*(C23^2-S23^2)-2*l2*x3*c2*S23-2*x3^2*(S23*C23)+ ...
        2*y3^2*(S23*C23))-2*I3xy*(C23^2-S23^2)+2*I3xx*(S23*C23)- ...
        2*I3yy*(S23*C23))*x(2)*x(14)+(2*m3*z3*(-x3*C23+y3*S23)- ...
        2*I3xz*C23+2*I3yz*S23)*x(8)*x(14)+ ...
        (m3*z3*(-l2*c2-x3*C23+y3*S23)+m2*z2*(-x2*c2+y2*s2)-I3xz*C23+ ...
        I3yz*S23-I2xz*c2+I2yz*s2)*x(8)^2+ ...
        (m3*z3*(-x3*C23+y3*S23)-I3xz*C23+I3yz*S23)*x(14)^2);


V2 = ((m3*(l1*l2*s2+l1*x3*S23+l1*y3*C23+l2*y3*(c2*C23-s2*S23)+ ...
        x3*y3*(C23^2-S23^2)+l2^2*s2*c2+l2*x3*(c2*S23+s2*C23)+ ...
        (x3^2-y3^2)*(S23*C23)) ...
        +m2*(l1*x2*s2+l1*y2*c2+x2*y2*(c2^2-s2^2)+(x2^2-y2^2)*s2*c2)+ ...
        I3xy*(C23^2-S23^2)+(I3yy-I3xx)*(S23*C23)+ ...
        I2xy*(c2^2-s2^2)-I2xx*s2*c2+I2yy*s2*c2)*x(2)^2- ...
        2*m3*l2*(x3*s3+y3*c3)*x(8)*x(14)-m3*l2*(x3*s3+y3*c3)*x(14)^2);


V3 =  ((m3*(l1*x3*S23+l2*x3*c2*S23+l1*y3*C23+l2*y3*c2*C23+ ...
        x3*y3*(C23^2-S23^2)+x3^2*(S23*C23)-y3^2*(S23*C23))+ ...
        I3xy*(C23^2-S23^2)+(-I3xx+I3yy)*(S23*C23))*x(2)^2+ ...
        (m3*l2*(x3*s3+y3*c3))*x(8)^2);


%assign estimated numerical values to parameters (hydraulic part)


%SWING

ratio_sw1 = 1 / 4;
ratio_sw2 = 1 / 4;

%parameters for hose #1
c1_sw = 1.585e-12*ratio_sw1;
i1_sw = 3.062e7*ratio_sw1;
r1_sw = 3.0329e8*ratio_sw1;

%parameters for hose #2
c2_sw = 1.585e-12*ratio_sw2;
i2_sw = 3.062e7*ratio_sw2;
r2_sw = 3.0329e8*ratio_sw2;

b_sw = 2.4964e4;

d_sw = 4.5064e-5/(2*pi);

Ri = 8.035e11;

Rel = 2.119e12;

Re2 = Rel;

N = (35.16*82) / 13;    %gear ratio


%two predefined terms

A = 1 / (1/r2_sw + 1/r1_sw + 1/Rel + 1/Re2);

B = 1 / (1/Ri + 1/r1_sw + 1/Rel);

C = (x(3)-x(4))/r1_sw - x(4)/Rel - N*d_sw*x(2);

D = 1 / (1/B - A*(1/r1_sw + 1/Rel)^2);

PRi = D * (C - A*(1/r1_sw + 1/Rel)*((x(3)-x(4))/r1_sw - x(4)/Rel - ...
       x(4)/Re2));

Pr2 = A * ((x(3)-PRi-x(4))/r1_sw - (PRi+x(4))/Rel - x(4)/Re2);


%force terms

omega_sw = x(2);

torque_sw = N * d_sw*PRi - b_sw*omega_sw;



%BOOM

ratio_bm1 = 1.6 / 4;
ratio_bm2 = 2.2 / 4;

%parameters for hose #1
c1_bm = 1.585e-12*ratio_bm1;
i1_bm = 3.062e7*ratio_bm1;
r1_bm = 4.987e5^2*ratio_bm1;

%parameters for hose #2
c2_bm = 1.585e-12*ratio_bm2;
i2_bm = 3.062e7*ratio_bm2;
r2_bm = 4.987e5^2*ratio_bm2;

%parameters for cylinder
GY1 = 1.824e-2;
GY2 = 1.368e-2;

b_bm = 1.0303e5;

%the force arm
xb_bm = sqrt(l1b^2 + l2b^2 - 2*l1b*l2b*cos(x(7) + delta + si2));

theta_bm = acos((l1b^2 + xb_bm^2 - l2b^2) / (2*l1b*xb_bm));

arm_bm = l1b * sin(theta_bm);

%figure out force
vs_bm = arm_bm * x(8);

F_bm = GY1*(x(9)-r1_bm*(GY1*vs_bm)^2*sign(vs_bm)) - ...
       GY2*(r2_bm*(GY2*vs_bm)^2*sign(vs_bm)+x(10)) ...
       - b_bm*vs_bm;

torque_bm = arm_bm * F_bm;
```

```
% STICK

ratio_sk1 =  3.8 / 4;
ratio_sk2 =  4.9 / 4;

%parameters for hose #1
c1_sk = 1.585e-12*ratio_sk1*2;
i1_sk = 3.062e7*ratio_sk1*2;
r1_sk = 4.987e5^2*ratio_sk1;

%parameters for hose #2
c2_sk = 1.585e-12*ratio_sk2*2;
i2_sk = 3.062e7*ratio_sk2*2;
r2_sk = 4.987e5^2*ratio_sk2;

%parameters for cylinder
GY1 = 1.824e-2;
GY2 = 1.368e-2;

b_sk = 1.0303e5;

%the force arm
xs_sk = sqrt(l1s^2+l2s^2+2*l1s*l2s*cos(x(13)+si1));

theta_sk = acos((l1s^2+xs_sk^2-l2s^2)/(2*l1s*xs_sk));

arm_sk = l1s * sin(theta_sk);

%figure out force
vs_sk = arm_sk * x(14);


F_sk =  GY1*(x(15)-r1_sk*(GY1*vs_sk)^2*sign(vs_sk)) - ...
        GY2*(r2_sk*(GY2*vs_sk)^2*sign(vs_sk)+x(16)) - b_sk*vs_sk;


torque_sk = arm_sk * F_sk;



R1 = torque_sw - V1 - G1;

R2 = torque_bm - V2 - G2;

R3 = torque_sk - V3 - G3;


%the state equations


%%%%%%%%%%%%%%%%%%%%%%%%%%%%%%%%%%%%%%%%%%%%%%%%%%%%%%%%%%%%%%%%%%%%%%%
%SWING


xdot(1) = x(2);

xdot(2) = im11*R1+im12*R2+im13*R3;

xdot(3) = (1/c1_sw) * (x(5) - (x(3)-PRi-Pr2-x(4))/r1_sw);

xdot(4) = (1/c2_sw) * ((x(3)-PRi-Pr2-x(4))/r1_sw - (PRi+Pr2+x(4))/Re1 ...
        - (x(4)+Pr2)/Re2 - x(6));

xdot(5) = (1/i1_sw) * (Ps - Crv1_sw*x(5)^2*sign(x(5)) - x(3));

xdot(6) = (1/i2_sw) * (x(4) - Crv2_sw*x(6)^2*sign(x(6)));
%%%%%%%%%%%%%%%%%%%%%%%%%%%%%%%%%%%%%%%%%%%%%%%%%%%%%%%%%%%%%%%%%%%%%%%



%%%%%%%%%%%%%%%%%%%%%%%%%%%%%%%%%%%%%%%%%%%%%%%%%%%%%%%%%%%%%%%%%%%%%%%
%BOOM

xdot(7) = x(8);

xdot(8) = im12*R1+im22*R2+im23*R3;

xdot(9) = (1/c1_bm) * (x(11) - GY1*vs_bm);

xdot(10) = (1/c2_bm) * (GY2*vs_bm - x(12));

xdot(11) = (1/i1_bm) * (Ps - Crv1_bm*x(11)^2*sign(x(11)) - x(9));

xdot(12) = (1/i2_bm) * (x(10) - Crv2_bm*x(12)^2*sign(x(12)));
%%%%%%%%%%%%%%%%%%%%%%%%%%%%%%%%%%%%%%%%%%%%%%%%%%%%%%%%%%%%%%%%%%%%%%%



%%%%%%%%%%%%%%%%%%%%%%%%%%%%%%%%%%%%%%%%%%%%%%%%%%%%%%%%%%%%%%%%%%%%%%%
%STICK

xdot(13) = x(14);

xdot(14) = im13*R1+im23*R2+im33*R3;

xdot(15) = (1/c1_sk) * (x(17) - GY1*vs_sk);

xdot(16) = (1/c2_sk) * (GY2*vs_sk - x(18));

xdot(17) = (1/i1_sk) * (Ps - Crv1_sk*x(17)^2*sign(x(17)) - x(15));

xdot(18) = (1/i2_sk) * (x(16) - Crv2_sk*x(18)^2*sign(x(18)));
```

IMAGE EVALUATION TEST TARGET (QA-3)

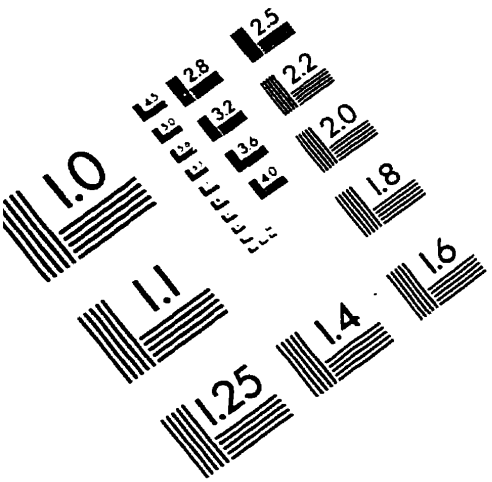

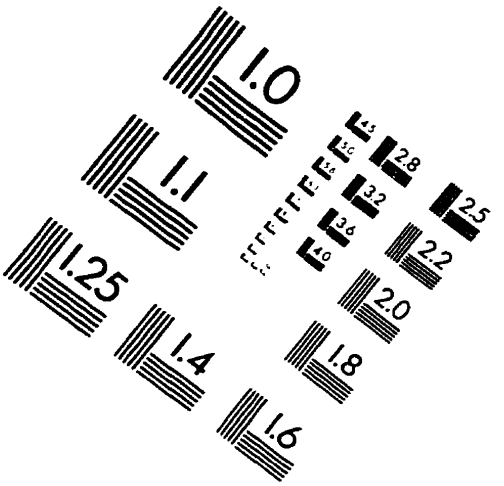

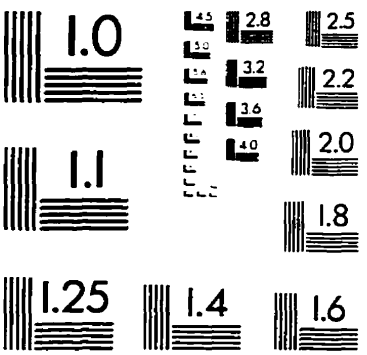

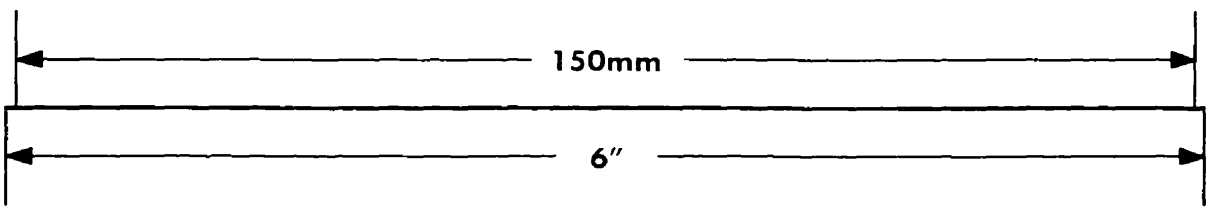

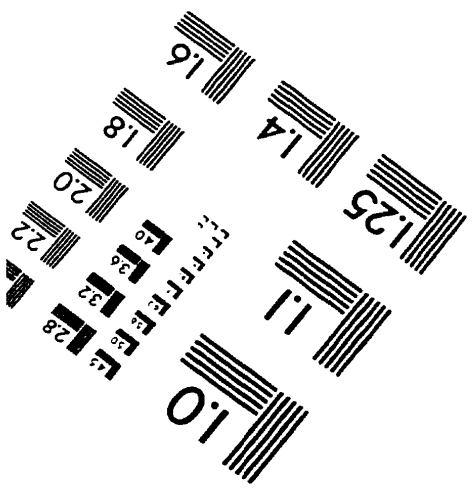

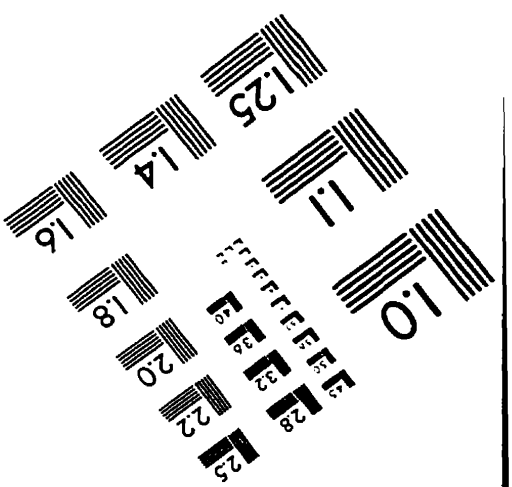

APPLIED IMAGE, Inc
1653 East Main Street
Rochester, NY 14609 USA
Phone: 716/482-0300
Fax: 716/288-5989